MODELING ASSESSMENT

Photochemical Modeling for the 2016 San Joaquin Valley Annual $PM_{2.5}$ State Implementation Plan

Prepared by

California Air Resources Board
San Joaquin Valley Air Pollution Control District

Prepared for

United States Environmental Protection Agency Region IX

July 26, 2016

TABLE OF CONTENTS

List of Figures

List of Tables

ACRONYMS

ARB – Air Resources Board

BCs – Boundary Conditions

CMAQ Model – Community Multi-scale Air Quality Model

CRPAQS – California Regional Particulate Air Quality Study

CSN – Chemical Speciation Network

DISCOVER-AQ – Deriving Information on Surface Conditions from Column and Vertically Resolved Observations Relevant to Air Quality

DV – Design Value

EC – Elemental Carbon

FEM – Federal Equivalent Method

FRM – Federal Reference Method

GEOS-5 – Goddard Earth Observing System Model, Version 5

GMAO – Global Modeling and Assimilation Office

ICs – Initial Conditions

MEGAN – Model of Emissions of Gases and Aerosols from Nature

MFB – Mean Fractional Bias

MFE – Mean Fractional Error

MOZART – Model for Ozone and Related chemical Tracers

NARR – North American Regional Reanalysis

NASA – National Aeronautics and Space Administration

NCR – National Center for Atmospheric Research

NMB – Normalized Mean Bias

NME – Normalized Mean Error

NO_x – Oxides of Nitrogen

OC – Organic Carbon

OM – Organic Matter

$PM_{2.5}$ – Particulate Matter of Aerodynamic Diameter less than 2.5 micrometers

RMSE – Root Mean Square Error

ROG – Reactive Organic Gases

RRF – Relative Response Factors

SANWICH – Sulfate, Adjusted Nitrate, Derived Water, Inferred Carbon Hybrid material balance

SAPRC – Statewide Air Pollution Research Center

SIP – State Implementation Plan

SJV – San Joaquin Valley

SOA – Secondary Organic Aerosol

SO_x – Sulfur oxides

U.S. EPA – United States Environmental Protection Agency

VOCs – Volatile Organic Compounds

WRF – Weather and Research Forecasting

1 INTRODUCTION

The purpose of this document is to summarize the findings of the modeling assessment for the annual $PM_{2.5}$ (12 µg/m^3) standard in the San Joaquin Valley nonattainment area (SJV or the Valley), which forms the scientific basis for the SJV 2016 annual $PM_{2.5}$ SIP. The 12 µg/m^3 standard was promulgated by the U.S. EPA in 2012, and EPA issued final designations in 2014. Currently, the Valley is designated as a Moderate nonattainment area for this standard with an attainment date of 2012. However, recent $PM_{2.5}$ trends in the Valley brought on by a sustained drought coupled with the modeling assessment described below, illustrates the impracticability of attaining the standard by 2021. This would lead to a reclassification of the Valley from a Moderate to Serious nonattainment area, as well as a new SIP timeline and attainment date of 2025.

The remainder of the document is organized as follows: Section 2 describes the general approach for projecting design values (DVs) to the future (2021), Section 3 discusses the meteorological modeling and evaluation, while Sections 4 and 5 describe the emissions inventory and $PM_{2.5}$ modeling and evaluation, respectively. A more detailed description of the modeling and development of the model-ready emissions inventory can be found in the Photochemical Modeling Protocol Appendix.

2 APPROACHES

This section briefly describes the Air Resources Board's (ARB's) procedures, based on U.S. EPA guidance (U.S. EPA, 2014), for projecting future year annual $PM_{2.5}$ Design Values (DVs) using model output and a Relative Response Factor (RRF) approach.

2.1 METHODOLOGY

The U.S. EPA modeling guidance (U.S. EPA, 2014) outlines the approach for using models to predict future year annual $PM_{2.5}$ DVs. The guidance recommends using model predictions in a "relative" rather than "absolute" sense. In this relative approach, the fractional change (or ratio) in $PM_{2.5}$ concentration between the model future year and model baseline year are calculated for all valid monitors. These ratios are called relative response factors (RRFs). Since $PM_{2.5}$ is comprised of different chemical species, which respond differently to changes in emissions of various pollutants, separate RRFs are calculated for the individual $PM_{2.5}$ species. Baseline DVs are then projected to the future on a species-by-species basis, where the DV is separated into individual $PM_{2.5}$ species and each species is multiplied by its corresponding RRF. The individual species are then summed to obtain the future year $PM_{2.5}$ DV.

A brief summary of the modeling procedures utilized in this attainment analysis, as prescribed by the U.S. EPA modeling guidance (U.S. EPA, 2014), is provided below. A

more detailed description can be found in the Photochemical Modeling Protocol Appendix.

2.2 MODELING PERIOD

Based on analysis of recent years' ambient $PM_{2.5}$ levels and meteorological conditions leading to elevated $PM_{2.5}$ concentrations, the year 2013 was selected for baseline modeling calculations. The National Aeronautics and Space Administration (NASA) launched the DISCOVER-AQ (Deriving Information on Surface Conditions from Column and Vertically Resolved Observations Relevant to Air Quality) field campaign in the SJV from January 16th to Mid-February, 2013. This field study provided unprecedented observations of wintertime $PM_{2.5}$ and its precursors not available in the SJV since the CRPAQS (i.e., California Regional Particulate Air Quality Study) study more than 15 years ago. These observations aided in development of the modeling platform used in this SIP work.

2.3 BASELINE DESIGN VALUES

Specifying the baseline DV is a key consideration in the model attainment test, because this value is projected forward to the future and used to test for future attainment of the standard at each monitor. U.S. EPA guidance (2014) defines the annual $PM_{2.5}$ DV for a given year as the 3-year average (ending in that year) of the annual average $PM_{2.5}$ concentrations, where the annual average is calculated as the average of the quarterly averages for each calendar quarter (e.g., January-March, April-June, July-September, October-December). For example, the 2012 $PM_{2.5}$ DV is the average of the annual $PM_{2.5}$ concentrations from 2010, 2011, and 2012.

To minimize the influence of year-to-year variability in demonstrating attainment, the U.S. EPA (2014) optionally allows the averaging of three DVs, where one of the years is the baseline emissions inventory and modeling year. This average DV is referred to as the baseline DV. For a baseline modeling year of 2013, this would typically mean that the average of the 2013, 2014, and 2015 DVs would be used. However, at the time of this work the 2015 DVs were still preliminary (i.e., 2015 measurements had not been finalized), so the average DV will instead include 2012, 2013, and 2014. Since each DV represents an average over three years, observational data from 2010, 2011, 2012, 2013, and 2014 will influence the average DV, with each year receiving a different weighting. Table 1 illustrates the observational data from each year that goes into the baseline DV.

Table1. Illustrates the data from each year that are utilized in the baseline Design Value calculation.

DV Year	Years averaged for the DV (average of quarterly average $PM_{2.5}$)				
2012	2010	2011	2012		
2013		2011	2012	2013	
2014			2012	2013	2014

Yearly weighting for the baseline DV calculation

$$2012-2014\ Average = \frac{PM2.5_{2010} + 2 \times PM2.5_{2011} + 3 \times PM2.5_{2012} + 2 \times PM2.5_{2013} + PM2.5_{2014}}{9}$$

Table 2 shows the 2012-2014 average DVs (or baseline DVs) for each Federal Reference Method (FRM) /Federal Equivalent Method (FEM) site in the SJV. For three sites with incomplete data, assumptions were made to calculate the baseline DVs and those assumptions were annotated following Table 2. The highest DV occurred at the Bakersfield – Planz site with a baseline DV of 17.3 µg/m^3.

Table 2. Average baseline DVs for each FRM monitoring site in the SJV, as well as the yearly design values from 2012-2014 utilized in calculating the baseline DVs.

AQS site ID	Monitoring Site Name	2012	2013	2014	2012-2014 Average Baseline
60290016	Bakersfield - Planz	15.6	16.9	19.3	17.3
60392010	Madera		18.1	15.8	16.9*
60311004	Hanford	15.8	17.0	16.8	16.5
60310004	Corcoran				16.3*
61072002	Visalia	14.8	16.6	17.2	16.2
60195001	Clovis	16.0	16.4	16.0	16.1
60290014	Bakersfield – California Ave.	14.5	16.4	17.2	16.0
60190011	Fresno –Garland	14.2	15.4	15.3	15.0
60990006	Turlock	14.9	15.7	14.1	14.9
60195025	Fresno –Hamilton & Winery	13.9	14.7	14.1	14.2

60771002	Stockton	11.6	13.8	14.1	13.1
60470003	Merced - Coffee	14.3	13.3	11.7	13.1
60990005	Modesto	12.9	13.6	12.5	13.0
60472510	Merced -Main Street	10.4	11.1	11.4	11.0
60772010	Manteca		10.2	9.9	10.1*
60192009	Tranquility	7.5	7.9	7.7	7.7

*: Because of incomplete data, at Madera and Manteca, only DVs from 2013 and 2014 were averaged to determine the baseline DV; at Corcoran, annual average concentrations from 2010, 2013, and 2014 were averaged to obtain baseline DV.

2.4 BASE, REFERENCE, AND FUTURE YEARS

The modeling assessment consists of the following three primary model simulations, which all used the same model inputs for meteorology, chemical boundary conditions, and biogenic emissions. The only difference between the simulations was the year represented by the anthropogenic emissions (2013 or 2021) and certain day-specific emissions.

1. *Base Year (or Base Case) Simulation*
   The base year simulation for 2013 was used to assess model performance and includes as much day-specific detail as possible in the emissions inventory such as hourly adjustments to the motor vehicle and biogenic inventories based on observed local meteorological conditions, as well as known wildfire and agricultural burning events.

2. *Reference (or Baseline) Year Simulation*
   The reference year simulation was identical to the base year simulation, except that certain emissions events which are either random and/or cannot be projected to the future were removed from the emissions inventory. For the 2013 reference year modeling, the only category/emissions source that was excluded was wildfires, which are difficult to predict in the future and can significantly influence the model response to anthropogenic emissions reductions in regions with large fires.

3. *Future Year Simulation*
   The future year simulation is identical to the reference year simulation, except that projected future year (2021) anthropogenic emission levels were used rather than 2013 emission levels. All other model inputs (e.g., meteorology, chemical

boundary conditions, biogenic emissions, and calendar for day-of-week specifications in the inventory) are the same as those used in the reference year simulation.

To summarize (Table 3), the base year 2013 simulation was used for evaluating model performance, while the reference (or baseline) 2013 and future year 2021 simulations were used to project the average DVs to the future as described in the Photochemical Modeling Protocol Appendix and in subsequent sections of this document.

Table 3. Description of CMAQ model simulations used to evaluate model performance and project baseline design values to the future.

Simulation	Anthropogenic Emissions	Biogenic Emissions	Meteorology	Chemical Boundary Conditions
Base year (2013)	2013 w/ wildfires	2013 MEGAN	2013 WRF	2013 MOZART
Reference year (2013)	2013 w/o wildfires	2013 MEGAN	2013 WRF	2013 MOZART
Future year (2021)	2021 w/o wildfires	2013 MEGAN	2013 WRF	2013 MOZART

2.5 $PM_{2.5}$ SPECIES CALCULATIONS

Since $PM_{2.5}$ consists of different chemical components, it is necessary to assess how each individual component will respond to emission reductions. As a first step in this process, the measured total $PM_{2.5}$ must be separated into its various components. In the SJV, the primary components on the filter based $PM_{2.5}$ measurements include sulfates, nitrates, ammonium, organic carbon (OC), elemental carbon (EC), particle-bound water, other primary inorganic particulate matter, and passively collected mass (blank mass). Species concentrations were obtained from the four chemical speciation network (CSN) sites in the SJV. These four CSN sites are located at: Bakersfield – California Avenue, Fresno – Garland, Visalia – North Church, and Modesto – 14th Street. Chemical species were measured once every three or six days at those sites. Since not all of the 16 FRM $PM_{2.5}$ sites in the Valley have collocated speciation monitors, it was necessary to utilize the speciated $PM_{2.5}$ measurements at one of the four CSN sites to represent the speciation profile at each of the FRM sites. The choice of which CSN site to represent the speciation profile at a given FRM monitor (Table 4) was determined based on geographic proximity, analysis of local emission sources, and

measurements from previous field studies (e.g., CRPAQS), and is consistent with previous $PM_{2.5}$ SIPs in the Valley.

Table 4. $PM_{2.5}$ speciation data used for each $PM_{2.5}$ design site.

AQS Site ID	$PM_{2.5}$ Design Site (FRM/FEM Monitor)	$PM_{2.5}$ Speciation Site
60290016	Bakersfield – Planz	Bakersfield – California
60392010	Madera	Fresno – Garland
60311004	Hanford	Visalia – Church
60310004	Corcoran	Visalia – Church
61072002	Visalia	Visalia – Church
60195001	Clovis	Fresno – Garland
60290014	Bakersfield – California Ave.	Bakersfield – California
60190011	Fresno – Garland	Fresno – Garland
60990006	Turlock	Modesto – 14th
60195025	Fresno – Hamilton & Winery	Fresno – Garland
60771002	Stockton	Modesto – 14th
60470003	Merced – Coffee	Modesto – 14th
60990005	Modesto	Modesto – 14th
60472510	Merced – Main Street	Modesto – 14th
60772010	Manteca	Modesto – 14th
60192009	Tranquility	Fresno – Garland

Since the FRM $PM_{2.5}$ monitors do not retain all of the $PM_{2.5}$ mass that is measured by the speciation samplers, the U.S. EPA (2014) recommends using the SANDWICH approach (Sulfate, Adjusted Nitrate, Derived Water, Inferred Carbon Hybrid material balance) described by Frank (2006) to apportion the FRM $PM_{2.5}$ mass to individual $PM_{2.5}$ species based on nearby CSN speciation data. A detailed description of the SANDWICH method can be found in the modeling protocol and in the U.S. EPA (2014) modeling guidance. In addition, based on completeness of the data, $PM_{2.5}$ speciation data from 2010 – 2013 were utilized. For each quarter, percent contributions from individual chemical species to FRM $PM_{2.5}$ mass were calculated as the average of the corresponding quarter from 2010-2013. In general, the inter-annual variability of the species fractions is small compared to the variability in the species concentrations and so the use of average data from 2010 – 2013 is appropriate.

2.6 FUTURE YEAR DESIGN VALUES

Projecting baseline annual $PM_{2.5}$ DVs to the future is a multi-step process as outlined below. See U.S. EPA (2014) and the Photochemical Modeling Protocol Appendix for additional details.

Step 1: Compute observed quarterly weighted average concentrations (consistent with the weighted average DV calculation) at each monitor for the following species: ammonium, nitrate, sulfate, organic carbon, elemental carbon, and other primary PM. This is done by multiplying quarterly weighted average FRM $PM_{2.5}$ concentrations by the fractional composition of $PM_{2.5}$ species for each quarter.

Step 2: Compute the component-specific RRF for each quarter and each species at each monitor based on the reference and future year modeling. The RRF for a specific component *j* is calculated using the following expression:

$$RRF_j = \frac{[C]_{j,\ future}}{[C]_{j,\ reference}} \quad (1)$$

Where $[C]_{j,\ future}$ is the modeled quarterly mean concentration for component *j* predicted for the future year averaged over the 3x3 array of grid cells surrounding the monitor, and $[C]_{j,reference}$ is the same, but for the reference year simulation. An RRF was calculated for each species in Step 1 and at each monitor and for each quarter.

Step 3: Apply the component specific RRF from Step 2 to the observed quarterly weighted average concentrations from Step 1 to obtain projected quarterly species concentrations.

Step 4: Use the online E-AIM model (http://www.aim.env.uea.ac.uk/aim/aim.php) to calculate future year particle-bound water for each quarter at each monitor based on projected ammonium sulfate and ammonium nitrate concentrations.

Step 5: The projected concentration for each quarter is summed over all species, including particle bound water from Step 4, as well as a blank mass of 0.5 µg/m^3 to obtain the future quarterly average $PM_{2.5}$ concentration. Finally, the future annual $PM_{2.5}$ DVs are calculated as the average of the projected $PM_{2.5}$ concentrations from the four quarters.

Projected future year $PM_{2.5}$ DVs are discussed in Section 5.3.

3 METEOROLOGICAL MODELING

California's proximity to the ocean, complex terrain, and diverse climate represent a unique challenge for developing meteorological fields that adequately represent the synoptic and mesoscale features of the regional meteorology. In summertime, the majority of the storm tracks are far to the north of the state and a semi-permanent Pacific high typically sits off the California coast. Interactions between this eastern Pacific subtropical high pressure system and the thermal low pressure further inland over the Central Valley or South Coast lead to conditions conducive to pollution buildup (Fosberg and Schroeder, 1966; Bao et al., 2008). In wintertime, periods of high atmospheric pressure bring light winds and, sometimes, low solar insolation (Daly et al. 2009) to the Central Valley. Because of the topographical features surrounding San Joaquin Valley, under such conditions, a layer of cold and wet air can be overlaid by warm air aloft creating strong and long-lasting stagnation in the area (Whiteman et al. 2001). It is under such conditions that high surface particulate matter concentrations typically occur (Gilles et al. 2010; Baker et al. 2011).

In the past, the ARB has utilized both prognostic and diagnostic meteorological models, as well as hybrid approaches in an effort to develop meteorological fields for use in air quality modeling that most accurately represent the meteorological processes which are important to air quality (e.g., Jackson et al., 2006). In this work, the state-of-the-science Weather and Research Forecasting (WRF) prognostic model (Skamarock et al., 2005) version 3.6 was utilized to develop the meteorological fields used in the subsequent photochemical model simulations.

3.1 WRF MODEL SETUP

The WRF meteorological modeling domain consisted of three nested Lambert projection grids of 36-km (D01), 12-km (D02), and 4-km (D03) uniform horizontal grid spacing (Figure 1). WRF was run simultaneously for the three nested domains with two-way feedback between the parent and the nest grids. The D01 and D02 grids were used to resolve the larger scale synoptic weather systems, while the D03 grid resolved the finer details of the atmospheric conditions and was used to drive the air quality model simulations. All three domains utilized 30 vertical sigma layers (defined in Table 5), with the major physics options for each domain listed in Table 6.

Initial and boundary conditions (IC/BCs) for the WRF modeling were based on the 32-km horizontal resolution North American Regional Reanalysis (NARR) data that are archived at the National Center for Atmospheric Research (NCAR). Boundary conditions to WRF were updated at 6-hour intervals for the 36-km grid (D01). In addition, surface and upper air observations obtained from NCAR were used to further refine the analysis data that were used to generate the IC/BCs. Analysis nudging was

employed in the outer 36-km grid (D01) to ensure that the simulated meteorological fields were adequately constrained and did not deviate from the observed meteorology. No nudging was used on the two inner domains to allow model physics to work fully without externally imposed forcing (Rogers et al., 2013).

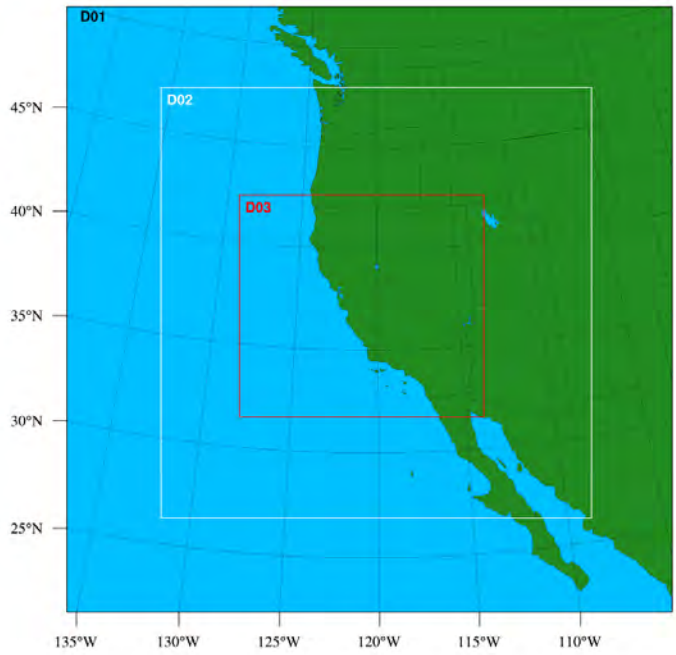

Figure 1. WRF modeling domains (D01 36km; D02 12km; and D03 4km).

Table 5. WRF vertical layer structure.

Layer Number	Height (m)	Layer Thickness (m)	Layer Number	Height (m)	Layer Thickness (m)
30	16082	1192	14	1859	334
29	14890	1134	13	1525	279
28	13756	1081	12	1246	233
27	12675	1032	11	1013	194
26	11643	996	10	819	162
25	10647	970	9	657	135
24	9677	959	8	522	113
23	8719	961	7	409	94
22	7757	978	6	315	79
21	6779	993	5	236	66
20	5786	967	4	170	55
19	4819	815	3	115	46
18	4004	685	2	69	38
17	3319	575	1	31	31
16	2744	482	0	0	0
15	2262	403			

Note: Shaded layers denote the subset of vertical layers used in the CMAQ photochemical model simulations.

Table 6. WRF Physics Options.

Physics Option	**Domain**		
	D01 (36 km)	**D02 (12 km)**	**D03 (4 km)**
Microphysics	WSM 6-class graupel scheme	WSM 6-class graupel scheme	WSM 6-class graupel scheme
Longwave radiation	RRTM	RRTM	RRTM
Shortwave radiation	Dudhia scheme	Dudhia scheme	Dudhia scheme
Surface layer	Revised MM5 Monin-Obukhov	Revised MM5 Monin-Obukhov	Revised MM5 Monin-Obukhov
Land surface	TD Scheme (Jan., Feb., Nov. and Dec.) Pleim-Xiu LSM (others)	TD Scheme (Jan., Feb., Nov. and Dec.) Pleim-Xiu LSM (others)	TD Scheme (Jan., Feb., Nov. and Dec.) Pleim-Xiu LSM (others)
Planetary Boundary Layer	YSU	YSU	YSU
Cumulus Parameterization	Kain-Fritsch scheme	Kain-Fritsch scheme	None

3.2 WRF MODEL RESULTS AND EVALUATION

Simulated surface wind speed, temperature, and relative humidity from the 4 km domain were validated against hourly observations at 77 surface stations in the SJV. Observational data for the surface stations were obtained from the ARB's archived meteorological database (http://www.arb.ca.gov/aqmis2/aqmis2.php). Table 7 lists the observational stations and the parameters measured at each station, including wind speed and direction (wind), temperature (T) and relative humidity (RH). The location of each of these sites is shown in Figure 2. Quarterly and annual quantitative performance metrics for 2013 were used to compare hourly surface observations and modeled estimates: mean bias (MB), mean error (ME) and index of agreement (IOA) based on recommendations from Simon et al. (2012). A summary of these statistics by performance region is shown in Tables 8 through 12. The performance regions cover roughly the Modesto, Fresno, Visalia, and Bakersfield regions, as well as one for the entire San Joaquin Valley (SJV), respectively. The region around Modesto includes sites 5737, 2833, and 2080. The region surrounding Fresno encompasses sites 5741, 2449, 2013, and 2844. The region around Visalia includes sites 2032, 5386, and 3250, while the region covering Bakersfield includes sites 5287 and 3146 (note that valid relative humidity observations in the Bakersfield area were only available at site 5287 for the months of January through May 2013). Model performance statistical metrics were calculated using all of the available data. All the sites in the valley are included in the SJV performance region (in addition to the sites mentioned above). The distribution of daily mean bias and mean error are shown in Figures 3 and 4. Figures 5 and 6 show observed vs. modeled scatter plots.

From a valley-wide perspective, the wind speed biases were positive in each quarter of 2013. At Bakersfield the biases turn slightly negative throughout the year, and are mostly less than 0.6 m/s. The annual temperature biases are less than 1 K in all performance regions, with the quarterly temperature biases reaching as high as -1.87 K in Bakersfield during the second quarter of 2013. Simulated temperature is generally in good agreement with the observations in all regions with the index of agreement (IOA) above 0.90 (1.0 represents perfect agreement). Relative humidity biases are positive except in the Modesto region. The annual bias values range from -1.53% to 12.47%, with the largest bias occurring in Visalia. These results are comparable to other recent WRF modeling efforts in California investigating ozone formation in Central California (e.g., Hu et al., 2012) and modeling analysis for the CalNex and CARES field studies (e.g., Fast et al., 2014; Baker et al., 2013; Kelly et al., 2014; Angevine et al., 2012). Detailed hourly time-series of surface temperature, relative humidity, wind speed, and wind direction for SJV can be found in the supplementary material, together with 2013 quarterly mean bias and mean error distributions of these parameters.

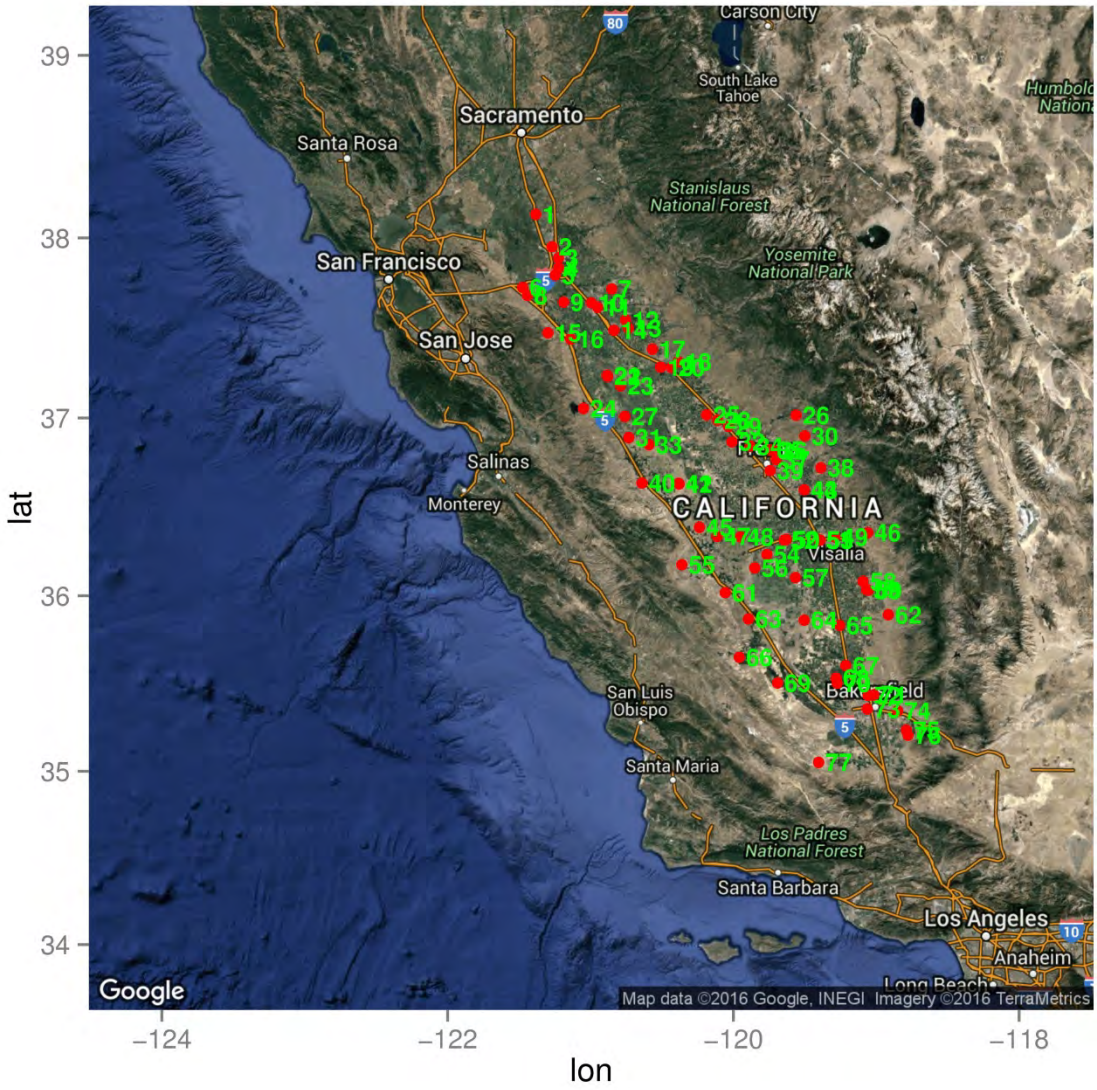

Figure 2. Meteorological observation sites in San Joaquin Valley. The numbers correspond to the sites listed in Table 7.

Table 7. Meteorological monitor location and parameter(s) measured.

Site	Site ID	Site Name	Parameter Measured	Site	Site ID	Site Name	Parameter Measured
1	5809	LodiWest	T, RH	40	3309	PanocheRd	Wind, T, RH
2	2094	Stockton-Haz	Wind, T, RH	41	3759	Tranquility	Wind, T
3	5362	StocktonArpt	Wind, T	42	5757	Westlands	T, RH
4	5736	Manteca	T, RH	43	5723	Parlier2	T, RH
5	3772	Manteca-Fish	Wind, T	44	2114	Parlier	Wind, T, RH
6	5810	Tracy	T, RH	45	5828	FivePointsSW	T, RH
7	5831	Oakdale2	T, RH	46	5746	Lindcove	T, RH
8	3696	Tracy_Air	Wind, T	47	5708	FivePoints2	T, RH
9	5737	Modesto3	T, RH	48	2544	Lemoore-Met	Wind, T
10	2833	Modesto-14th	Wind	49	2032	Visalia-NChu	Wind, T
11	2080	Modesto-Met	Wind, T	50	5308	HanfordMuni	Wind, T
12	7233	DenairII	T, RH	51	5386	VisaliaMuni	Wind, T
13	3303	RosePeak	Wind, T, RH	52	3129	Hanford-Irwn	Wind, T
14	2996	Turlock-SMin	Wind, T	53	3250	Visalia-Airp	Wind, T, RH
15	3449	Pulgas	Wind, T, RH	54	3712	StRosaRnchria	Wind, T
16	5805	Patterson2	T, RH	55	6028	CoalingaCIM	T, RH
17	2814	Merced-AFB	Wind, T	56	5715	Stratford2	T, RH
18	5793	Merced	T, RH	57	3194	Corcoran-Pat	Wind, T
19	5318	MercedMuni	Wind, T	58	5812	Portervl	T, RH
20	3022	Merced-SCofe	Wind, T	59	5351	PortervlMuni	Wind, T
21	6079	MERCED 23WSW	T	60	3763	Portrvlle-Ne	Wind, T
22	5752	Kesterson	T, RH	61	3330	KettlemanHls	Wind, T, RH
23	3647	SanLuisNWR	Wind, T, RH	62	3350	FountnSpr	Wind, T, RH
24	3307	LosBanos	Wind, T, RH	63	5717	Kettleman	T, RH
25	5790	Madera	T, RH	64	6813	Alpaugh	T, RH
26	3522	Hurley1	Wind, T, RH	65	5823	Delano2	T, RH
27	5730	LosBanos2	T, RH	66	5729	BlackwllCnr	T, RH
28	5317	MaderaMuni	Wind, T	67	5783	Famoso	T, RH
29	3771	Madera-Av14	Wind, T, RH	68	5709	ShafterUSDA	T, RH
30	3346	FancherCreek	Wind, T, RH	69	5791	Belridge	T, RH
31	5770	Panoche	T, RH	70	2981	Shafter-Wlkr	Wind, T, RH
32	3211	Madera-Rd29	Wind, T, RH	71	2772	Oildale-3311	Wind, T
33	5711	Firebgh-Tel	T, RH	72	5287	MeadowsFld	Wind, T
34	2844	Fresno-Sky#2	Wind, T	73	3146	Baker-5558Ca	Wind, T, RH
35	5741	FSU2	T, RH	74	2312	Edison	Wind, T
36	3026	Clovis	Wind, T, RH	75	3758	Arvin-DiG	Wind, T
37	2449	Fresno-FAT	Wind, T	76	5771	Arvin-Edison	T, RH
38	5787	OrangeCove	T, RH	77	2919	Maricopa-Stn	Wind, T
39	2013	Fresno-Drmnd	Wind, T				

Table 8. Hourly surface wind speed, temperature and relative humidity statistics in Modesto.

Quarter	Observed Mean	Modeled Mean	Mean Bias	Mean Error	IOA
		Wind Speed (m/s)			
Q1	2.08	2.62	0.54	1.16	0.74
Q2	3.04	3.51	0.46	1.43	0.73
Q3	2.64	2.94	0.30	1.18	0.65
Q4	1.66	2.35	0.69	1.23	0.68
Annual	2.41	2.89	0.49	1.26	0.73
		Temperature (K)			
Q1	282.62	282.93	0.31	2.16	0.94
Q2	293.18	292.86	-0.32	2.07	0.96
Q3	295.98	297.06	1.07	2.35	0.93
Q4	283.95	285.73	1.78	2.73	0.93
Annual	288.93	289.65	0.71	2.33	0.97
		Relative Humidity (%)			
Q1	73.52	74.38	0.86	9.14	0.89
Q2	57.03	53.28	-3.75	10.99	0.86
Q3	62.17	55.26	-6.91	13.98	0.72
Q4	67.75	71.40	3.66	11.48	0.85
Annual	65.10	63.57	-1.53	11.40	0.86

Table 9. Hourly surface wind speed, temperature and relative humidity statistics in Fresno.

Quarter	Observed Mean	Modeled Mean	Mean Bias	Mean Error	IOA
		Wind Speed (m/s)			
Q1	1.47	1.90	0.43	1.11	0.56
Q2	2.54	3.12	0.58	1.53	0.59
Q3	2.14	2.65	0.51	1.42	0.47
Q4	1.12	1.69	0.57	1.05	0.52
Annual	1.85	2.37	0.52	1.29	0.61
		Temperature (K)			
Q1	283.76	282.90	-0.86	1.79	0.96
Q2	295.23	294.04	-1.19	2.16	0.95
Q3	299.69	299.22	-0.47	2.22	0.94
Q4	285.65	286.01	0.36	1.93	0.96
Annual	291.18	290.65	-0.53	2.03	0.98
		Relative Humidity (%)			
Q1	71.46	76.39	4.93	10.71	0.86
Q2	48.01	53.07	5.06	11.88	0.83
Q3	45.12	51.45	6.33	14.95	0.65
Q4	64.03	70.79	6.77	13.49	0.83
Annual	57.09	62.87	5.78	12.77	0.86

Table 10. Hourly surface wind speed, temperature and relative humidity statistics in Visalia.

Quarter	Observed Mean	Modeled Mean	Mean Bias	Mean Error	IOA
		Wind Speed (m/s)			
Q1	1.48	1.64	0.16	0.82	0.55
Q2	2.07	2.53	0.45	1.04	0.65
Q3	1.91	2.22	0.31	0.86	0.59
Q4	1.62	1.58	-0.04	0.73	0.60
Annual	1.77	2.00	0.24	0.88	0.65
		Temperature (K)			
Q1	283.66	282.87	-0.79	1.85	0.95
Q2	294.38	293.09	-1.29	2.23	0.95
Q3	298.73	298.42	-0.31	2.56	0.91
Q4	285.19	286.03	0.84	2.11	0.95
Annual	290.03	289.55	-0.48	2.16	0.97
		Relative Humidity (%)			
Q1	73.28	80.72	7.44	11.11	0.82
Q2	47.80	59.94	12.13	17.23	0.73
Q3	47.08	63.07	15.99	21.49	0.49
Q4	61.22	75.43	14.21	16.36	0.77
Annual	57.37	69.84	12.47	16.56	0.76

Table 11. Hourly surface wind speed, temperature and relative humidity statistics in Bakersfield (valid RH data available from January through May only; statistics are based on the available data).

Quarter	Observed Mean	Modeled Mean	Mean Bias	Mean Error	IOA
		Wind Speed (m/s)			
Q1	1.84	1.80	-0.04	0.88	0.59
Q2	2.63	2.47	-0.15	1.03	0.74
Q3	2.12	2.10	-0.02	1.10	0.68
Q4	2.23	1.86	-0.37	0.98	0.61
Annual	2.21	2.09	-0.12	1.00	0.70
		Temperature (K)			
Q1	284.94	283.97	-0.97	1.91	0.95
Q2	295.66	293.78	-1.87	2.44	0.94
Q3	301.17	299.54	-1.63	2.63	0.90
Q4	286.85	286.97	0.12	1.73	0.97
Annual	291.33	290.17	-1.16	2.16	0.97
		Relative Humidity (%)			
Q1	62.65	72.70	10.04	15.15	0.81
Q2	36.94	51.46	14.52	16.82	0.74
Annual	52.27	64.12	11.85	15.83	0.83

Table 12. Hourly surface wind speed, temperature and relative humidity statistics in the San Joaquin Valley.

Quarter	Observed Mean	Modeled Mean	Mean Bias	Mean Error	IOA
		Wind Speed (m/s)			
Q1	2.08	2.62	0.54	1.16	0.74
Q2	3.04	3.51	0.46	1.43	0.73
Q3	2.64	2.94	0.30	1.18	0.65
Q4	1.66	2.35	0.69	1.23	0.68
Annual	2.41	2.89	0.49	1.26	0.73
		Temperature (K)			
Q1	283.31	283.30	-0.01	2.17	0.94
Q2	294.23	293.42	-0.81	2.46	0.94
Q3	298.22	298.21	-0.02	2.82	0.90
Q4	285.08	286.20	1.12	2.65	0.93
Annual	290.19	290.25	0.07	2.52	0.96
		Relative Humidity (%)			
Q1	69.36	71.65	2.29	12.87	0.81
Q2	47.95	52.53	4.57	13.73	0.79
Q3	46.35	54.48	8.12	17.33	0.59
Q4	58.62	68.35	9.72	16.00	0.75
Annual	55.70	61.84	6.14	14.96	0.79

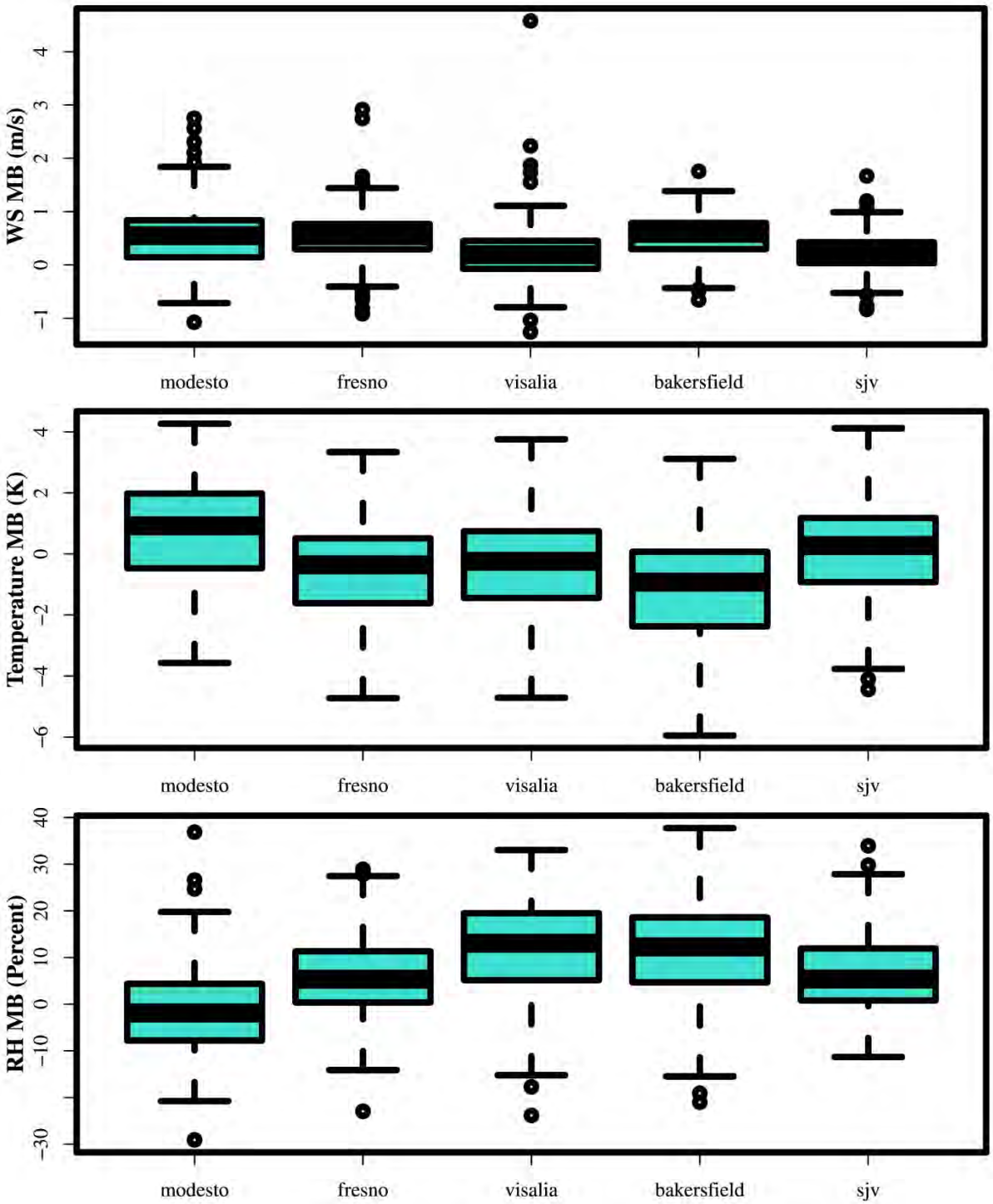

Figure 3. Distribution of model daily mean bias for Modesto, Fresno, Visalia, Bakersfield and SJV. Results are shown for wind speed (top), temperature (middle), and Relative Humidity (bottom).

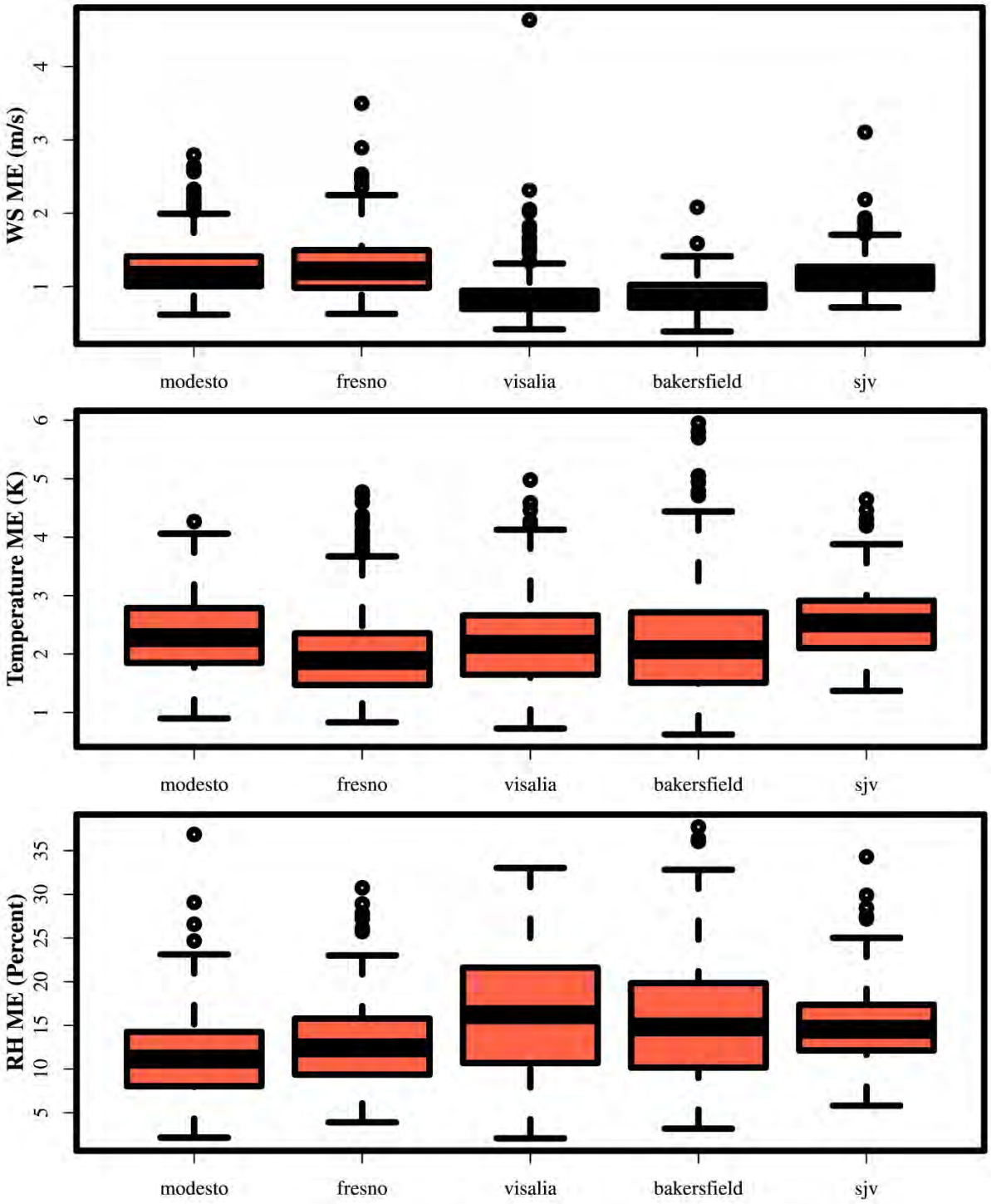

Figure 4. Distribution of model daily mean error for Modesto, Fresno, Visalia, Bakersfield and SJV. Results are shown for wind speed (top), temperature (middle), and Relative Humidity (bottom).

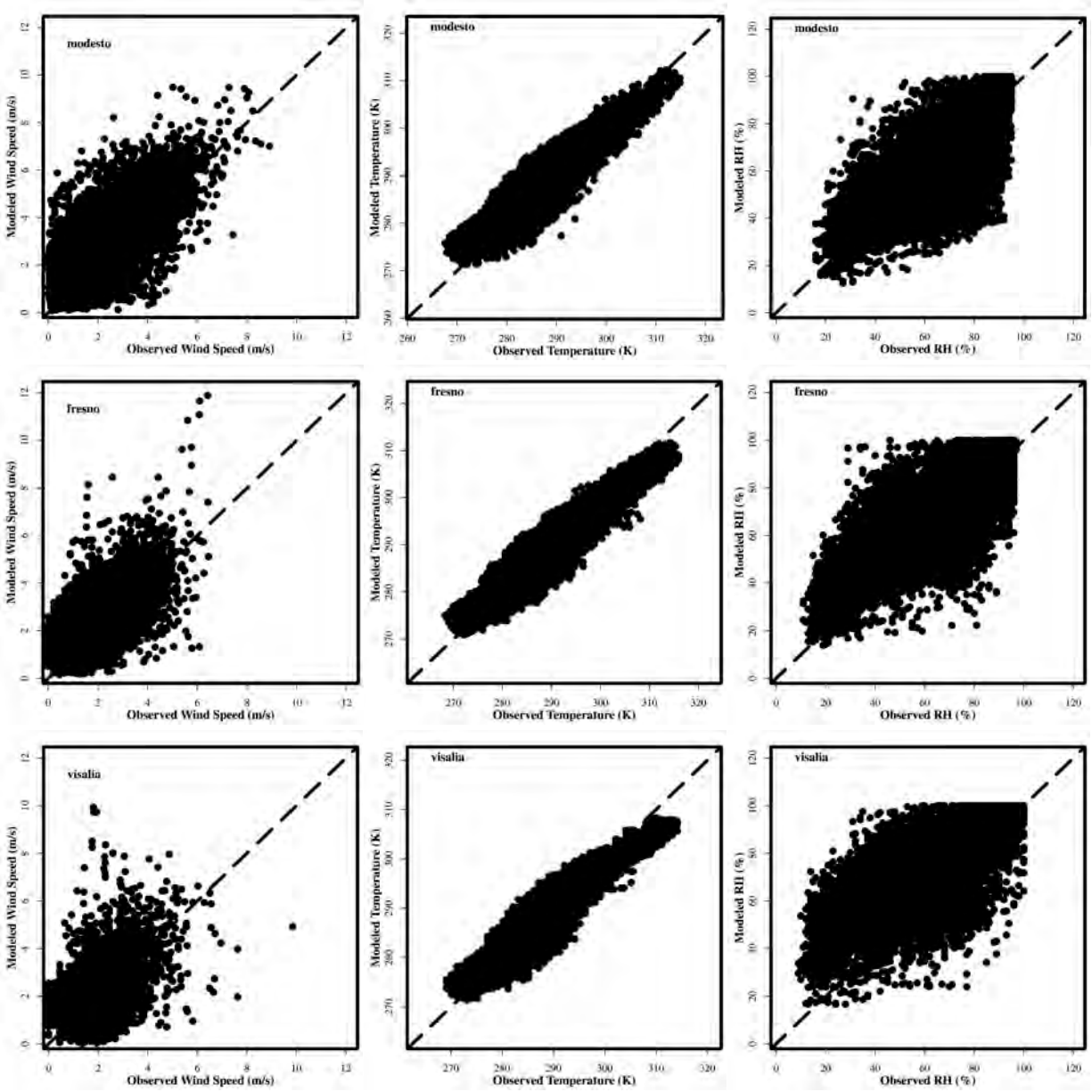

Figure 5. Comparison of modeled and observed hourly wind speed (left column), 2-meter temperature (middle column), and relative humidity (right column). Results for Modesto are shown in the top row, Fresno in the middle row, and Visalia in the bottom row.

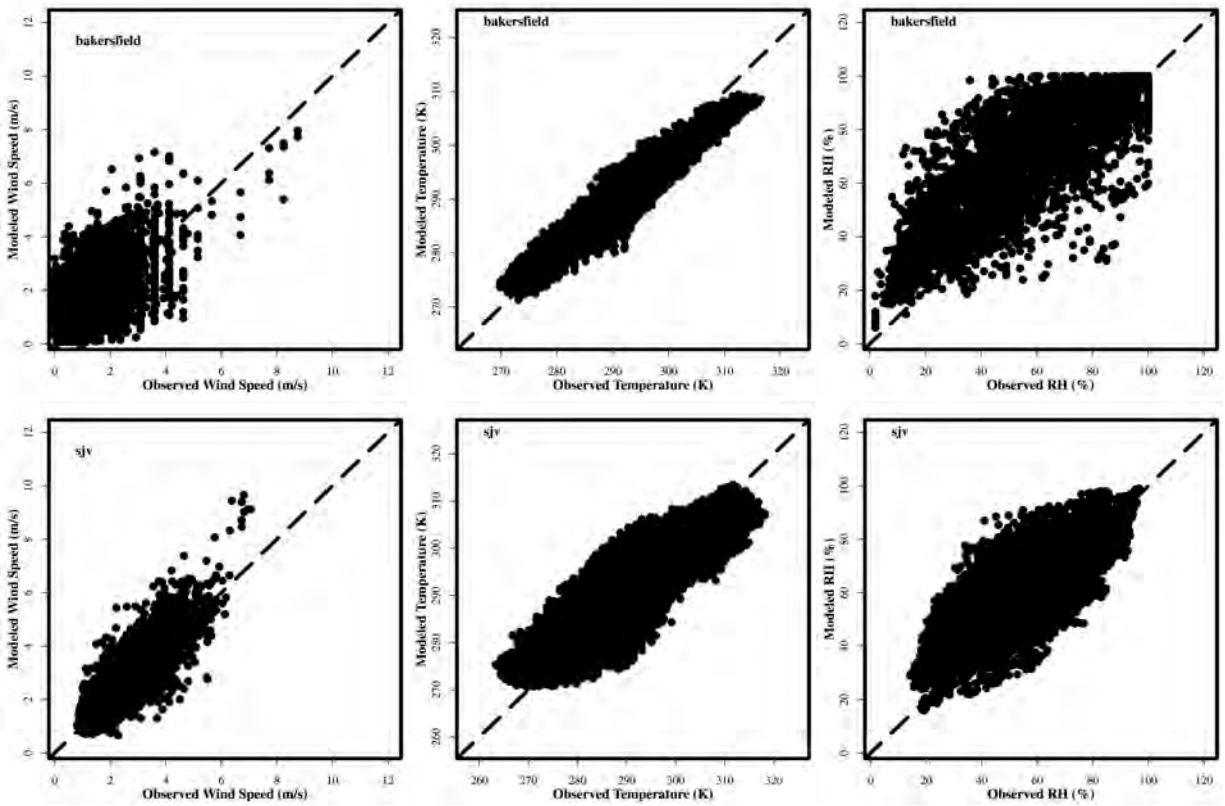

Figure 6. Comparison of modeled and observed hourly wind speed (left column), 2-meter temperature (middle column), and relative humidity (right column). Results for Bakersfield are shown in the top row and SJV in the bottom row.

3.2.1 PHENOMENOLOGICAL EVALUATION

Conducting a detailed phenomenological evaluation for all modeled days can be resource intensive given that the entire year was modeled. However, some insight and confidence that the model is able to reproduce the meteorological conditions leading to elevated particulate matter can be gained by investigating the meteorological conditions during a period of peak PM within the Valley in more detail. The highest $PM_{2.5}$-conducive meteorological conditions in the Valley occurred around January 20, 2013. Surface weather analysis shows that on January 20, the western US was under a typical Great Basin high pressure system. In the 500 hPa map (not shown), a strong high pressure ridge extends from Northern California along the west Pacific coast all the way to Alaska. As shown in Figures 7, 8, and 9, the winds, though weak, are mainly offshore along the northern California coast. Under this type of weather system, conditions in SJV are driven by diurnal cycles of the local winds. Figure 7 shows that at 13:00 PST, January 20, the upslope flows along the eastern side of the Coastal Ranges and the western side of the Sierras, lead to a weak northwesterly flow on the floor of the valley. The downslope winds form at nighttime and in the early morning (Figure 8 and Figure 9). They converge towards the valley and the winds in the center of the valley floor turn southeasterly. At the southern end of the valley, an eddy-like pattern occurs due to the interaction of the katabatic flows. The surface wind distributions of the modeled and observed winds indicate the model was able to capture many of the important features of the meteorological fields in the SJV.

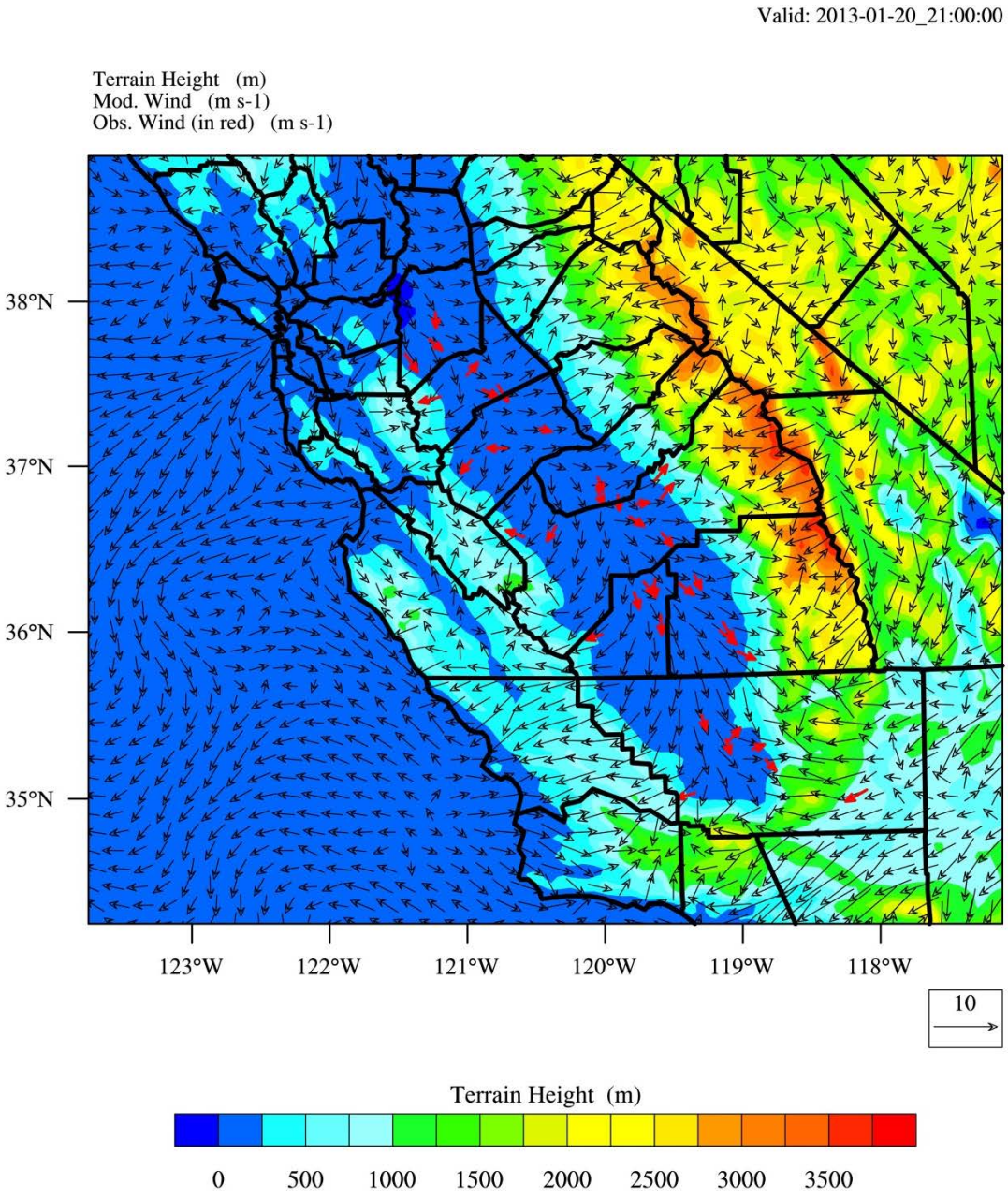

Figure 7. Surface wind field at 13:00 PST January 20, 2013.

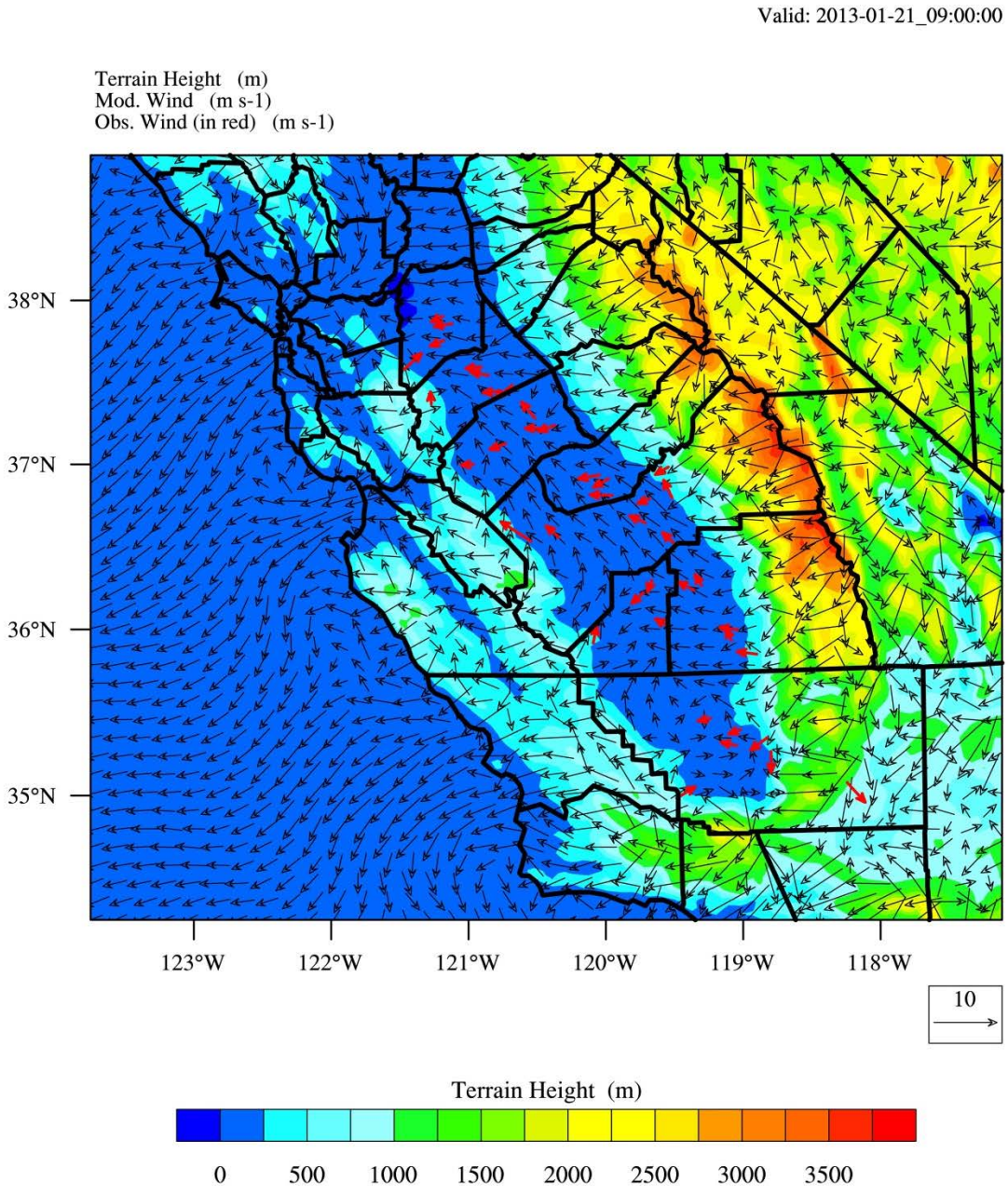

Figure 8. Surface wind field at 01:00 PST January 21, 2013.

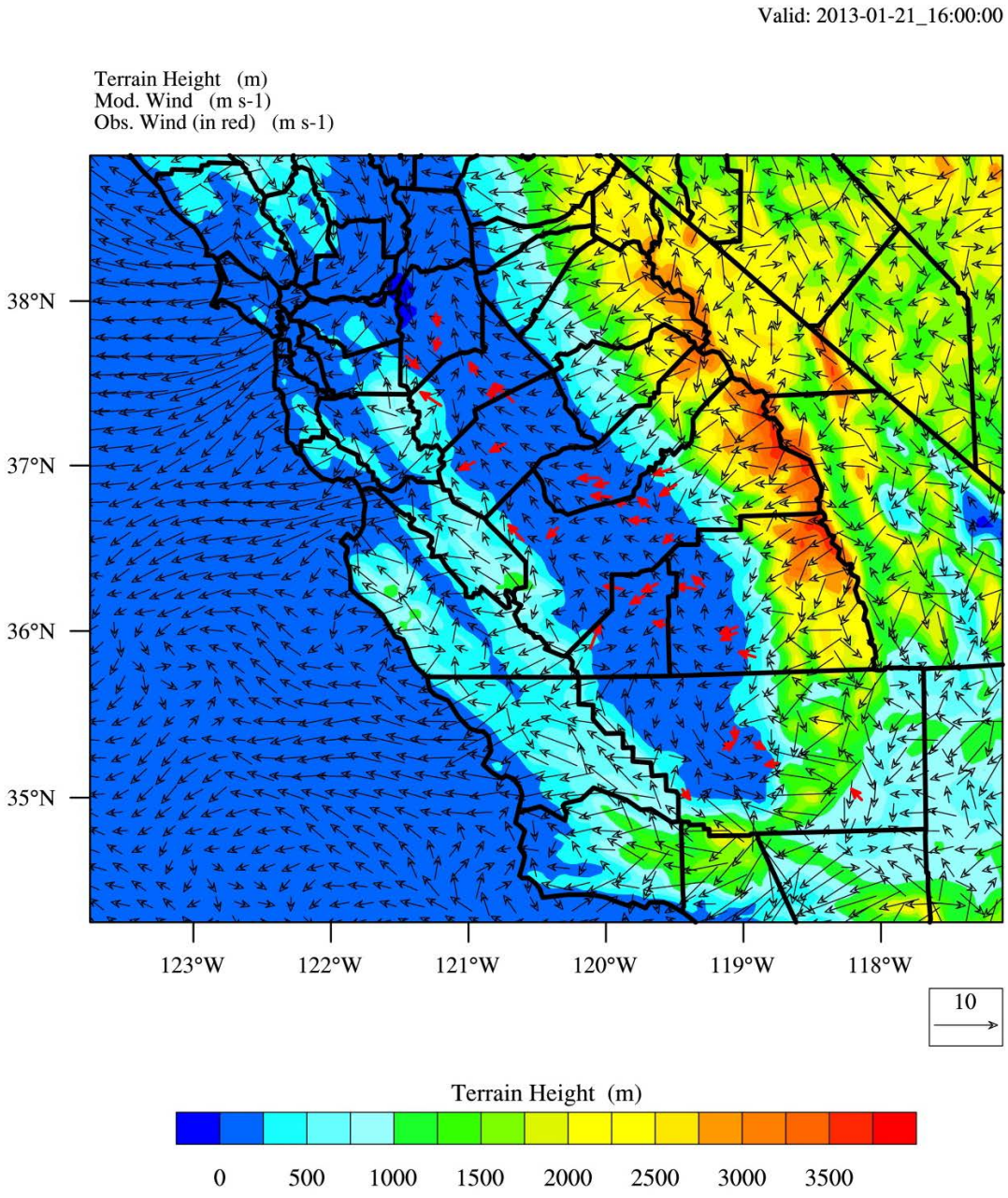

Figure 9. Surface wind field at 08:00 PST January 21, 2013.

4 EMISSIONS

The emissions inventory used in this modeling was based on the most recent inventory submitted to the U.S. EPA, with base year 2012 and projected to 2013 under growth and control conditions (http://www.arb.ca.gov/planning/sip/2012iv/2012iv.htm). For a detailed description of the emissions inventory, updates to the inventory, and how it was processed from the planning totals to a gridded inventory for modeling, see the Modeling Emissions Inventory Appendix.

4.1 EMISSIONS SUMMARIES

Table 13 summarizes 2013, 2021, and 2025 SJV annual anthropogenic emissions for the five $PM_{2.5}$ precursors. Emissions totals in Table 13 do not reflect reductions to residential wood burning (RWC) emissions applied to the modeling inventory to reflect actual no burn days in 2013 and projected no burn days in 2021/2025. Under the 2014 amendment to the RWC rule (two curtailment levels), 2021 emissions were reduced by 85% (level 1: no burning unless registered) and 90% (level 2: no burning for all) on projected no burn days. In addition, emissions totals also do not reflect the 20% reduction in commercial charbroiling applied to the modeling inventory per commitments made in the SJV 2012 24-hour $PM_{2.5}$ SIP. From 2013 to 2021, anthropogenic emissions in the SJV will drop approximately 38%, 8%, 7%, 2%, and 1% for NO_x, ROG, primary $PM_{2.5}$, SO_x, and NH_3, respectively. Among these five precursors, anthropogenic NO_x emissions show the largest relative reduction, dropping from 318.2 tons/day in 2013 to 196.1 tons/day in 2021. Anthropogenic ROG emissions will drop from 319.2 tons/day to 292.8 tons/day, reflecting an 8% reduction from 2013 to 2021. From 2021 to 2025, NO_x emissions will further drop by 24%, while emissions of other pollutants will stay nearly flat. Monthly biogenic ROG totals for 2013 in the SJV are shown in Figure 10 (note that the 2013 biogenic emissions were used for all model runs). Biogenic ROG emissions are highest in the summer at nearly 1800 tons/day in July when temperature, insolation, and leaf area are generally at their peak, and drop to near zero during winter months.

Table 13. SJV Annual Planning Emissions for 2013, 2021, and 2025

Category	NO_x	ROG	$PM_{2.5}$	SO_x	NH_3
2013 (tons/day)					
Stationary	38.6	85.1	8.9	7.2	13.8
Area	8.1	150.3	42.3	0.3	310.7
On-road Mobile	183.2	49.9	6.4	0.6	4.5
Other Mobile	88.3	33.9	5.8	0.2	0.0
Total	318.2	319.2	63.5	8.4	329.1
2021 (tons/day)					
Stationary	29.8	90.5	9.1	6.9	15.3
Area	8.1	152.4	41.9	0.3	306.4
On-road Mobile	88.0	23.3	3.3	0.6	4.2
Other Mobile	70.2	26.7	5.0	0.3	0.0
Total	196.1	292.8	59.3	8.2	325.9
2025 (tons/day)					
Stationary	29.2	94.3	9.3	7.1	16.3
Area	8.0	154.1	42.2	0.3	304.3
On-road Mobile	54.3	18.9	3.3	0.6	4.3
Other Mobile	58.3	24.1	4.3	0.3	0.0
Total	149.8	291.4	59.1	8.4	324.9

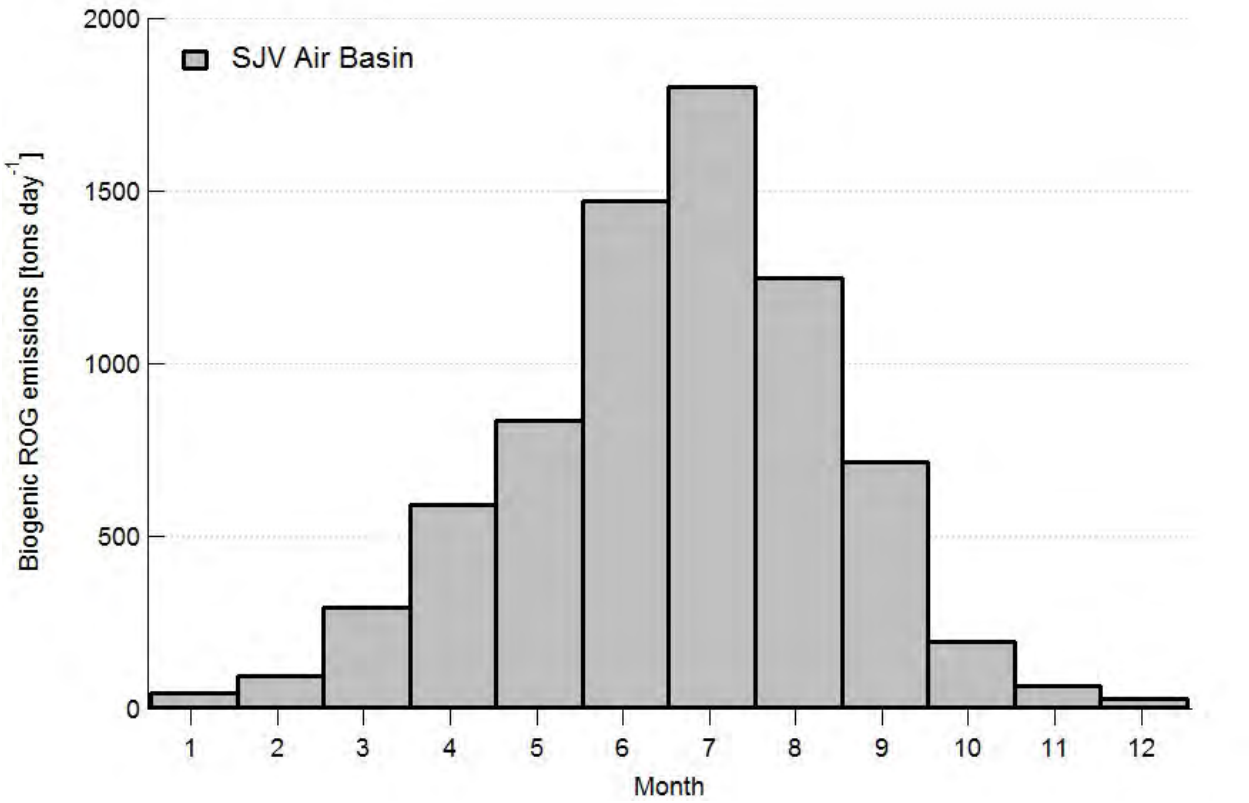

Figure 10. Monthly average biogenic ROG emissions for 2013.

5 $PM_{2.5}$ MODELING

5.1 CMAQ MODEL SETUP

Figure 11 shows the CMAQ modeling domains used in this work. The larger domain covering all of California has a horizontal grid resolution of 12 km with 107 x 97 lateral grid cells for each vertical layer and extends from the Pacific Ocean in the west to Eastern Nevada in the east and runs from the U.S.-Mexico border in the south to the California-Oregon border in the north. The smaller nested domain covering the SJV region has a finer scale 4 km grid resolution and includes 87 x 103 lateral grid cells. While the nested domain is smaller than that used for ozone modeling in the Valley (see the Photochemical Modeling Protocol), as long as the larger statewide 12 km domain is utilized to provide dynamic boundary condition inputs to the smaller 4 km domain, there is no appreciable difference in simulated $PM_{2.5}$ predictions between the smaller domain utilized for $PM_{2.5}$ modeling and the larger domain used for ozone modeling. Both the 12 km and 4 km domains are based on a Lambert Conformal Conic projection with reference longitude at – 120.5ºN and 60ºN, which is consistent with WRF domain settings. The 30 vertical layers from WRF were mapped onto 18 vertical layers for CMAQ, extending from the surface to 100 mb such that a majority of the vertical layers

fall within the planetary boundary layer (see the Photochemical Modeling Protocol for details).

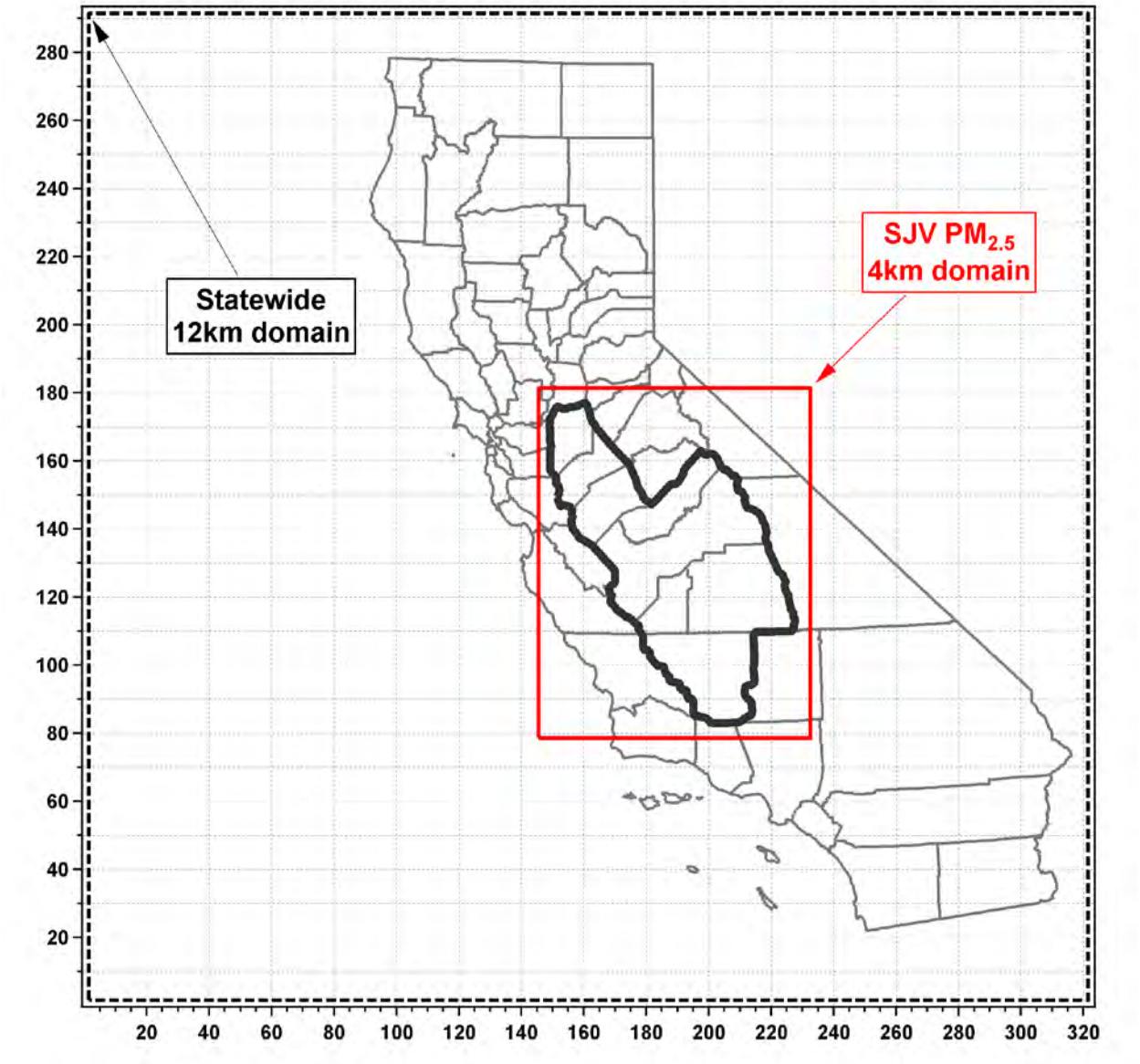

Figure 11. CMAQ modeling domains utilized in the modeling assessment.

The CMAQ model version 5.0.2 (http://www.airqualitymodeling.org/cmaqwiki/index.php?title=CMAQ_version_5.0.2_%28April_2014_release%29_Technical_Documentation) released by the U.S. EPA in May 2014 was used for all air quality model simulations. The SAPRC07 chemical mechanism and aerosol module aero6 were selected as the gas-phase and aerosol modules, respectively. Further details of the CMAQ configuration can be found in

Table14 and in the Photochemical Modeling Protocol. The same configuration was used for all simulations.

Annual simulations were conducted on a simultaneous month-by-month basis, rather than one single continuous simulation. For each month, the CMAQ simulations included a seven day spin-up period (i.e., the last seven days of the previous month) for the outer 12 km domain, where initial conditions were set to the default CMAQ initial conditions. These outer domain simulations were used to provide initial and lateral boundary conditions for the inner 4 km simulation, which utilized a three day spin-up period.

Chemical boundary conditions for the outer 12 km domain were extracted from the global chemical transport Model for Ozone and Related chemical Tracers, version 4 (MOZART-4; Emmons et al., 2014). The MOZART-4 model output for 2013 was obtained from the National Center for Atmospheric Research (NCAR; https://www2.acom.ucar.edu/gcm/mozart) using the simulations driven by meteorological fields from the NASA GMAO GEOS-5 model. The same MOZART derived BCs for the 12 km outer domain were used in all simulations.

Table 14. CMAQ configuration and settings.

Process	**Scheme**
Horizontal advection	Yamo (Yamartino scheme for mass-conserving advection)
Vertical advection	WRF-based scheme for mass-conserving advection
Horizontal diffusion	Multi-scale
Vertical diffusion	ACM2 (Asymmetric Convective Model version 2)
Gas-phase chemical mechanism	SAPRC-07 gas-phase mechanism version “B”
Chemical solver	EBI (Euler Backward Iterative solver)
Aerosol module	Aero6 (the sixth-generation CMAQ aerosol mechanism with extensions for sea salt emissions and thermodynamics; includes a new formulation for secondary organic aerosol yields)

Cloud module	ACM_AE6 (ACM cloud processor that uses the ACM methodology to compute convective mixing with heterogeneous chemistry for AERO6)
Photolysis rate	phot_inline (calculate photolysis rates in-line using simulated aerosols and ozone concentrations)

5.2 CMAQ MODEL EVALUATION

CMAQ model performance was evaluated for $PM_{2.5}$ mass, individual $PM_{2.5}$ chemical species, as well as a number of gas-phase species based on observations from an extensive network of monitors in the SJV.

Time series of observed and modeled $PM_{2.5}$ chemical species based on CSN measurements are shown in the supplemental material (Figures S37-S40 of the supplemental materials for Bakersfield, Fresno, Modesto, and Visalia, respectively). $PM_{2.5}$ species are measured every 3 or 6 days at these sites. Generally, observed $PM_{2.5}$ concentrations are higher in winter months and are much lower in summer months. During winter months, $PM_{2.5}$ in the SJV is dominated by ammonium nitrate and directly emitted OC. The CMAQ model was able to reasonably reproduce these key characteristics of $PM_{2.5}$ pollution in the SJV, including successfully capturing many elevated wintertime nitrate events, which is key for accurately simulating both peak wintertime $PM_{2.5}$ as well as annual average $PM_{2.5}$ in the SJV.

Tables 15-18 summarize the key model performance metrics for major $PM_{2.5}$ chemical species at the four CSN sites. Model performance was evaluated quarterly as well as on an annual basis. Average observations, average modeled values, mean bias, mean error, mean fractional bias (MFB), and mean fractional error (MFE) are given for individual $PM_{2.5}$ species at these four sites. Detailed definitions for these metrics can be found in the Photochemical Modeling Protocol Appendix. In general, model performance was consistent across different quarters and at different monitors. Mean bias of the simulated annual average $PM_{2.5}$ was within +/-1 $\mu g/m^3$ at all the CSN sites except Bakersfield, which showed an annual mean bias of -2.5 $\mu g/m^3$. The larger negative bias at Bakersfield was the result of a slight over prediction during winter months, which was offset by a larger under prediction during summer months (likely due to uncertainty in the unspecified $PM_{2.5}$ category – not shown). This is consistent with the other sites, which also generally showed over predictions in the first and fourth quarters, and under predictions in the second and third quarters. The two primary components of $PM_{2.5}$ in

the SJV, nitrate and OC, exhibited somewhat different quarterly biases, with nitrate closely following total $PM_{2.5}$ and OC being under predicted during most quarters and at most sites.

A graphical representation of the annual MFB and MFE values in Tables 15-18 is shown in Figure 12 for each CSN site, along with suggested model performance goals and criteria (green and red lines, respectively) from Boylan and Russell (2006). According to Boylan and Russell (2006), model performance goals are defined as the level of accuracy that is considered to be close to the best a model can achieve while model performance criteria are defined as the level of accuracy that is considered to be acceptable for modeling applications. Based on these metrics, the current CMAQ modelling system met the model performance criteria and in many instances exceeded model performance goals.

Table 15. Quarterly and annual $PM_{2.5}$ model performance based on CSN measurement at Fresno – Garland.

Quarter	Species	# of Obs.	Avg. Obs. (µg/m^3)	Avg. Mod. (µg/m^3)	Mean bias (µg/m^3)	Mean error (µg/m^3)	MFB	MFE
1	$PM_{2.5}$	30	21.1	22.7	1.6	6.5	0.18	0.36
1	Ammonium	30	1.7	2.8	1.1	1.3	0.56	0.67
1	Nitrate	30	5.8	9.4	3.6	4.1	0.46	0.60
1	Sulfate	30	0.8	1.0	0.2	0.3	0.28	0.41
1	OC	28	4.9	4.1	-0.8	1.6	-0.03	0.34
1	EC	28	1.2	1.4	0.1	0.5	0.27	0.45
2	$PM_{2.5}$	30	7.8	6.4	-1.4	2.4	-0.23	0.37
2	Ammonium	30	0.4	0.3	-0.2	0.2	-0.50	0.62
2	Nitrate	30	0.9	0.6	-0.2	0.4	-0.53	0.72
2	Sulfate	30	1.1	0.7	-0.4	0.4	-0.37	0.46
2	OC	29	1.8	1.9	0.2	0.5	0.02	0.25
2	EC	29	0.3	0.6	0.3	0.3	0.61	0.62
3	$PM_{2.5}$	30	9.4	6.4	-3.0	3.7	-0.35	0.44
3	Ammonium	30	0.4	0.2	-0.2	0.2	-0.61	0.77
3	Nitrate	30	0.7	0.3	-0.4	0.5	-1.18	1.25
3	Sulfate	30	0.9	0.8	-0.2	0.3	-0.10	0.33
3	OC	30	2.4	1.8	-0.6	0.9	-0.21	0.34
3	EC	30	0.5	0.6	0.1	0.2	0.23	0.32
4	$PM_{2.5}$	29	25.8	25.1	-0.7	8.5	0.07	0.36
4	Ammonium	29	2.9	2.7	-0.2	1.4	0.06	0.52
4	Nitrate	28	9.0	9.4	0.4	3.6	0.02	0.43
4	Sulfate	28	1.0	1.0	-0.1	0.3	-0.03	0.26
4	OC	29	6.0	4.6	-1.4	2.1	-0.13	0.38
4	EC	29	1.6	1.6	0.0	0.5	0.14	0.41
Annual	$PM_{2.5}$	119	16.0	15.1	-0.9	5.2	-0.08	0.38
Annual	Ammonium	119	1.3	1.5	0.2	0.8	-0.12	0.65
Annual	Nitrate	118	4.0	4.9	0.9	2.1	-0.32	0.75
Annual	Sulfate	118	1.0	0.9	-0.1	0.3	-0.06	0.36
Annual	OC	116	3.8	3.1	-0.7	1.3	-0.09	0.33
Annual	EC	116	0.9	1.0	0.1	0.4	0.31	0.45

Table 16. Quarterly and annual $PM_{2.5}$ model performance based on CSN measurement at Visalia.

Quarter	Species	# of Obs.	Avg. Obs. ($\mu g/m^3$)	Avg. Mod. ($\mu g/m^3$)	Mean bias ($\mu g/m^3$)	Mean error ($\mu g/m^3$)	MFB	MFE
1	$PM_{2.5}$	15	20.5	22.8	2.4	4.9	0.17	0.29
1	Ammonium	15	2.0	3.1	1.2	1.4	0.50	0.65
1	Nitrate	15	6.7	10.6	4.0	4.4	0.45	0.55
1	Sulfate	15	1.0	0.8	-0.3	0.4	-0.20	0.36
1	OC	15	4.6	3.5	-1.1	1.3	-0.18	0.27
1	EC	15	0.9	1.1	0.3	0.3	0.37	0.40
2	$PM_{2.5}$	15	9.8	8.0	-1.8	2.6	-0.30	0.37
2	Ammonium	15	0.7	0.5	-0.2	0.2	-0.33	0.45
2	Nitrate	10	2.2	1.9	-0.2	0.8	-0.21	0.48
2	Sulfate	15	1.6	0.7	-0.9	0.9	-0.77	0.77
2	OC	17	2.6	1.8	-0.8	0.8	-0.46	0.46
2	EC	17	0.4	0.6	0.2	0.2	0.36	0.37
3	$PM_{2.5}$	17	10.5	7.4	-3.2	3.8	-0.31	0.41
3	Ammonium	17	0.6	0.3	-0.2	0.3	-0.47	0.63
3	Nitrate	17	1.6	0.7	-0.9	1.0	-0.91	0.95
3	Sulfate	17	1.4	0.8	-0.5	0.5	-0.41	0.43
3	OC	17	2.9	1.8	-1.1	1.3	-0.49	0.53
3	EC	17	0.5	0.6	0.2	0.2	0.26	0.30
4	$PM_{2.5}$	16	33.1	33.1	-0.1	13.0	0.11	0.38
4	Ammonium	16	4.3	4.0	-0.3	2.1	0.11	0.48
4	Nitrate	16	14.3	13.9	-0.4	6.9	0.14	0.48
4	Sulfate	16	1.4	1.0	-0.4	0.6	-0.28	0.41
4	OC	16	5.8	4.4	-1.4	1.8	-0.27	0.36
4	EC	16	1.3	1.5	0.3	0.5	0.17	0.32
Annual	$PM_{2.5}$	63	18.5	17.7	-0.7	6.1	-0.09	0.37
Annual	Ammonium	63	1.9	2.0	0.1	1.0	-0.06	0.55
Annual	Nitrate	58	6.5	7.1	0.6	3.5	-0.15	0.64
Annual	Sulfate	63	1.4	0.8	-0.5	0.6	-0.41	0.49
Annual	OC	65	3.9	2.8	-1.1	1.3	-0.36	0.41
Annual	EC	65	0.7	1.0	0.2	0.3	0.29	0.35

Table 17. Quarterly and annual $PM_{2.5}$ model performance based on CSN measurement at Bakersfield.

Quarter	Species	# of Obs.	Avg. Obs. ($\mu g/m^3$)	Avg. Mod. ($\mu g/m^3$)	Mean bias ($\mu g/m^3$)	Mean error ($\mu g/m^3$)	MFB	MFE
1	$PM_{2.5}$	21	20.5	23.2	2.7	8.7	0.34	0.49
1	Ammonium	21	2.2	2.8	0.7	1.6	0.57	0.74
1	Nitrate	19	7.9	9.4	1.5	3.9	0.28	0.47
1	Sulfate	21	0.9	0.9	0.1	0.4	0.26	0.52
1	OC	22	3.9	4.6	0.7	1.3	0.27	0.36
1	EC	22	1.1	1.5	0.4	0.4	0.36	0.41
2	$PM_{2.5}$	25	11.0	7.8	-3.3	4.0	-0.36	0.45
2	Ammonium	25	0.6	0.4	-0.2	0.3	-0.52	0.59
2	Nitrate	25	1.1	0.9	-0.2	0.6	-0.46	0.74
2	Sulfate	25	1.4	0.8	-0.6	0.6	-0.49	0.54
2	OC	22	2.2	2.4	0.2	0.5	0.09	0.24
2	EC	22	0.4	0.7	0.4	0.4	0.75	0.75
3	$PM_{2.5}$	19	15.5	8.2	-7.3	8.0	-0.55	0.60
3	Ammonium	19	0.5	0.3	-0.2	0.3	-0.61	0.68
3	Nitrate	19	0.8	0.6	-0.2	0.6	-0.69	0.93
3	Sulfate	19	1.3	0.9	-0.5	0.5	-0.38	0.38
3	OC	17	2.6	2.5	0.0	0.9	-0.05	0.33
3	EC	17	0.5	0.8	0.4	0.4	0.58	0.58
4	$PM_{2.5}$	0	NA	NA	NA	NA	NA	NA
4	Ammonium	0	NA	NA	NA	NA	NA	NA
4	Nitrate	0	NA	NA	NA	NA	NA	NA
4	Sulfate	0	NA	NA	NA	NA	NA	NA
4	OC	0	NA	NA	NA	NA	NA	NA
4	EC	0	NA	NA	NA	NA	NA	NA
Annual	$PM_{2.5}$	65	15.4	12.9	-2.5	6.7	-0.19	0.50
Annual	Ammonium	65	1.1	1.2	0.1	0.7	-0.19	0.67
Annual	Nitrate	63	3.0	3.4	0.3	1.6	-0.30	0.71
Annual	Sulfate	65	1.2	0.9	-0.3	0.5	-0.22	0.49
Annual	OC	61	2.9	3.2	0.3	0.9	0.11	0.31
Annual	EC	61	0.7	1.0	0.4	0.4	0.56	0.58

Table 18. Quarterly and annual $PM_{2.5}$ model performance based on CSN measurement at Modesto.

Quarter	Species	# of Obs.	Avg. Obs. ($\mu g/m^3$)	Avg. Mod. ($\mu g/m^3$)	Mean bias ($\mu g/m^3$)	Mean error ($\mu g/m^3$)	MFB	MFE
1	$PM_{2.5}$	15	17.3	18.4	1.1	4.2	0.18	0.34
1	Ammonium	15	1.0	2.2	1.2	1.2	0.70	0.73
1	Nitrate	15	5.0	7.1	2.1	2.3	0.27	0.42
1	Sulfate	15	0.8	1.1	0.3	0.4	0.31	0.41
1	OC	14	5.5	3.9	-1.6	2.2	-0.09	0.37
1	EC	14	1.2	1.2	0.0	0.4	0.21	0.42
2	$PM_{2.5}$	15	6.5	5.4	-1.1	2.2	-0.18	0.36
2	Ammonium	15	0.3	0.4	0.1	0.1	0.27	0.48
2	Nitrate	13	0.7	0.6	-0.1	0.4	-0.35	0.63
2	Sulfate	15	1.0	0.8	-0.1	0.3	-0.10	0.33
2	OC	15	1.6	1.3	-0.3	0.4	-0.20	0.27
2	EC	15	0.3	0.4	0.1	0.1	0.38	0.38
3	$PM_{2.5}$	14	7.9	6.0	-1.8	3.2	-0.13	0.37
3	Ammonium	15	0.3	0.2	0.0	0.1	0.22	0.50
3	Nitrate	15	0.7	0.2	-0.5	0.5	-1.12	1.12
3	Sulfate	15	1.1	1.0	-0.1	0.3	-0.04	0.28
3	OC	15	2.6	1.7	-1.0	1.1	-0.29	0.36
3	EC	15	0.4	0.5	0.1	0.2	0.18	0.34
4	$PM_{2.5}$	17	25.6	30.3	4.7	6.5	0.25	0.31
4	Ammonium	17	2.4	3.3	0.9	1.0	0.50	0.53
4	Nitrate	17	8.2	11.2	3.0	3.5	0.42	0.48
4	Sulfate	17	1.1	1.2	0.1	0.3	0.12	0.25
4	OC	17	6.2	4.7	-1.6	1.8	-0.20	0.29
4	EC	17	1.6	1.5	-0.1	0.3	0.02	0.24
Annual	$PM_{2.5}$	61	14.8	15.7	0.9	4.1	0.04	0.34
Annual	Ammonium	62	1.0	1.6	0.6	0.6	0.43	0.56
Annual	Nitrate	60	3.9	5.1	1.2	1.8	-0.17	0.66
Annual	Sulfate	62	1.0	1.0	0.0	0.3	0.07	0.32
Annual	OC	61	4.0	2.9	-1.1	1.4	-0.19	0.32
Annual	EC	61	0.9	0.9	0.0	0.2	0.19	0.34

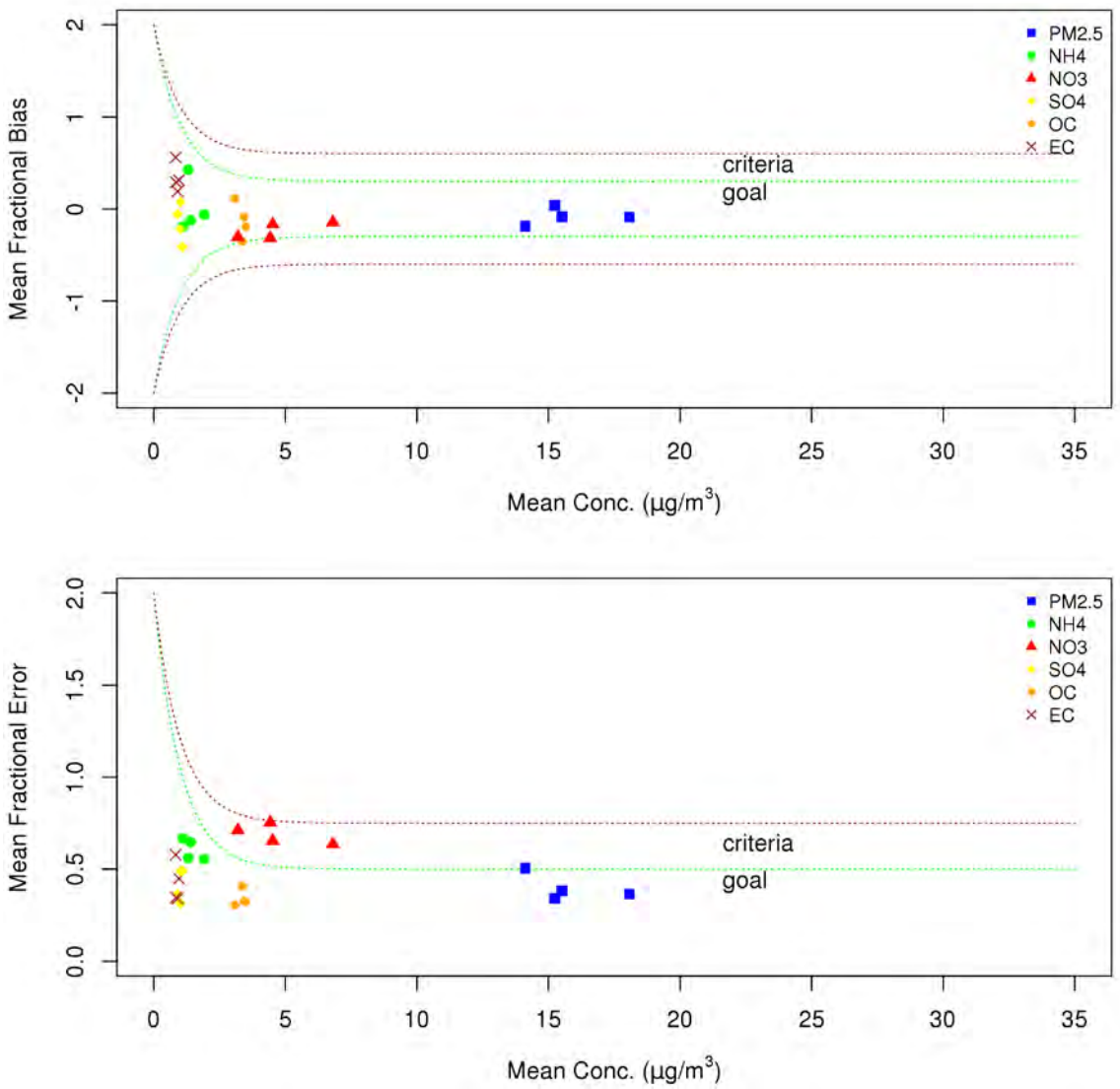

Figure 12. Bugle plot of annual $PM_{2.5}$ model performance in terms of MFB and MFE at four CSN sites in the SJV (i.e., Bakersfield, Fresno, Modesto, and Visalia).

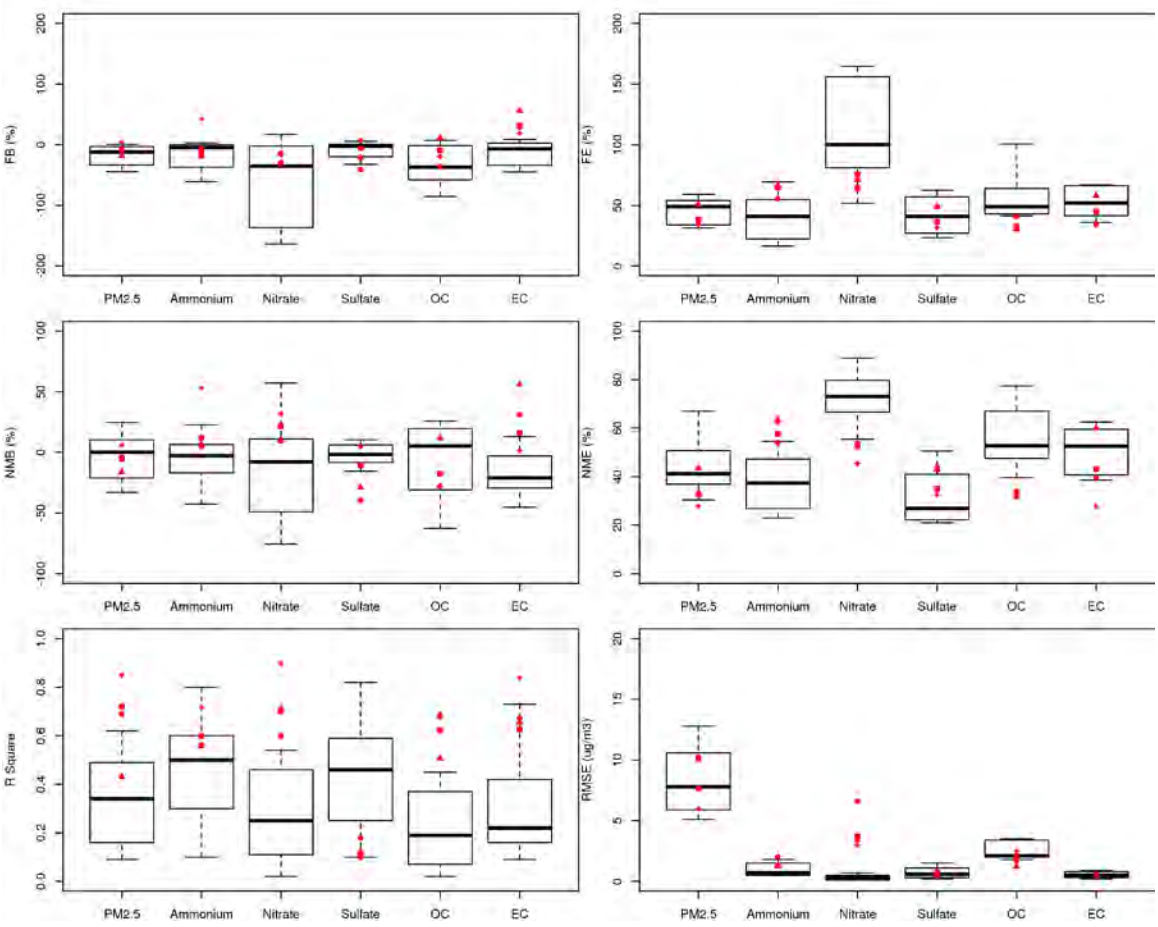

Figure 13. Comparison of annual $PM_{2.5}$ model performance to other modeling studies in Simon et al. (2012). Red symbols represent performance at the four CSN sites in the SJV.

In addition to evaluating the standard statistical performance metrics, it is also informative to put these performance statistics in the context of other studies published in the scientific literature. Figure 13 compares key performance statistics from the modeling platform presented in this document to the range of published performance statics from 2006 to 2012 and summarized in Simon et al. (2012). In Figure 13, the black centerline shows the median value (i.e., median model performance) from those studies, the boxes outline the 25th and 75th percentile values, and the whiskers show the 10th and 90th percentile values. The model performance for each of the four CSN sites in the SJV is shown in red. Performance metrics including MFB, MFE, normalized mean bias (NMB), normalized mean error (NME), R squared, and root mean square error (RMSE) are compared. Definitions of the statistics can be found in the Photochemical

Modeling Protocol or Simon et al. (2012). Model performance metrics in the SJV are typically equal to or better than the corresponding statistics from other studies. One exception is the higher RMSE for nitrate in the SJV, which is simply a reflection of the higher nitrate concentrations in the SJV compared to other regions. In fact, MFB, MFE, NME, and R squared for nitrate in the SJV is consistently better than the majority of the model studies summarized in Simon et al. (2012).

Since CSN monitors do not measure $PM_{2.5}$ on a daily basis, it is also advantageous to compare modeled 24-hour average $PM_{2.5}$ concentrations to observations from continuous $PM_{2.5}$ samplers, which typically report 24-hour average $PM_{2.5}$ concentrations on a daily basis. Figures S-41 – S-52 show the time series of modeled and observed 24-hour average $PM_{2.5}$ concentrations at these sites located throughout the SJV. Distinct seasonal variations in $PM_{2.5}$ concentrations are observed throughout the Valley, and are also reasonably captured by the model. Of particular importance, the modeling system was able to capture the elevated $PM_{2.5}$ events during the winter months and the lower $PM_{2.5}$ common in the summer months. In addition, Table 19 summarizes the corresponding model performance statistics at these sites. All the sites met or exceeded the $PM_{2.5}$ model performance criteria defined in Boyland and Russell (2006).

In addition to the $PM_{2.5}$ performance evaluation, gas phase model performance was also evaluated for NO_2 and ozone, which are key products of the photochemical processes in the atmosphere. Scatter plots of observed and modeled one-hour NO_2 mixing ratios at 16 sites are shown in Figures S-53 to S-68 in the supplemental materials. On average, there is good agreement between observed and modeled NO_2 mixing ratios. The slope of the regression line between the observed and modeled hourly NO_2 mixing ratios is within ±30% of the 1:1 line at most of the sites. Scatter plots of observed and modeled hourly O_3 mixing ratios at 25 sites are shown in Figures S-69 to S-93 in the supplemental materials. Modeled O_3 mixing ratios showed excellent agreement with observed mixing ratios and the slopes of the regression lines between observed and modeled O_3 are all within ±15% of the 1:1 line.

Table 19. Model performance for 24-hour $PM_{2.5}$ concentrations measured from continuous $PM_{2.5}$ monitors

Sites	# of Obs.	Avg. Obs. ($\mu g/m^3$)	Avg. Mod. ($\mu g/m^3$)	Mean bias ($\mu g/m^3$)	Mean error ($\mu g/m^3$)	MFB	MFE
Fresno-Drummond Street	246	14.8	13.5	-1.2	4.4	-0.16	0.36
Clovis	300	16.4	14.5	-1.9	5.6	-0.22	0.42
Bakersfield-California Avenue	267	20.2	16.2	-4.0	7.0	-0.29	0.44
Tranquility	301	8.5	10.1	1.5	5.0	-0.11	0.52
Fresno-Garland	312	19.3	15.7	-3.6	6.1	-0.33	0.44
Stockton	302	18.0	13.1	-4.9	7.3	-0.55	0.63
Merced	326	13.2	13.3	0.1	5.3	-0.14	0.44
Hanford	329	18.0	15.8	-2.2	5.9	-0.27	0.46
Madera	323	18.0	13.1	-4.9	7.7	-0.51	0.64
Manteca	325	11.7	13.4	1.7	6.2	-0.10	0.55
Visalia	309	18.6	19.1	0.5	6.9	-0.09	0.41
Modesto	315	14.4	14.5	0.1	5.0	-0.05	0.42
Turlock	316	14.8	14.6	-0.2	4.5	-0.05	0.41

5.3 FUTURE YEAR DESIGN VALUES

Future DVs for each site are given in Table 20. Correspondingly, Relative Response Factors (RRFs) and the base and the projected future year annual $PM_{2.5}$ composition at each monitor are given in Tables 21-23 (Note that the annual RRFs and composition are for reference only and that in the actual future year DV calculation, separate calculations were performed for each quarter and not on the annual average). The Bakersfield-Planz site has the highest projected future year DV at 14.8 $\mu g/m^3$, which is well above the 2012 annual $PM_{2.5}$ standard of 12 $\mu g/m^3$, but below the 2006 annual $PM_{2.5}$ standard of 15 $\mu g/m^3$. From the base to future year, there are significant reductions projected for ammonium nitrate and EC, modest reduction in OM, almost no change in sulfate, and a slight increase in crustal material (i.e., other primary $PM_{2.5}$ such as fugitive dust emissions).

Table 20. Projected future year $PM_{2.5}$ DVs at each monitor

Site AQS ID	Name	Base DV ($\mu g/m^3$)	Future 2021 DV ($\mu g/m^3$)
60290016	Bakersfield - Planz	17.3	14.8
60392010	Madera	16.9	14.4
60311004	Hanford	16.5	13.4
60310004	Corcoran	16.3	14.4
61072002	Visalia	16.2	13.7
60195001	Clovis	16.1	14.1
60290014	Bakersfield - California	16.0	13.6
60190011	Fresno-Garland	15.0	12.9
60990006	Turlock	14.9	12.8
60195025	Fresno - Hamilton & Winery (H &W)	14.2	12.2
60771002	Stockton	13.1	11.7
60470003	Merced - S Coffee	13.1	11.2
60990005	Modesto	13.0	11.2
60472510	Merced - Main Street	11.0	9.7
60772010	Manteca	10.1	8.8
60192009	Tranquility	7.7	6.5

Table 21. Annual RRFs for $PM_{2.5}$ components

Site	RRF for $PM_{2.5}$	RRF for NH_4	RRF for NO_3	RRF for SO_4	RRF for OM	RRF for EC	RRF for Crustal
Bakersfield - Planz	0.85	0.68	0.69	0.97	0.90	0.51	1.02
Madera	0.85	0.74	0.70	1.00	0.93	0.69	1.01
Hanford	0.81	0.71	0.67	1.02	0.94	0.70	0.92
Corcoran	0.88	0.70	0.68	1.04	0.97	0.76	0.95
Visalia	0.85	0.69	0.70	1.01	0.89	0.63	1.02
Clovis	0.87	0.70	0.70	1.00	0.91	0.66	1.07
Bakersfield - California	0.85	0.67	0.67	0.97	0.90	0.52	1.03
Fresno-Garland	0.86	0.72	0.72	0.99	0.89	0.59	1.05
Turlock	0.86	0.77	0.75	1.00	0.92	0.67	1.05

Fresno - H&W	0.86	0.74	0.74	0.99	0.89	0.58	1.05
Stockton	0.89	0.80	0.76	1.02	0.95	0.70	1.05
Merced - S Coffee	0.85	0.73	0.71	1.01	0.93	0.68	1.04
Modesto	0.86	0.77	0.74	1.01	0.92	0.67	1.05
Merced - Main Street	0.88	0.72	0.71	1.01	0.93	0.69	1.04
Manteca	0.87	0.81	0.77	1.02	0.92	0.68	1.04
Tranquility	0.84	0.69	0.63	1.00	0.96	0.73	1.02

Table 22. Base year $PM_{2.5}$ compositions*

Name	Base $PM_{2.5}$ ($\mu g/m^3$)	Base NH_4 ($\mu g/m^3$)	Base NO_3 ($\mu g/m^3$)	Base SO_4 ($\mu g/m^3$)	Base OM ($\mu g/m^3$)	Base EC ($\mu g/m^3$)	Base Crustal ($\mu g/m^3$)
Bakersfield - Planz	17.3	1.1	2.6	1.7	7.0	1.0	2.5
Madera	16.9	1.4	4.1	1.5	6.4	0.9	1.2
Hanford	16.5	1.9	5.5	1.5	4.1	0.7	1.2
Corcoran	16.3	1.2	2.9	1.5	7.4	0.7	1.2
Visalia	16.2	1.2	3.0	1.4	7.3	0.7	1.2
Clovis	16.1	0.9	2.1	1.3	8.7	0.9	1.1
Bakersfield – California	16.0	1.1	2.6	1.5	6.4	0.9	2.2
Fresno - Garland	15.0	0.9	2.2	1.1	8.0	0.8	0.9
Turlock	14.9	1.4	3.9	1.2	5.4	0.8	0.9
Fresno - H&W	14.2	0.8	2.1	1.0	7.6	0.8	0.8
Stockton	13.1	1.1	3.3	1.1	4.9	0.7	0.8
Merced - S Coffee	13.1	1.1	3.3	1.1	4.8	0.7	0.8
Modesto	13.0	1.2	3.4	1.1	4.7	0.7	0.8
Merced – Main Street	11.0	0.7	1.7	0.9	5.6	0.6	0.6
Manteca	10.1	0.9	2.6	0.8	3.6	0.5	0.6
Tranquility	7.7	0.6	1.9	0.6	2.8	0.4	0.5

*: Base year $PM_{2.5}$ compositions were based on CSN speciation measurement adjusted by the EPA SANDWICH method. Particle-bound water and blank mass are not shown.

Table 23. Projected future year $PM_{2.5}$ compositions

Name	Future $PM_{2.5}$ ($\mu g/m^3$)	Future NH_4 ($\mu g/m^3$)	Future NO_3 ($\mu g/m^3$)	Future SO_4 ($\mu g/m^3$)	Future OM ($\mu g/m^3$)	Future EC ($\mu g/m^3$)	Future Crustal ($\mu g/m^3$)	Future Water ($\mu g/m^3$)	Blank ($\mu g/m^3$)
Bakersfield - Planz	14.8	0.8	1.8	1.6	6.2	0.5	2.6	0.7	0.5
Madera	14.4	1.1	2.8	1.5	5.9	0.6	1.2	0.8	0.5
Hanford	13.4	1.4	3.6	1.5	3.8	0.5	1.1	0.9	0.5
Corcoran	14.4	0.8	2.0	1.5	7.1	0.5	1.1	0.7	0.5
Visalia	13.7	0.8	2.1	1.5	6.5	0.4	1.2	0.7	0.5
Clovis	14.1	0.6	1.5	1.3	7.9	0.6	1.1	0.6	0.5
Bakersfield - California	13.6	0.7	1.7	1.4	5.8	0.5	2.3	0.6	0.5
Fresno - Garland	12.9	0.6	1.6	1.1	7.1	0.5	0.9	0.5	0.5
Turlock	12.8	1.0	3.0	1.2	4.9	0.5	0.9	0.7	0.5
Fresno - H&W	12.2	0.6	1.5	1.0	6.7	0.4	0.9	0.5	0.5
Stockton	11.7	0.9	2.5	1.2	4.6	0.5	0.9	0.6	0.5
Merced - S Coffee	11.2	0.8	2.3	1.1	4.5	0.5	0.8	0.6	0.5
Modesto	11.2	0.9	2.5	1.1	4.3	0.4	0.8	0.6	0.5
Merced – Main Street	9.7	0.5	1.2	0.9	5.2	0.4	0.6	0.4	0.5
Manteca	8.8	0.7	2.0	0.8	3.3	0.3	0.6	0.5	0.5
Tranquility	6.5	0.4	1.2	0.6	2.7	0.3	0.5	0.3	0.5

5.4 PRECURSOR SENSITIVITY ANALYSIS

To evaluate the impact of reducing emissions of different $PM_{2.5}$ precursors on the projected future $PM_{2.5}$ DVs, a series of model sensitivity simulations were conducted, where emissions of the precursor species were scaled by ±15% from the future year baseline emissions. Comparing the difference in $PM_{2.5}$ DVs from the ±15% perturbations essentially produces the sensitivity of the future year $PM_{2.5}$ DVs to a 30% change in future year baseline precursor emissions. Specifically, the effect of reductions in the following $PM_{2.5}$ precursors was investigated: direct $PM_{2.5}$ (or primary $PM_{2.5}$), nitrogen oxides (NO_x), sulfur oxides (SO_x), ammonia, and volatile organic compounds (VOCs). For each precursor, only anthropogenic emissions in California were perturbed. Natural emissions and emissions outside of California (e.g., Mexico) were not perturbed.

Tables 24-28 show the change in $PM_{2.5}$ DV at each site from the 30% perturbation of controllable NO_x, direct $PM_{2.5}$, NH_3, VOCs, and SO_x emissions, respectively. The DV change is calculated as the difference in the projected DV from the +15% perturbation minus the projected DV from the -15% perturbation case. In addition, the differences are calculated for both the aggregate $PM_{2.5}$ DV as well as the component specific portion of the DV that is directly linked to each precursor. The $PM_{2.5}$ component(s) corresponding to each emissions precursor are as follows: NO_x is linked to ammonium nitrate; direct $PM_{2.5}$ is linked to primary sulfate, organic matter (OM), EC, and other primary $PM_{2.5}$ components; NH_3 is linked to ammonium nitrate plus the ammonium associated with ammonium sulfate (i.e., all ammonium); VOCs are linked to secondary organic aerosol (SOA); and SO_x is linked to the sulfate component of ammonium sulfate.

A threshold of 0.2 $\mu g/m^3$ for the annual $PM_{2.5}$ DV was used to determine the significance of a precursor to $PM_{2.5}$ formation (e.g., if a 30% change in precursor emissions leads to a change in component DV less than or equal to 0.2 $\mu g/m^3$ then the precursor is deemed not significant). For NO_x (Table 24), a 30% change in emissions resulted in a response of the component DV that is greater than 0.2 $\mu g/m^3$ at all sites, so NO_x is deemed a significant precursor. The same is true for direct $PM_{2.5}$ (Table 25), where sites show a response between 0.8 $\mu g/m^3$ at Tranquility and 2.8 $\mu g/m^3$ at Bakersfield-Planz and Clovis. For the other major precursors, ammonia, VOC, and SO_x (Tables 26-28), all are shown to be not significant based on the 0.2 $\mu g/m^3$ threshold and a 30% change in precursor emissions.

Table 24. Difference in $PM_{2.5}$ and ammonium nitrate DVs from a 30% perturbation in anthropogenic NO_x emissions.

Site	Difference in $PM_{2.5}$ DVs ($\mu g/m^3$)	Difference in component (i.e., ammonium nitrate, $\mu g/m^3$)
Bakersfield - Planz	0.8	0.7
Madera	1.1	1.0
Hanford	1.5	1.3
Corcoran	0.9	0.8
Visalia	0.9	0.8
Clovis	0.7	0.5
Bakersfield - California	0.8	0.7
Fresno-Garland	0.6	0.5
Turlock	1.1	1.0
Fresno - Hamilton & Winery	0.6	0.5
Stockton	0.9	0.8
Merced - S Coffee	0.9	0.8
Modesto	0.9	0.8
Merced - Main Street	0.5	0.4
Manteca	0.7	0.6
Tranquility	0.5	0.4

Table 25. Difference in $PM_{2.5}$ and components (including sulfate, OM, EC, and other) DVs from a 30% perturbation in anthropogenic $PM_{2.5}$ emissions

Site	Difference in $PM_{2.5}$ DVs ($\mu g/m^3$)	Difference in component (including sulfate, OM, EC, and other $PM_{2.5}$, $\mu g/m^3$)
Bakersfield - Planz	2.9	2.8
Madera	2.3	2.1
Hanford	1.6	1.5
Corcoran	2.4	2.3
Visalia	2.4	2.3
Clovis	2.9	2.8
Bakersfield - California	2.7	2.6
Fresno-Garland	2.7	2.6
Turlock	2.0	1.9
Fresno - Hamilton & Winery	2.6	2.5
Stockton	1.9	1.8
Merced - S Coffee	1.7	1.6
Modesto	1.8	1.7
Merced - Main Street	1.8	1.8
Manteca	1.3	1.2
Tranquility	0.9	0.8

Table 26. Difference in $PM_{2.5}$ and ammonium nitrate DVs from a 30% perturbation in ammonia emissions

Site	Difference in $PM_{2.5}$ DVs ($\mu g/m^3$)	Difference in component (i.e., ammonium nitrate, $\mu g/m^3$)
Bakersfield - Planz	0.1	0.1
Madera	0.2	0.2
Hanford	0.2	0.2
Corcoran	0.1	0.1
Visalia	0.1	0.1
Clovis	0.1	0.1
Bakersfield - California	0.1	0.1
Fresno-Garland	0.1	0.1
Turlock	0.2	0.1
Fresno - Hamilton & Winery	0.1	0.1
Stockton	0.1	0.1
Merced - S Coffee	0.1	0.1
Modesto	0.1	0.1
Merced - Main Street	0.1	0.1
Manteca	0.1	0.1
Tranquility	0.1	0.1

Table 27. Difference in $PM_{2.5}$ and SOA DVs from a 30% perturbation in VOCs emissions

Site	Difference in $PM_{2.5}$ DVs ($\mu g/m^3$)	Difference in component (i.e., SOA, $\mu g/m^3$)
Bakersfield - Planz	0.0	0.1
Madera	0.0	0.1
Hanford	-0.1	0.1
Corcoran	0.0	0.1
Visalia	0.0	0.1
Clovis	0.1	0.1
Bakersfield - California	0.0	0.1
Fresno-Garland	0.1	0.1
Turlock	0.0	0.0
Fresno - Hamilton & Winery	0.0	0.1
Stockton	0.0	0.0
Merced - S Coffee	0.0	0.1
Modesto	0.0	0.0
Merced - Main Street	0.0	0.1
Manteca	0.0	0.0
Tranquility	0.0	0.0

Table 28. Difference in $PM_{2.5}$ and sulfate DVs from a 30% perturbation in SO_x emissions

Site	Difference in $PM_{2.5}$ DVs ($\mu g/m^3$)	Difference in component (i.e., sulfate only, $\mu g/m^3$)
Bakersfield - Planz	0.1	0.1
Madera	0.2	0.1
Hanford	0.2	0.1
Corcoran	0.1	0.1
Visalia	0.2	0.1
Clovis	0.1	0.1
Bakersfield - California	0.1	0.1
Fresno-Garland	0.1	0.1
Turlock	0.2	0.1
Fresno - Hamilton & Winery	0.1	0.1
Stockton	0.2	0.1
Merced - S Coffee	0.2	0.1
Modesto	0.2	0.1
Merced - Main Street	0.1	0.1
Manteca	0.2	0.1
Tranquility	0.1	0.0

5.5 DISCUSSION ON PRECURSOR SENSITIVITY

In this section, we address three questions regarding precursor sensitivity:

1.) NO_x as the limiting precursor for ammonium nitrate vs. benefits of ammonia reductions on ammonium nitrate formation;
2.) On VOCs' indirect role in ammonium nitrate formation;
3.) Current status of secondary organic aerosol (SOA)

Ammonia's role in ammonium nitrate formation in the SJV

During the DISCOVER-AQ field campaign, aircraft measurements of $PM_{2.5}$ and its precursors were made in the planetary boundary layer over agricultural and urban areas within the SJV. Among the suite of measurements made, the measurements of total nitric acids (gas + particle phases, or g + p), gaseous ammonia, particulate ammonium, and sulfate allowed for an observation based evaluation of the precursor limitation for ammonium nitrate formation. The excess NH_3 in the atmosphere can be defined as the sum of gaseous NH_3 and particulate ammonium minus 2x particulate sulfate and total nitric acids (g + p) (Blanchard et al., 2000). While the calculation of excess NH_3 in Blanchard et al. (2000) also incorporated the impact from other ions, such as calcium, magnesium, potassium and chloride, those species should only have a minor effect on the analysis and so were not considered in order to maximize the data availability. If the value of excess NH_3 is greater than zero, this indicates that secondary particulate nitrate is in a NO_x-limited regime. Conversely, a value less than zero demonstrates an ammonia-limited regime.

Figure 14 shows the excess NH_3 in the bottom 1 km of the atmosphere, collected by NASA aircraft in the SJV on January 18 and 20, during which $PM_{2.5}$ concentrations in the SJV were elevated. Each data point of excess NH_3 was calculated based on 10 second observational data with no further averaging. For nearly all data points, excess NH_3 is clearly above zero, indicating that nitrate formation in the SJV is in a NO_x-limited regime, which is consistent with past observations (Lurmann et al., 2006; Markovic, 2014).

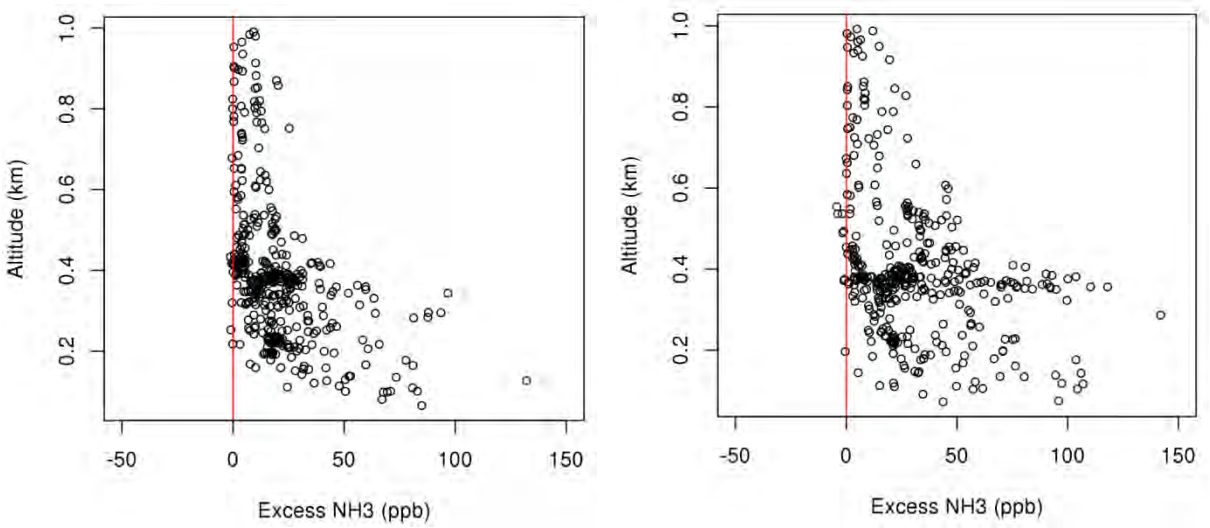

Figure 14. Excess NH_3 in the SJV on January 18 (Left) and January 20 (Right) based on NASA aircraft measurements in 2013.

While ammonium nitrate formation is in a NO_x limited regime, this does not conflict with modeling results that showed a small sensitivity of ammonium nitrate formation to ammonia emission reductions. At equilibrium state, the product of gaseous nitric acid and ammonia mixing ratios in the atmosphere is a constant, and the equilibrium constant depends on ambient conditions as well as particulate compositions (Seinfeld and Pandis, 2006). Even in a NO_x-limited regime, the perturbation of ammonia mixing ratios influences the partitioning of nitric acids. As ammonia becomes more and more excessive, the partitioning of nitric acids shifts towards the particulate phase. After the vast majority of nitric acids are in the particulate phase (e.g., > 98% of nitric acids in particulate phase), the formation of ammonium nitrate becomes far less sensitive to the excessive ammonia. In addition, the dry deposition velocity difference between gaseous nitric acid and particulate nitrate further adds to the complexity. When the partitioning of gaseous and particulate nitric acids is perturbed by changing ammonia, due to the different removal rates of gaseous and particulate nitric acids (Meng et al., 1997; Pusede et al., 2016), the mass of total nitric acids is perturbed as well, which could amplify the response to ammonia emissions changes. In the SJV, because of the excessive ammonia, the formation of ammonium nitrate is much more sensitive to the reductions of NO_x than to the reductions of ammonia, which has been widely documented in past modeling studies. Nevertheless, limited sensitivity of ammonium nitrate formation to large ammonia reductions has been shown in previous modeling studies as well (Kleeman et al., 2005). Overall, modeling demonstrated that ammonia is not a significant precursor to $PM_{2.5}$ as $PM_{2.5}$ DVs only exhibited a limited sensitivity to a reasonable level of ammonia reductions.

Indirect role of VOCs in ammonium nitrate formation

The integrated reaction rate (IRR) analysis in CMAQv5.0.2 was used to understand the impact of VOC emission reductions on nitrate formation in the model. IRR outputs the production or loss rates for individual gas-phase chemical pathways. Heterogeneous nitric acid formation rates were obtained from the aerosol module. Two separate simulations using the January 2013 meteorological fields were conducted for two future year emission scenarios. One utilized the baseline future year emissions inventory for 2025 and the other involved a 25% reduction in VOC emissions from the baseline scenario. When VOC emissions were reduced by 25%, daytime and nighttime nitric acid formation rates were only slightly impacted by the VOC emission reductions. Daytime homogeneous nitric acid formation is primarily through the gas-phase reaction of NO_2 and the hydroxyl radical. When VOC emissions were reduced, at urban locations such as Bakersfield, the daytime nitric acid formation rate decreased slightly because of the slight decrease in hydroxyl radical mixing ratios associated with VOC reductions. More specifically, reduced hydroxyl radical mixing ratio was due to reduced photolysis from formaldehyde (Pusede et al., 2016).

In addition to the effect that VOCs can have on daytime nitric acid formation rates, they can also indirectly affect nighttime heterogeneous nitric acid formation, which involves the heterogeneous reaction of N_2O_5 on particles. N_2O_5 is formed from NO_2 and NO_3, the latter of which is a product of the reaction between NO_2 and O_3 (Seinfeld and Pandis, 2006). In places like Visalia, the nighttime heterogeneous nitric acid formation rate above the surface was slightly enhanced when VOC emissions were reduced. Model output showed reduced peroxyacetyle nitrate (PAN) formation under reduced VOC emissions. The reduced PAN formation then resulted in increased availability of NO_2, which in turn enhanced N_2O_5 formation (Meng et al., 1997) and slightly increased its heterogeneous formation rate.

Overall, reducing VOC emissions by 25% increased ammonium nitrate only slightly (~ 1%) at $PM_{2.5}$ design sites, which is the net outcome of different chemical processes in competition with each other, as well as the physical transport and mixing processes in the atmosphere.

Current status of secondary organic aerosol (SOA)

Secondary organic aerosol (SOA) is formed in the atmosphere by oxidation of VOCs followed by gas to particle partitioning of the oxidation products (Kanakidou et al., 2005). In general, the importance of SOA is higher during the ozone season when VOC emissions are at their peak (e.g., Foley et al., 2010; Liu et al., 2012; Rollins et al., 2012;

Zhao et al., 2013) and is much smaller in winter (Lurmann et al., 2006). However, in the SJV, $PM_{2.5}$ concentrations are typically lower in summer compared to winter. In recent years, Aerosol Mass Spectrometer (AMS) measurements made in Fresno during winter showed that approximately a third of organic aerosol is oxygenated organic aerosol (OOA) and the remaining is primary (Ge et al., 2013; Young et al., 2016).At present, the sources and/or formation processes for OOA are not known yet. Potential sources for OOA could include SOA, atmospherically processed POA, or directly emitted POA as well.

In the CMAQ model, SOA is simulated using the two-product absorption model (Odum et al., 1996). Detailed description of the SOA model in CMAQ can be found in Carlton et al. (2010) and Simon et al. (2012). Briefly, CMAQ considers SOA formation from the following precursors: long chain alkanes, high-yield aromatics (e.g., toluene), low-yield aromatics (e.g., xylene), benzene, isoprene, monoterpenes, and sesquiterpenes. For most anthropogenic VOCs, SOA is formed via oxidation by the hydroxyl radical. For biogenic VOCs, such as monoterpenes and sesquiterpenes, SOA is also formed from oxidation by nitrate and ozone, in addition to oxidation by the hydroxyl radical (Carlton et al., 2010). CMAQ also incorporates a NO_x dependence on SOA yield, in-cloud SOA formation from glyoxal and mythylglyoxal, particle-phase oligomerization (Carlton et al., 2010) and aging of primary organic aerosol (Simon et al., 2012). Overall, CMAQ's SOA module represents a state-of-the-science treatment of known SOA precursors and processes. Various daytime and nighttime formation processes of SOA considered important at Bakersfield (Liu et al., 2012; Rollins et al., 2012; Zhao et al., 2013) are treated in the CMAQ model.

In general, current state-of-the-science SOA models are believed to under-predict the levels of SOA formation in the atmosphere. The under-prediction of SOA is not limited to the two-product SOA model used in CMAQ. Other SOA modeling formulations, such as the volatility bin based model (e.g., Ciarelli et al., 2015; Woody et al., 2015) and the statistical oxidation model (e.g., Jathar et al., 2016) under-predict SOA concentrations to a similar degree, especially when these models are calibrated to the same chamber SOA yield data and are based on the same SOA precursors

Two important issues have emerged in recent years that were deemed to be promising in reducing the gaps between modeled and observed SOA concentrations in the atmosphere. Robinson et al. (2007) demonstrated that SOA formation from emissions of intermediate-volatile/semi-volatile organic compounds (IVOCs/SVOCs) from combustion sources far exceeded known SOA precursors and that those emissions were not accounted for in the current emission inventories. Characterization and quantification of the emission factors and SOA formation potentials of the IVOCs/SVOCs are not trivial. In the past several years, collaborations among Professor Robinson's group at

Carnegie Mellon University (CMU), EPA, and CARB have been focusing on the characterization of IVOCs/SVOCs emissions from mobile sources. Follow-up studies have demonstrated the importance of SOA formation from motor vehicle emitted IVOCs/SVOCs (e.g., Jathar et al., 2014; Zhao et al., 2015), although these studies were based on 0-D calculations. Given the challenge of characterizing those emissions and SOA formation potentials, there is also a discrepancy regarding the relative importance of SOA formation from different motor vehicle sources (Bahreini et al., 2012; Gentner et al., 2012; Jathar et al., 2014; Zhao et al., 2015). However, CMU's latest 3-D air quality modeling assessment in Southern California including those IVOCs/SVOCs emissions shows only modest difference of OA prediction compared to the traditional method in CMAQv4.7 and that mobile sources (including gasoline and diesel vehicles/equipments) only contributed one-quarter of the OA burden in Southern California, as strict regulations have dramatically reduced motor vehicle emissions (Robinson, 2016). Zhang et al. (2014) found that SOA yield data measured from laboratory chamber experiments may be substantially suppressed due to losses of SOA-forming vapors to chamber walls. This can lead to an underestimate of SOA in air quality models because parameterizations in SOA models are calibrated against chamber measured SOA yields. While the significance of vapor wall loss has been recognized, more work is needed to understand the mechanisms of vapor wall loss and to correct the vapor wall loss for past experimental data (Krechmer et al., 2016; Yeh and Ziemann, 2015; Zhang et al., 2015).

Many ambient or laboratory measurements have demonstrated potential SOA formation from different chemical pathways beyond the absorption process treated in typical SOA models. For example, Zhao et al (2013) showed that SOA production from phthalic acid was substantially increased by reaction with ammonia to form ammonium salts that favor their partitioning into the particle phase. Smith (2014) demonstrated that aqueous oxidation of phenols can lead to SOA formation. While those findings are important under certain conditions, more coordinated ambient measurement, laboratory experiments, and computational modeling are needed to develop models that describe those formation pathways rigorously under different atmospheric conditions. From there, the importance of those processes and the implication to control programs can be assessed. Arbitrary use of findings may itself lead to simulated SOA formation that is not a true representation of the relevant atmospheric processes, even though the model performance of SOA/OA is improved. For example, Jathar et al. (2016) cautioned that the use of an unconstrained multi-generational aging scheme, commonly adopted in models recently (e.g., Lane et al., 2008; Shrivastava et al., 2008), is not an indication of improved representation of atmospheric chemistry, though it improved the agreement between observed and modeled OA concentrations. Hayes et al. (2015) showed that including SOA formation from IVOCs/SVOCs based on three different parameterizations

shows very large differences (e.g., a factor of 3 in SOA mass concentrations), which underscored the uncertainties associated with the current understanding. These all demonstrated that caution needs to be taken in terms of development and choice of parameterizations of SOA precursors/formation, particularly when these models are used for regulatory purposes.

Overall, continued assessment of SOA formation in the SJV is warranted as the scientific understanding of SOA contributing sources and formation mechanisms continues to be improved. However, based on modeling result from the current state-of-the-science SOA module in CMAQv5.0.2, VOC is not a significant precursor to $PM_{2.5}$ formation in the SJV based on its contribution to SOA formation.

6 REFERENCES

Angevine, W. M., Eddington, L., Durkee, K., Fairall, C., Bianco, L., Brioude, J., 2012: Meteorological model evaluation for CalNex 2010, Monthly Weather Review, 140, 3885-3906.

Bahreini, R., et al., 2012: Gasoline emissions dominate over diesel in formation of secondary organic aerosol mass, Geophysical Research Letters, 39, doi:10.1029/2011GL050718.

Baker, K. R., H. Simon, and J. T. Kelly, 2011: Challenges to modeling “cold pool” meteorology associated with high pollution episodes. Environ. Sci. and Technol., 45(17), 7118–9.

Baker, K. R., Misenis, C., Obland, M. D., Ferrare, R. A., Scarino, A. J., and Kelly, J. T., 2013: Evaluation of surface and upper air fine scale WRF meteorological modeling of the May and June 2010 CalNex period in California, Atmos. Environ., 80, 299-309.

Bao, J.W., Michelson, S.A., Persson, P.O.G., Djalalova, I.V., Wilczak, J.M., 2008: Observed and WRF-simulated low-level winds in a high-ozone episode during the Central California ozone study, Journal of Applied Meteorology and Climatology, 47, 2372-2394.

Blanchard, C.L., Roth, P.M., Tanenbaum, S.J., Ziman, S.D., Seinfeld, J.H., 2000, The use of ambient measurements to identify which precursor species limit aerosol nitrate formation, Journal of Air Waste Management Association, 50, 2073-2084.

Boylan, J.W. and Russell, A.G., 2006, PM and light extinction model performance metrics, goals, and criteria for three-dimensional air quality models, Atmospheric Environment, 40, 4946-4959.

Carlton, A. G., P. V. Bhave, S. L. Napelenok, E. O. Edney, G. Sarwar, R. W. Pinder, G. A. Pouliot, and M. Houyoux, 2010, Model Representation of Secondary Organic Aerosol in CMAQv4.7., Env. Sci. & Techno., 44, 8553-8560.

Ciarelli, G., et al., 2015, European air quality modelled by CAMx including the volatility basis set scheme, Atmospheric Chemistry Physics Discussion, 15, 35645-35691.

Daly, C., D. Conklin, and M. Unsworth, 2009: Local atmospheric decoupling in complex topography alters climate change impacts. Int. J. Climatol., 30, 1857–1864.

Emmons, L. K., Apel, E.C., Lamarque, J.F., Hess, P.G., Avery, M., Blake, D., Brune, W., Campos, T., Crawford, J., DeCarlo, P.F., Hall, S., Heikes, B., Holloway, J., Jimenez, J.L., Knapp, D.J., Kok, G., Mena-Carrasco, M., Olson, J., O'Sullivan, D., Sachse, G., Walega, J., Weibring, P., Weinheimer, A., and Wiedinmyer, C., 2010, Impact of Mexico City emissions on regional air quality from MOZART-4 simulations, Atmospheric Chemistry and Physics, 10, 6195-6212.

Fast, J. D., Gustafson Jr, W. I., Berg, L. K., Shaw, W. J., Pekour, M., Shrivastava, M., Barnard, J. C., Ferrare, R. A., Hostetler, C. A., Hair, J. A., Erickson, M., Jobson, B. T., Flowers, B., Dubey, M. K., Springston, S., Pierce, R. B., Dolislager, L., Pederson, J., and Zaveri, R. A., 2012: Transport and mixing patterns over Central California during the carbonaceous aerosol and radiative effects study (CARES), Atmos. Chem. Phys., 12, 1759-1783, doi:10.5194/acp-12-1759-2012.

Foley, K. M., et al., 2010, Incremental testing of the Community Multiscale Air Quality (CMAQ) modeling system version 4.7, Geosci. Model Dev., 3, 205-226, doi:10.5194/gmd-3-205-2010.

Fosberg, M.A., Schroeder, M.J., 1966: Marine air penetration in Central California, Journal of Applied Meteorology, 5, 573-589.

Frank, N.H., 2006, Retained nitrate, hydrated sulfates, and carbonaceous mass in federal reference method fine particulate matter for six eastern U.S. cities, Journal of Air & Waste Management Association, 56, 500-511.

Ge, X. L., A. Setyan, Y. L. Sun, Q. Zhang, 2012, Primary and Secondary Organic Aerosols in Fresno California during Wintertime: Results from High Resolution Aerosol Mass Spectrometry, Journal of Geophysical Research – Atmospheres, 117, D19301, 15p,10.1029/2012JD018026.

Gentner, D.R., et al., 2012, Elucidating secondary organic aerosol from diesel and gasoline vehicles through detailed characterization of organic carbon emissions, Proceedings of the National Academy of Sciences, 109, 18318-18323.

Gillies, R. R., S. Wang, and M. R. Booth, 2010: Atmospheric scale interaction on wintertime intermountain west low-level inversions. Weather Forecasting, 25, 1196–1210.

Hayes, P.L., et al., 2015, Modeling the formation and aging of secondary organic aerosols in Los Angeles during CalNex 2010, Atmospheric Chemistry Physics, 15, 5773-5801.

Hu, J., Howard, C. J., Mitloehner, F., Green, P. G., and Kleeman, M. J., 2012: Mobile Source and Livestock Feed Contributions to Regional Ozone Formation in Central California, Environmental Science & Technology, 46, 2781-2789.

Jackson, B.S., Chau, D., Gurer, K., Kaduwela, A., 2006: Comparison of ozone simulations using MM5 and CALMET/MM5 hybrid meteorological fields for the July/August 2000 CCOS episode, Atmos. Environ., 40, 2812-2822.

Jathar, S. H., Cappa, C. D., Wexler, A. S., Seinfeld, J. H., and Kleeman, M. J., 2016, Simulating secondary organic aerosol in a regional air quality model using the statistical oxidation model – Part 1: Assessing the influence of constrained multi-generational ageing, Atmos. Chem. Phys., 16, 2309-2322.

Jathar, S.H., Gordon, T.D., Hennigan, C.J., Pye, H.O.T., Pouliot G., Adams, P.J., Donahue, N.M., Robinson, A.L., 2014, Unspeciated organic emissions from combustion sources and their influence on the secondary organic aerosol budget in the United State, Proceedings of the National Academy of Sciences, 111, 10473-10478.

Kanakidou et al., 2005, Organic aerosol and global climate modeling: a review, Atmospheric Chemistry Physics, 5, 1053-1123.

Kelly, J. T., Baker, K. R., Nowak, J. B., Murphy, J. G., Milos, Z. M., VandenBoer, T. C., Ellis, R. A., Neuman, J. A., Weber, R. J., Roberts, J. M., Veres, P. R., de Gouw, J. A., Beaver, M. R., Newman, S., and Misenis, C., 2014: Fine-scale simulation of ammonium and nitrate over the South Coast Air Basin and San Joaquin Valley of California during CalNex-2010, J. Geophysical Research, 119, 3600-3614, doi:10.1002/2013JD021290.

Kleeman, M.J., Ying, Q., and Kaduwela, A., 2005, Control strategies for the reduction of airborne particulate nitrate in California's San Joaquin Valley, Atmospheric Environment, 39, 5325-5341.

Krechmer, J., Pagonis, D., Ziemann, P.J., Jimenez, J.L., 2016, Quantification of gas-wall partitioning in Teflon environmental chambers using rapid bursts of low-volatility oxidized species generated in situ, Environmental Science & Technology, doi:10.1021/acs.est.6b00606.

Lane, T.E., Donahue, N.M., Pandis, S.N., 2008, Simulating secondary organic aerosol formation using the volatility basis-set approach in a chemical transport model, Atmospheric Environment, 42, 7439-7451.

Liu, S., et al., 2012, Secondary organic aerosol formation from fossil fuel sources contribute majority of summertime organic mass at Bakersfield, J. Geophys. Res., 117, D00V26, doi:10.1029/2012JD018170.

Lurmann, F.W., Brown, S.G., McCarthy, M.C., and Roberts, P.T., 2006, Processes Influencing Secondary Aerosol Formation in the San Joaquin Valley during Winter, Journal of Air and Waste Management Association, 56, 1679-1693.

Markovic, M. Z., VandenBoer, T. C., Baker, K. R., Kelly, J. T., and Murphy, J. G., 2014, Measurements and modeling of the inorganic chemical composition of fine particulate matter and associated precursor gases in California's San Joaquin Valley during CalNex 2010, Journal of Geophysical Research - Atmosphere,119, 6853–6866, doi:10.1002/2013JD021408.

Meng, Z., Dabdub, D., Seinfeld, J.H., 1997, Chemical coupling between atmospheric ozone and particulate matter, Science, 277, 116-119.

Odum, J.R., T. Hoffmann, F. Bowman, D. Collins, R.C. Flagan, J.H. Seinfeld, 1996, Gas/particle partitioning and secondary organic aerosol yields, Environmental Science & Technology, 30, 2580-2585.

Pusede, S.E., et al., 2016, On the effectiveness of nitrogen oxide reductions as a control over ammonium nitrate aerosol, Atmospheric Chemistry Physics, 16, 2575-2596.

Robinson, A. 2016, Linking Tailpipe to Ambient: Phase 4 Executive Summary, prepared by Carnegie Mellon University for the Coordinating Research Council, Inc., available at http://www.crcao.com/reports/recentstudies2016/A-74_E-96%20Phase%204/A-74-E-96%20Phase%204%20Executive%20Summary.pdf, accessed in July 2016.

Rogers, R.E., Deng, A., Stauffer, D. Gaudet, B.J., Jia, Y., Soong, S.-T., Tanrikulu, S., 2013, Application of the Weather Research and Forecasting model for air quality modeling in the San Francisco Bay area, Journal of Applied Meteorology and Climatology, 52, 1953-1973.

Rollins, A. W., et al., 2012, Evidence for NOx Control over Nighttime SOA Formation, Science, 337, 1210-1212, doi:10.1126/science.1221520.

Seinfeld, J.H., Pandis, S.N., 2006, Atmospheric Chemistry and Physics: From Air Pollution to Climate Change, 2nd Edition, Wiley, Inc., New York.

Shrivastava, M.K., Lane, T.E., Donahue, N.M., Pandis, S.N., Robinson, A.L., 2008, Effects of gas particle partitioning and aging of prigram emissions on urban and regional organic aerosol concentrations, Journal of Geophysical Research, 113, D18301, doi:10.1029/2007JD009735.

Skamarock, W. C., J. B. Klemp, J. Dudhia, D. O. Gill, D. M. Barker, W. Wang, and J. G. Powers, 2005: A description of the Advanced Research WRF Version 2. NCAR Tech Notes-468+STR.

Simon, H., Baker, K.R., and Phillips, S., 2012, Compilation and interpretation of photochemical model performance statistics published between 2006 and 2012, Atmospheric Environment, 61, 124-139.

Simon, H., Bhave, P.V., 2012, Simulating the degree of oxidation in atmospheric organic particles. Environ. Sci. Technol., 46, 331-339.

Smith, J.D., Sio, V., Yu, L., Zhang, Q., Anastasio, C., 2014, Secondary organic aerosol production from aqueous reactions of atmospheric phenols with an organic triplet excited state, Environmental Science & Technology, 48, 1049-1057.

Whiteman, C. D., S. Zhong, W. J. Shaw, J. M. Hubbe, X. Bian, and J. Mittelstadt, 2001: Cold pools in the Columbia Basin. Weather Forecasting, 16, 432–447.

Woody, M. C., Baker, K. R., Hayes, P. L., Jimenez, J. L., Koo, B., and Pye, H. O. T., 2015: Understanding sources of organic aerosol during CalNex-2010 using the CMAQ-VBS, Atmos. Chem. Phys. Discuss., 15, 26745-26793, doi:10.5194/acpd-15-26745-2015.

Yeh, G.K., Ziemann, P.J., 2015, Gas-wall partitioning of oxygenated organic compounds: Measurements, structure-activity relationships, and correlation with gas chromatographic retention factor, Aerosol Science & Technology, 49, 727-738.

Young, D., Kim, H. J., Parworth, C., Zhou, S., Zhang, X. L., Cappa, C., Seco, R., Kim, S., and Zhang, Q., 2016, Influences of emission sources and meteorology on aerosol chemistry in a polluted urban environment: Results from DISCOVER-AQ California, Atmospheric Chemistry & Physics, 16, 5427-5451.

Zhao, Y., et al., 2013, Sources of organic aerosol investigated using organic compounds as tracers measured during CalNex in Bakersfield, J. Geophys. Res. Atmos., 118, doi:10.1002/jgrd.50825.

Zhao, Y., Nguyen, N.T., Presto, A.A., Hennigan C.J., May A.A., Robinson, A.L., 2015, Intermediate volatility organic compound emissions from on-road diesel vehicles: chemical composition, emission factors, and estimated secondary organic aerosol production, Environmental Science Technology, 49, 11516-11526.

Zhang, X., Schwantes, R.H., McVay, R.C., Lignell, H., Coggon, M.M., Flagan, R.C., Seinfeld, J.H., 2015, Vapor wall deposition in Teflon chambers, Atmospheric Chemistry Physics, 15, 4197-4214.

Zhang, X., Cappa, C.D., Jathar, S.H., McVay, R.C., Ensberg, J.J., Kleeman, M.J., and Seinfeld, J.H., 2014, Influence of vapor wall loss in laboratory chambers on yields of secondary organic aerosol, Proceedings of the National Academy of Sciences of the United States of America, 111, 5802-5807, doi:10.1073/pnas.1404727111.

U.S. EPA, 2014, Draft Modeling Guidance for Demonstrating Attainment of Air Quality Goals for Ozone, PM2.5 and Regional Haze, available at http://www.epa.gov/scram001/guidance/guide/Draft_O3-PM-RH_Modeling_Guidance-2014.pdf

SUPPLEMENTAL MATERIALS

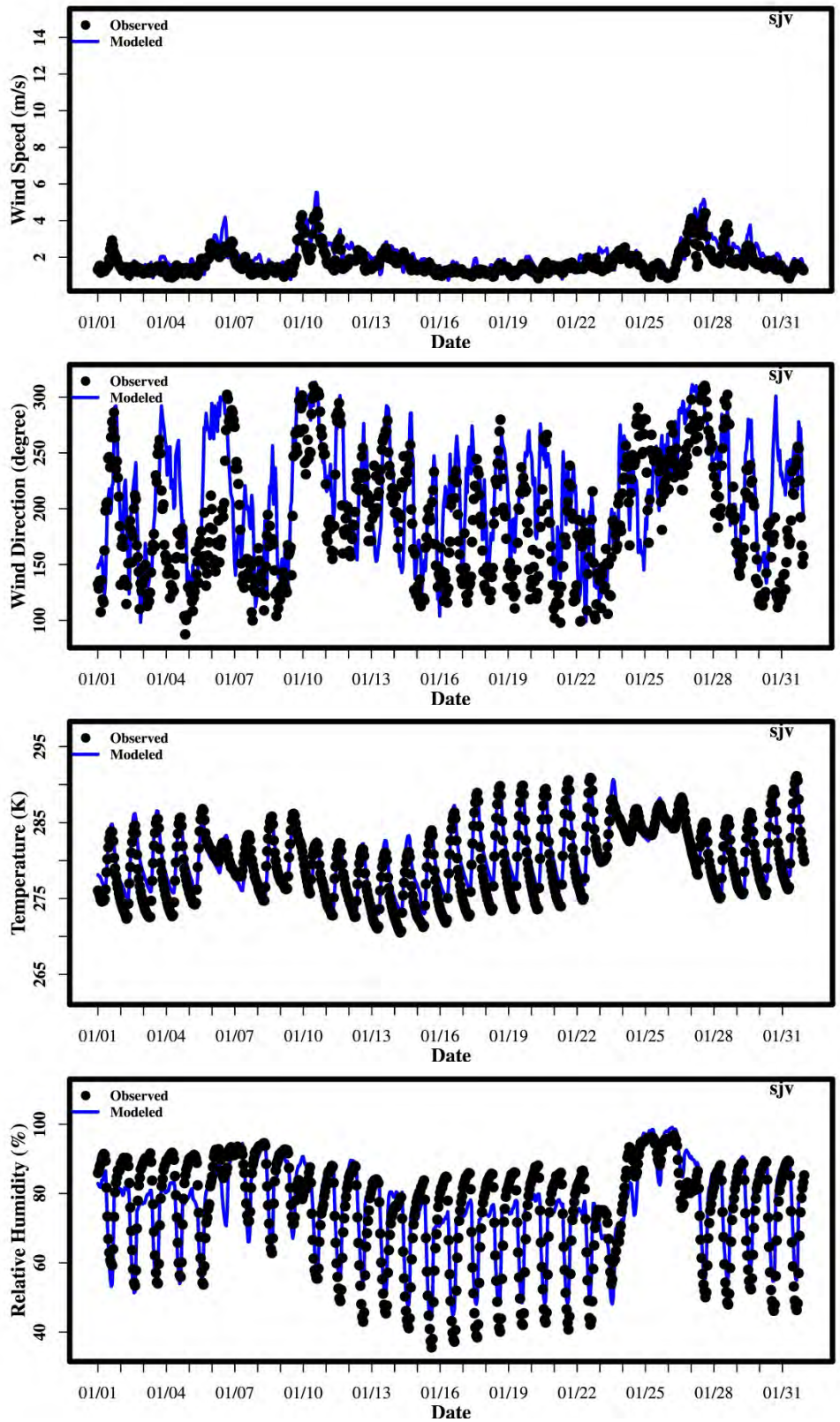

Figure S. 1 Time series of wind speed, direction, temperature and relative humidity for San Joaquin Valley in January 2013.

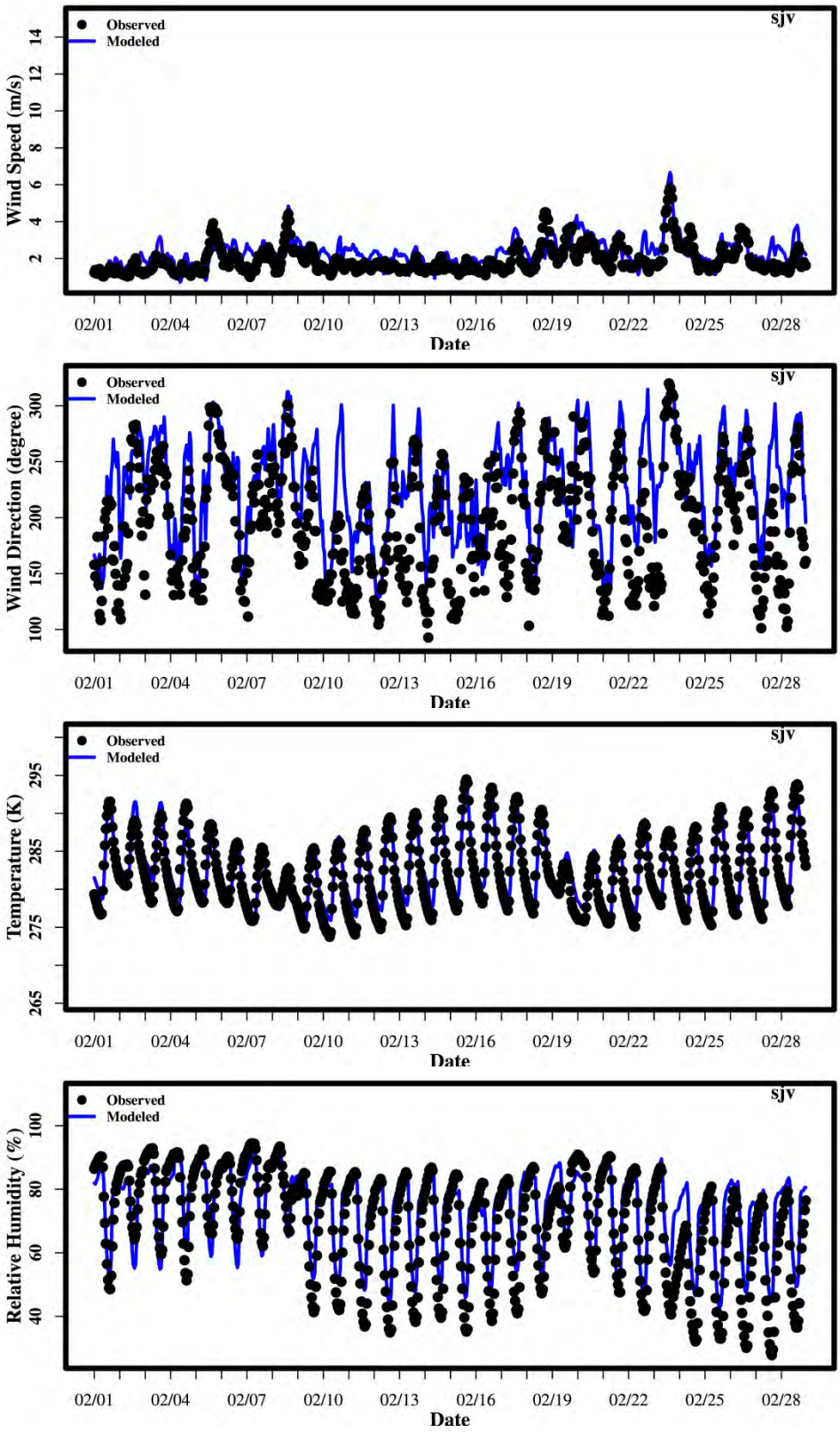

Figure S. 2 Time series of wind speed, direction, temperature and relative humidity for San Joaquin Valley in February 2013.

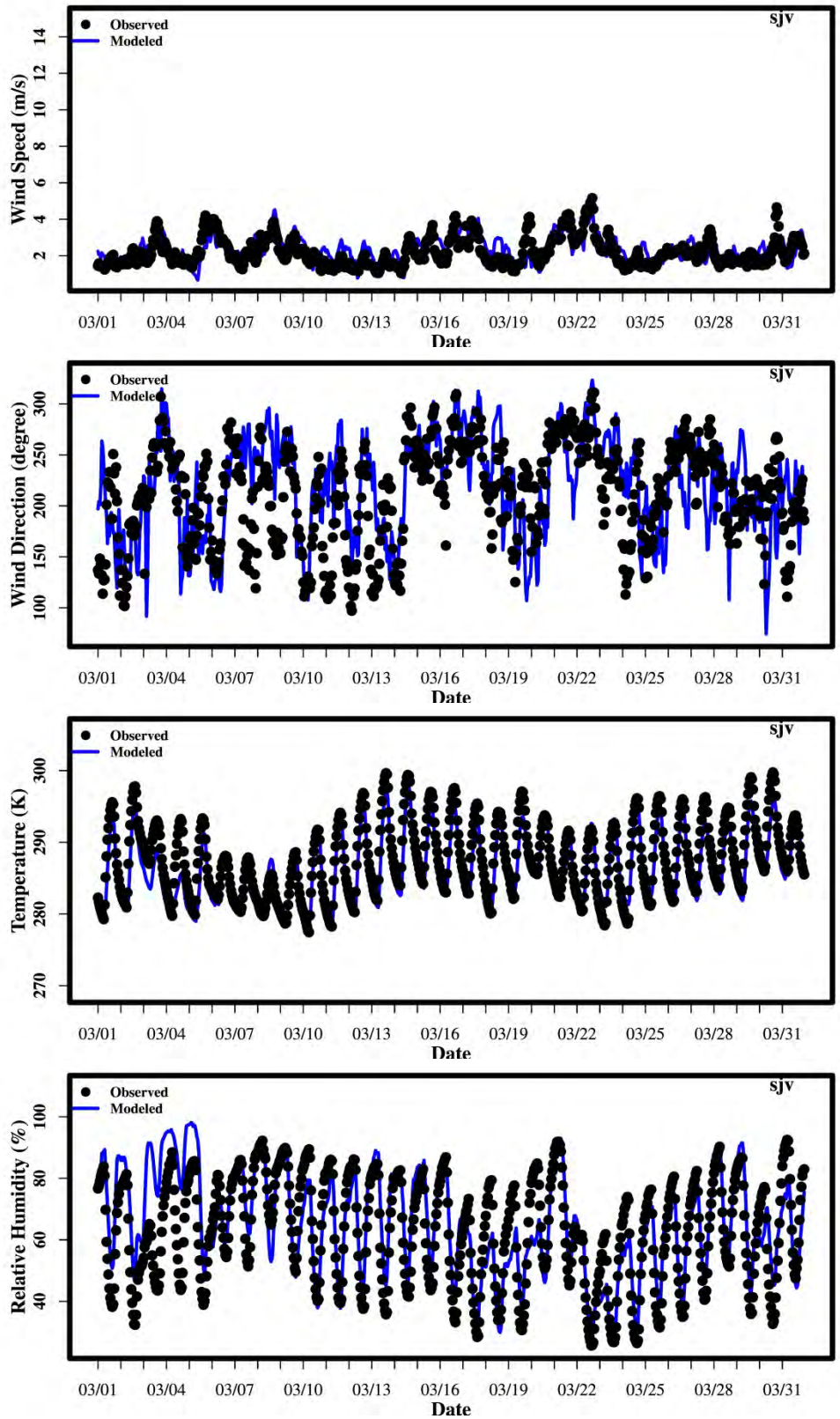

Figure S. 3 Time series of wind speed, direction, temperature and relative humidity for San Joaquin Valley in March 2013.

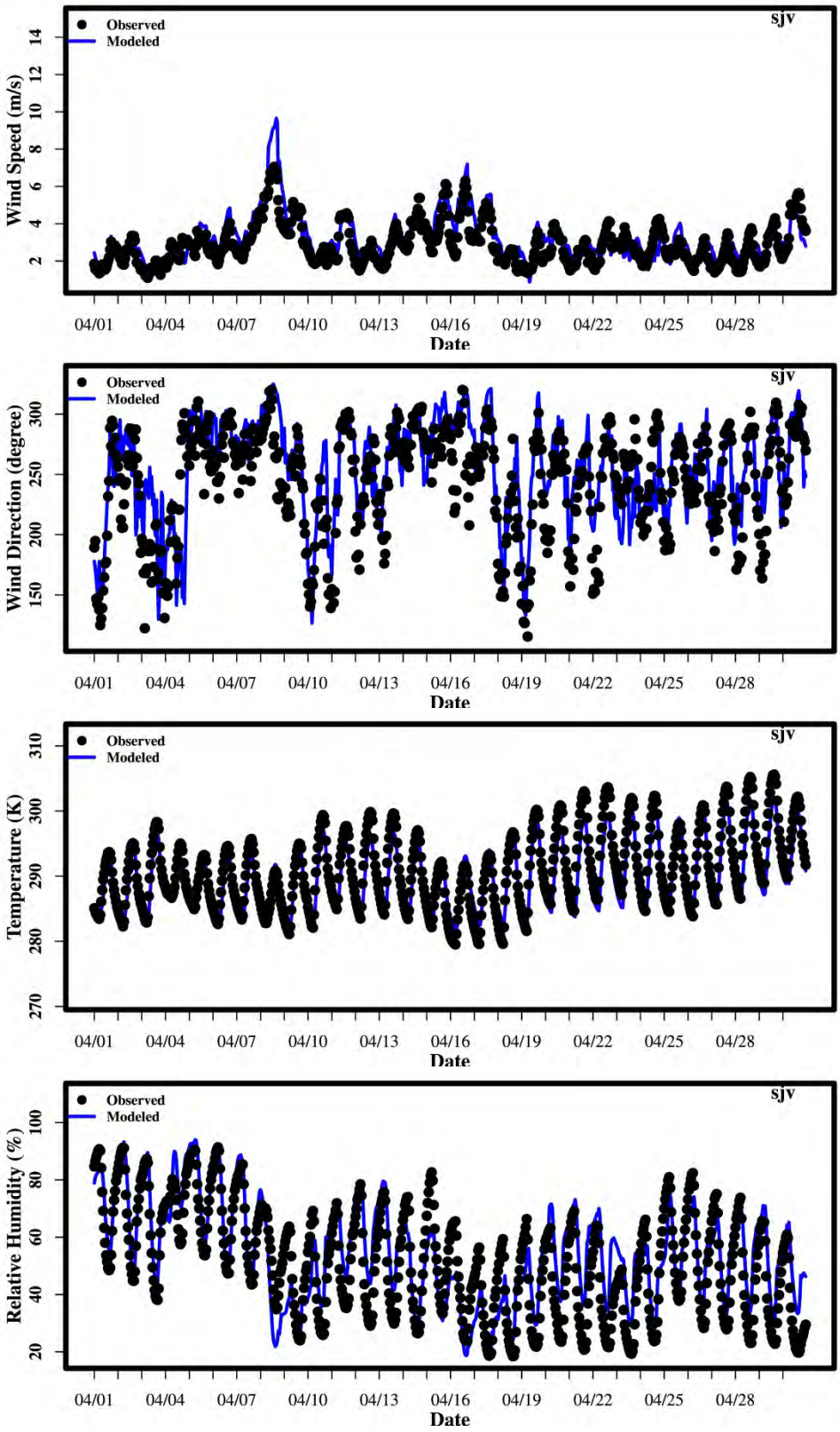

Figure S. 4 Time series of wind speed, direction, temperature and relative humidity for San Joaquin Valley in April 2013.

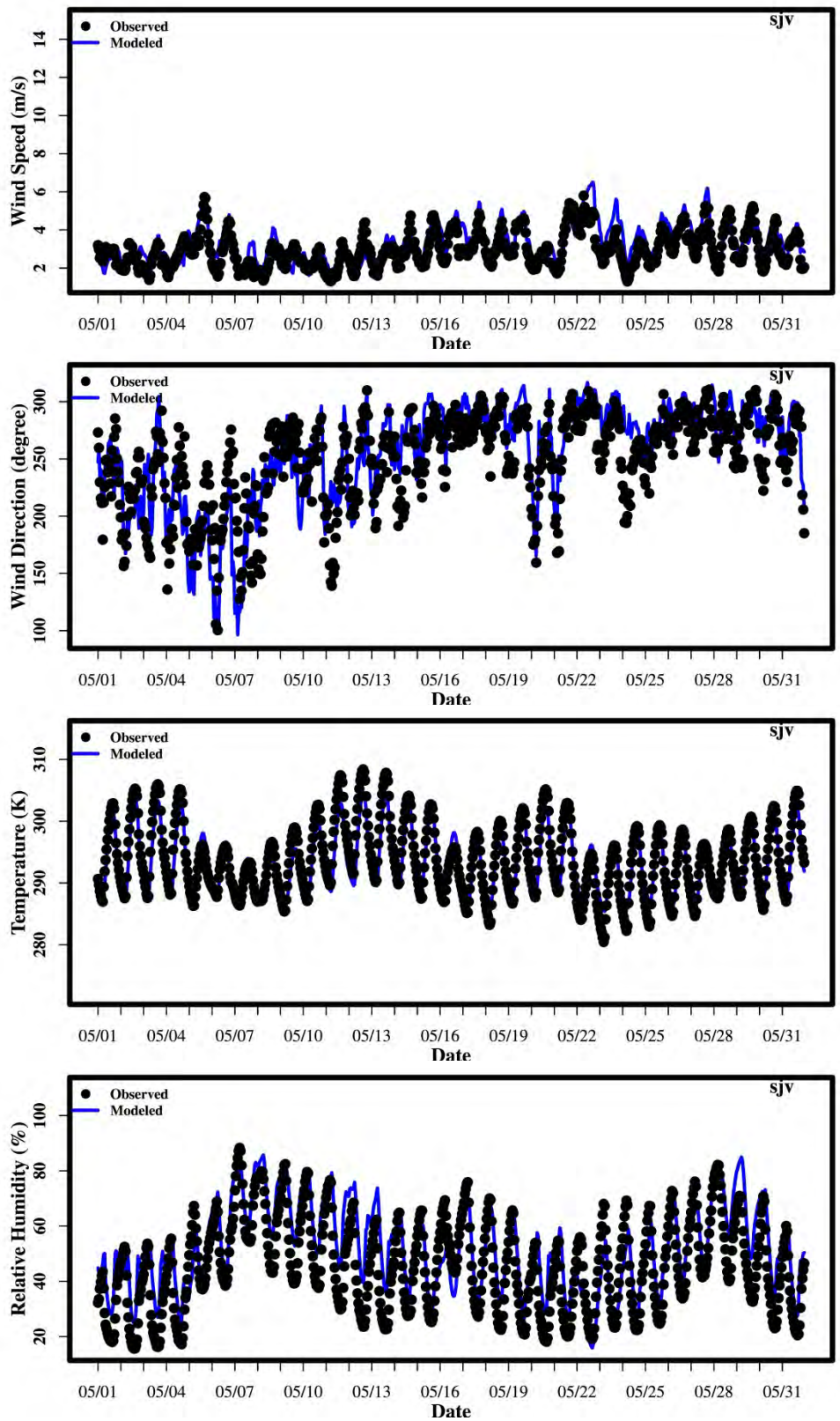

Figure S. 5 Time series of wind speed, direction, temperature and relative humidity for San Joaquin Valley in May 2013.

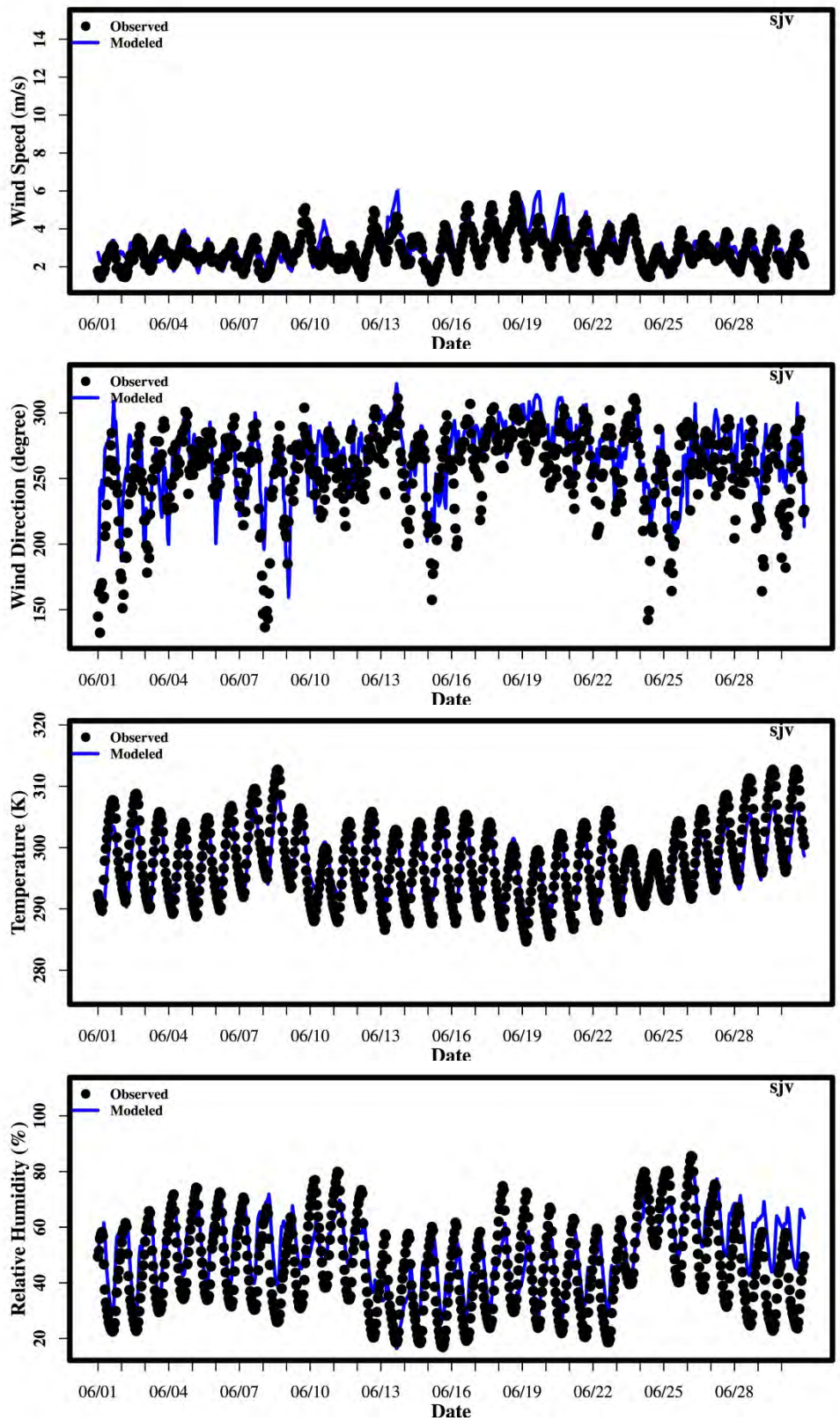

Figure S. 6 Time series of wind speed, direction, temperature and relative humidity for San Joaquin Valley in June 2013.

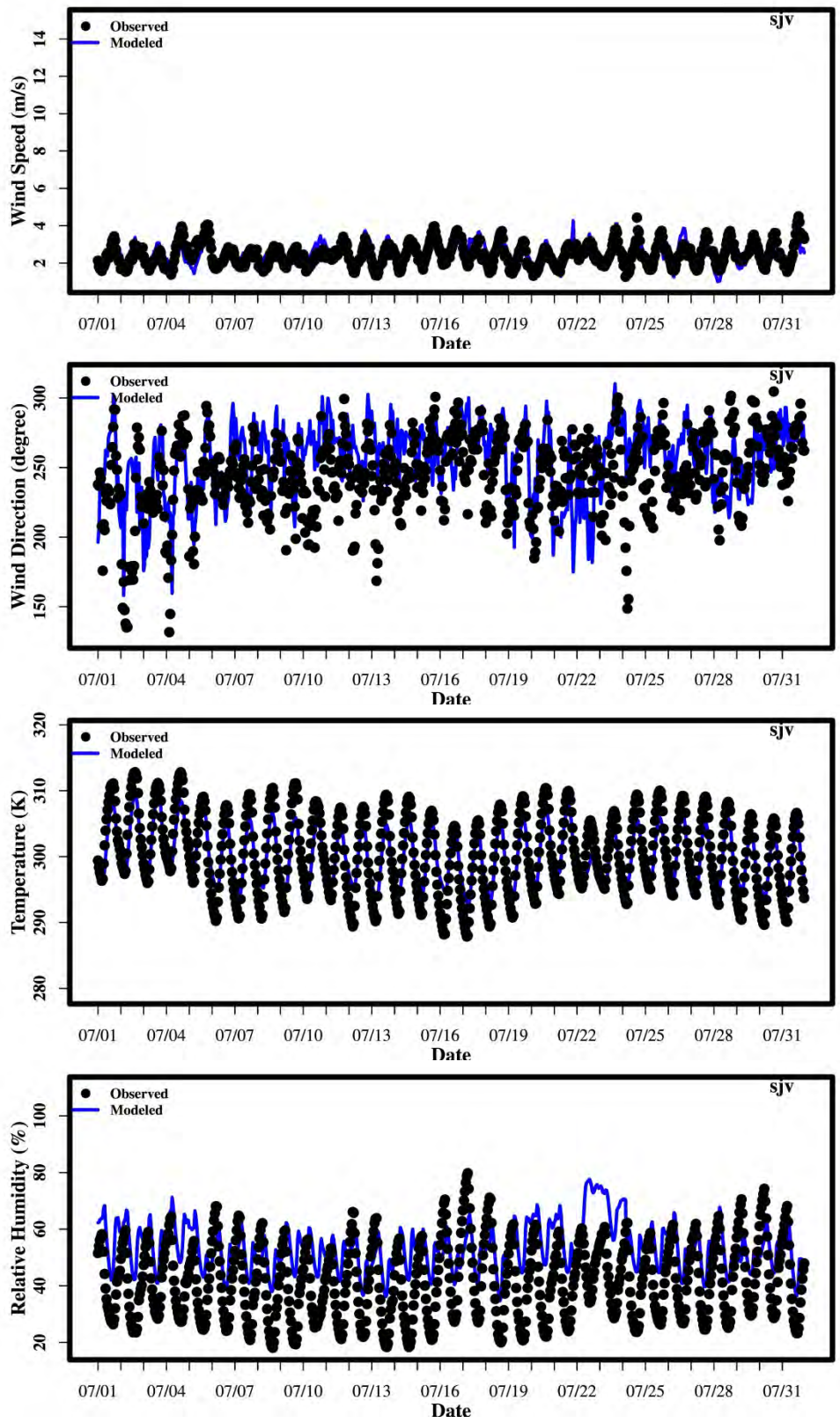

Figure S. 7 Time series of wind speed, direction, temperature and relative humidity for San Joaquin Valley in July 2013.

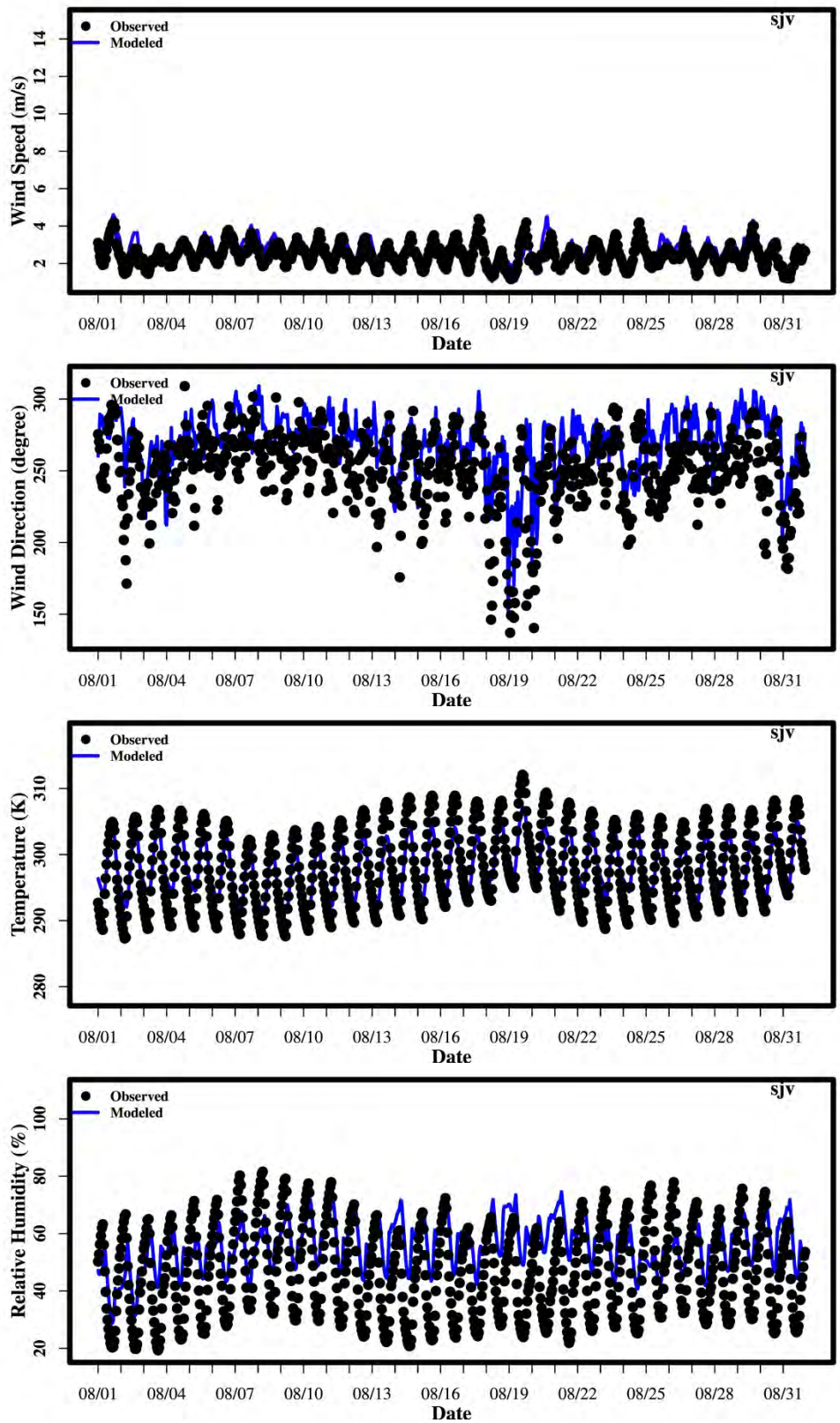

Figure S. 8 Time series of wind speed, direction, temperature and relative humidity for San Joaquin Valley in August 2013.

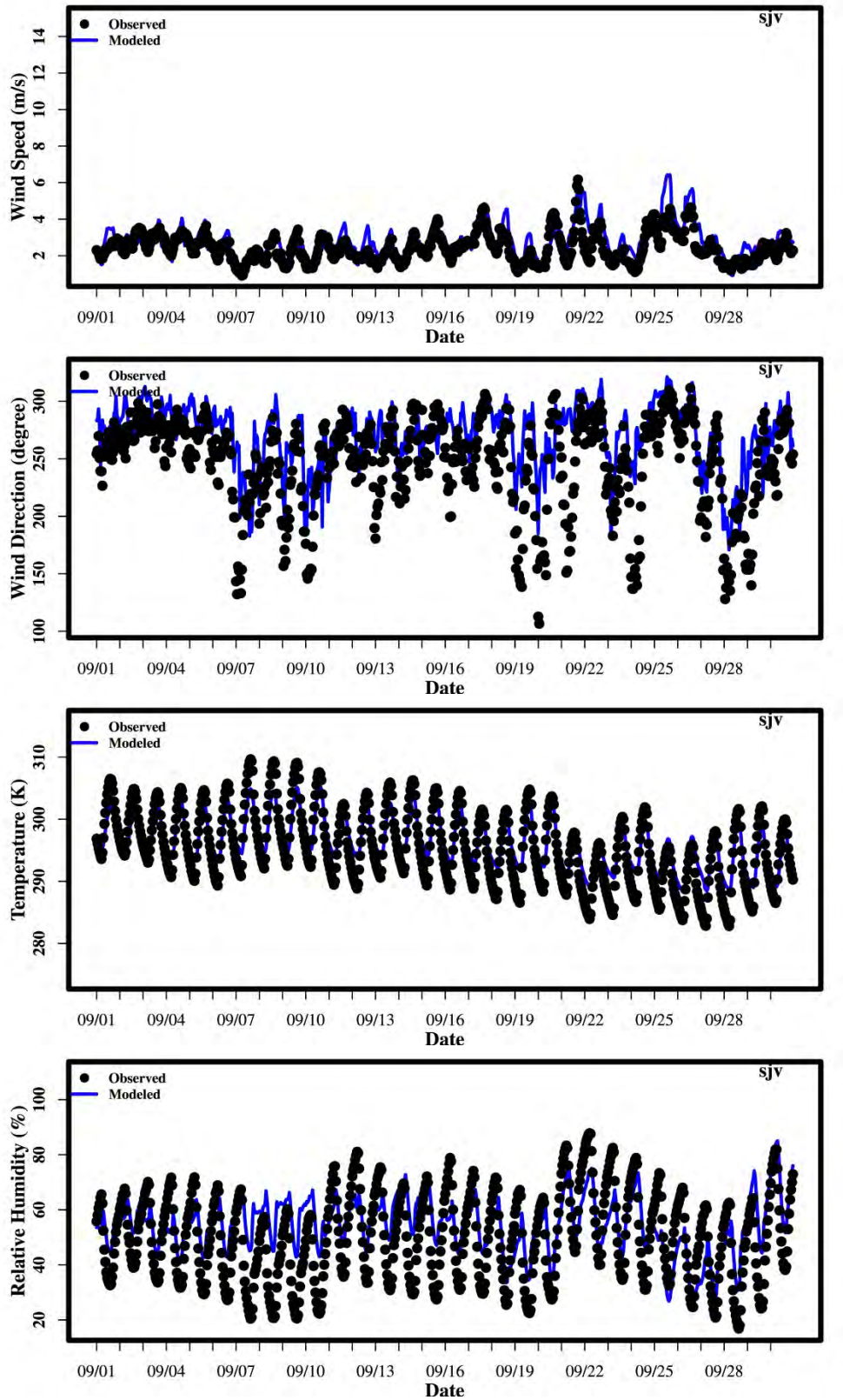

Figure S. 9 Time series of wind speed, direction, temperature and relative humidity for San Joaquin Valley in September 2013.

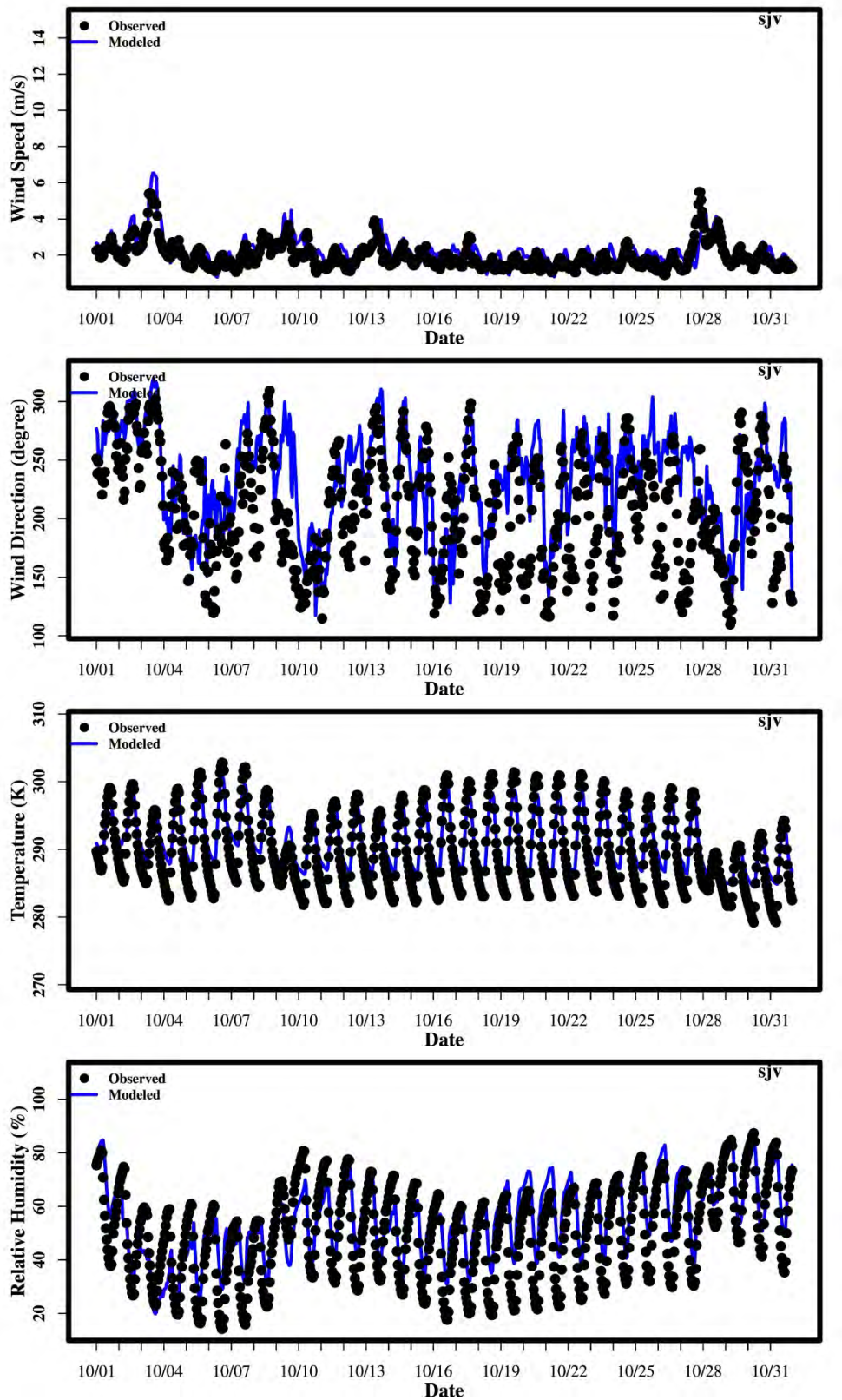

Figure S. 10 Time series of wind speed, direction, temperature and relative humidity for San Joaquin Valley in October 2013.

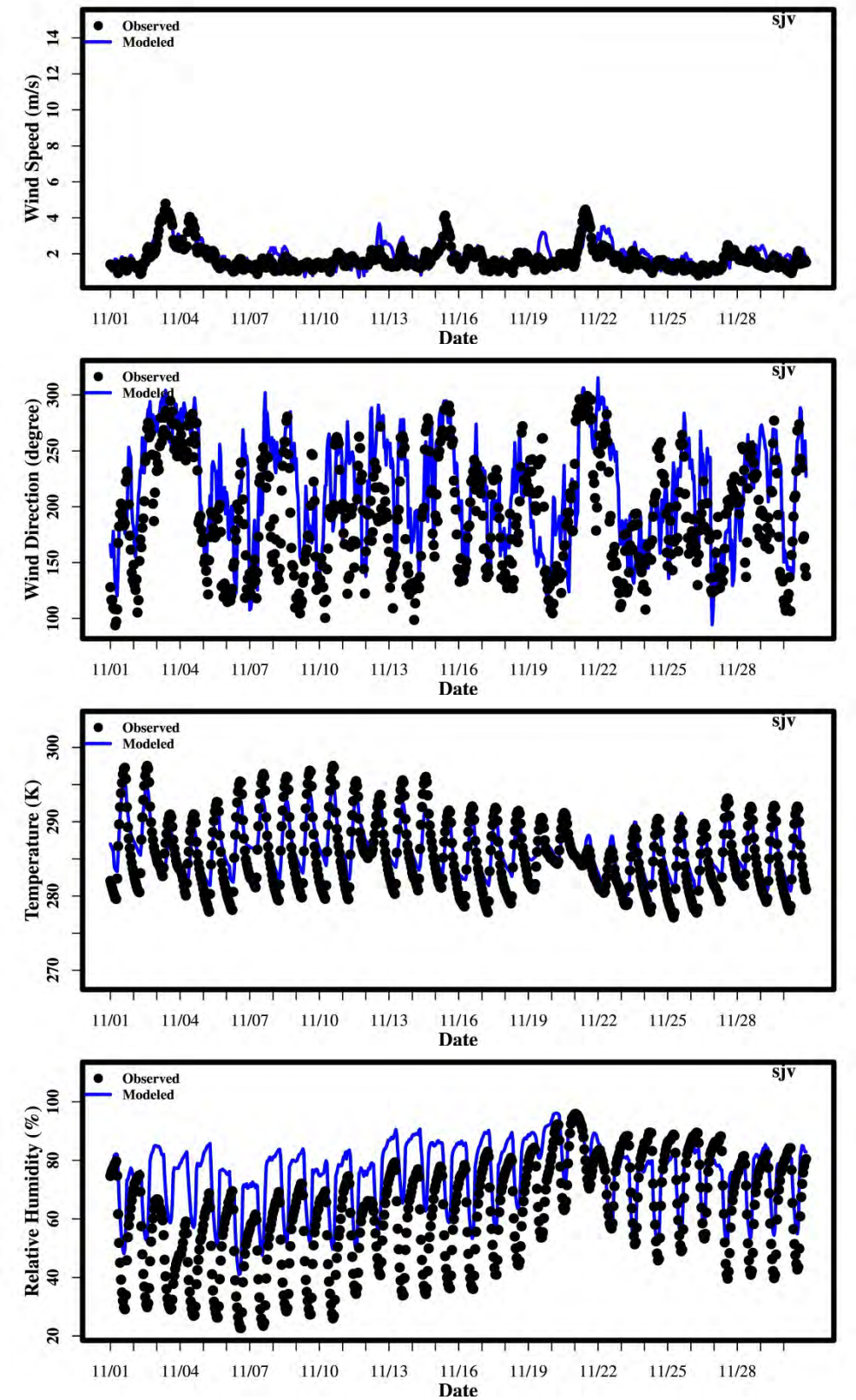

Figure S. 11 Time series of wind speed, direction, temperature and relative humidity for San Joaquin Valley in November 2013.

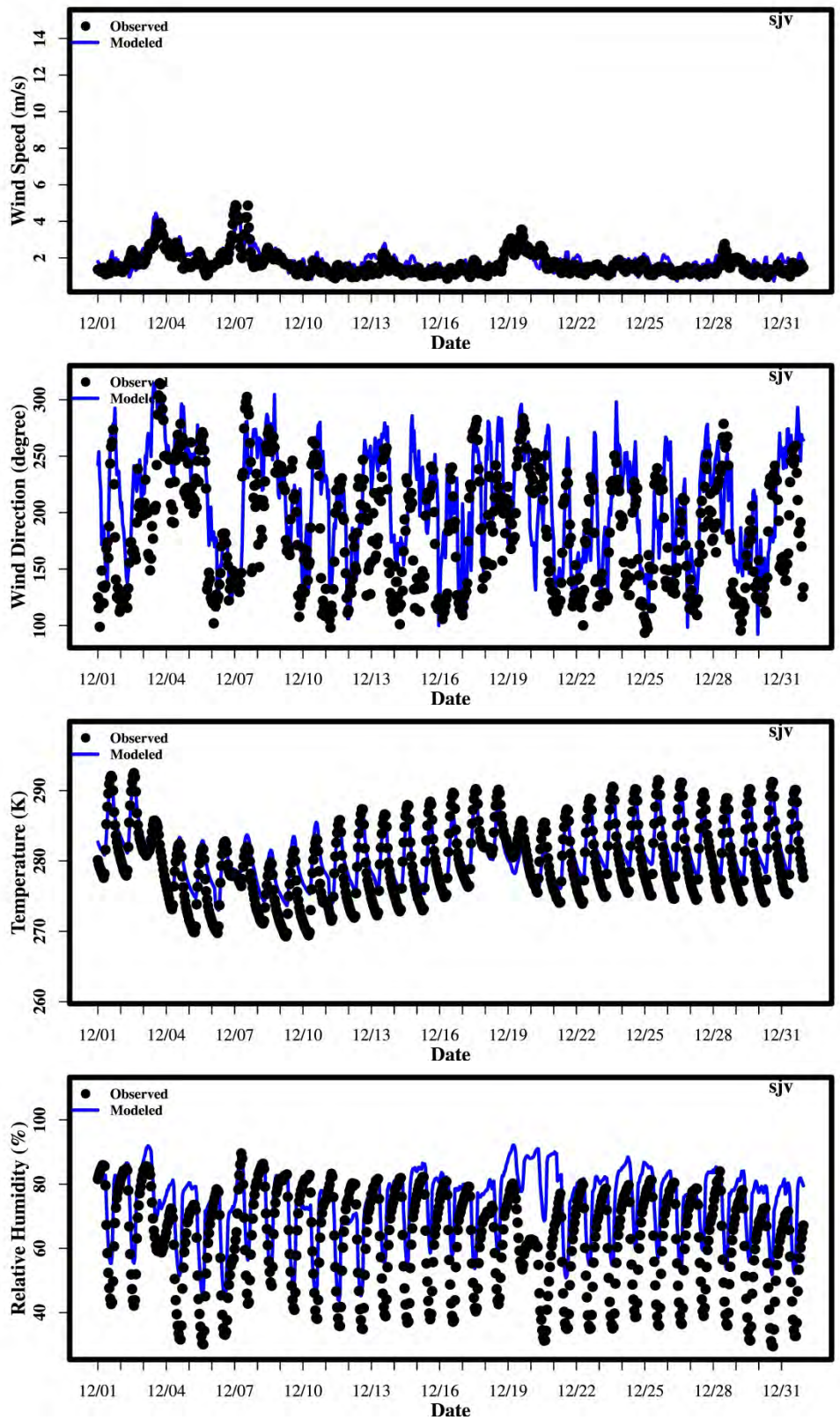

Figure S. 12 Time series of wind speed, direction, temperature and relative humidity for San Joaquin Valley in December 2013.

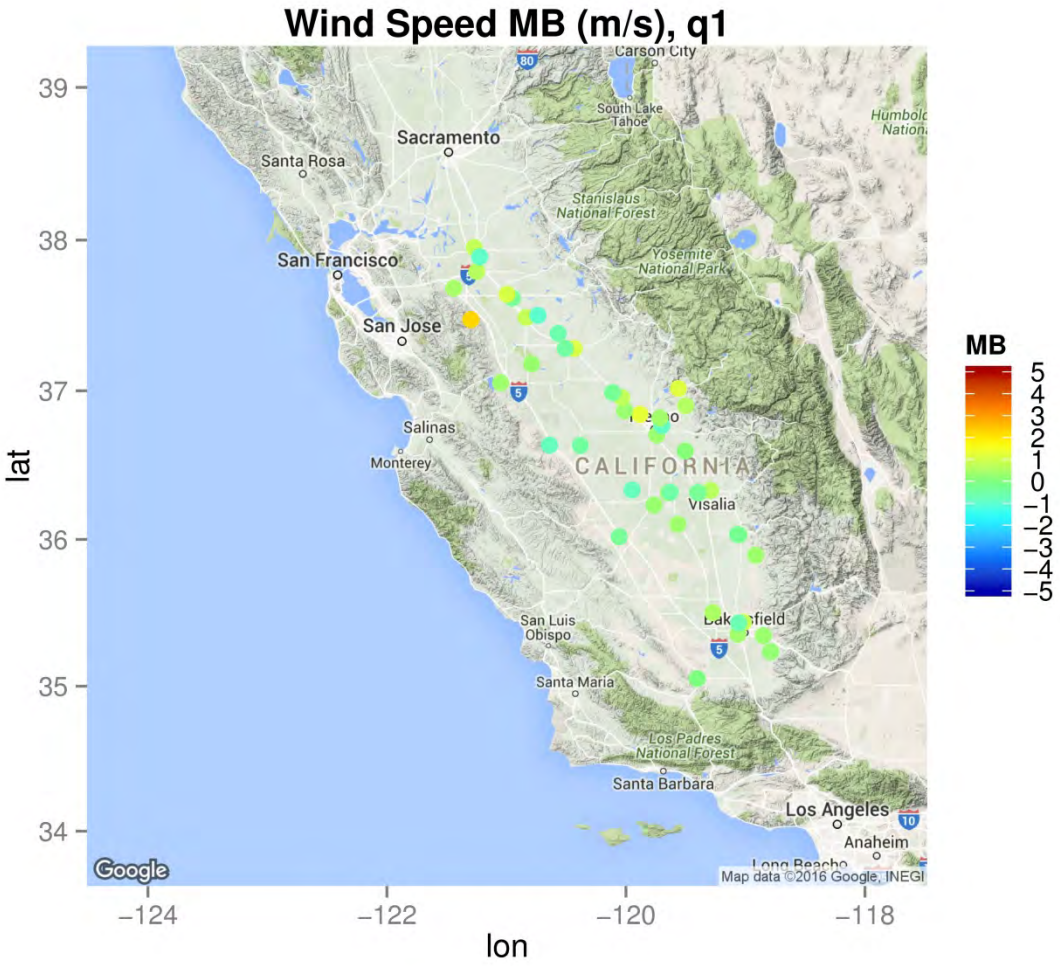

Figure S. 13 Hourly wind speed mean error in the first quarter of 2013

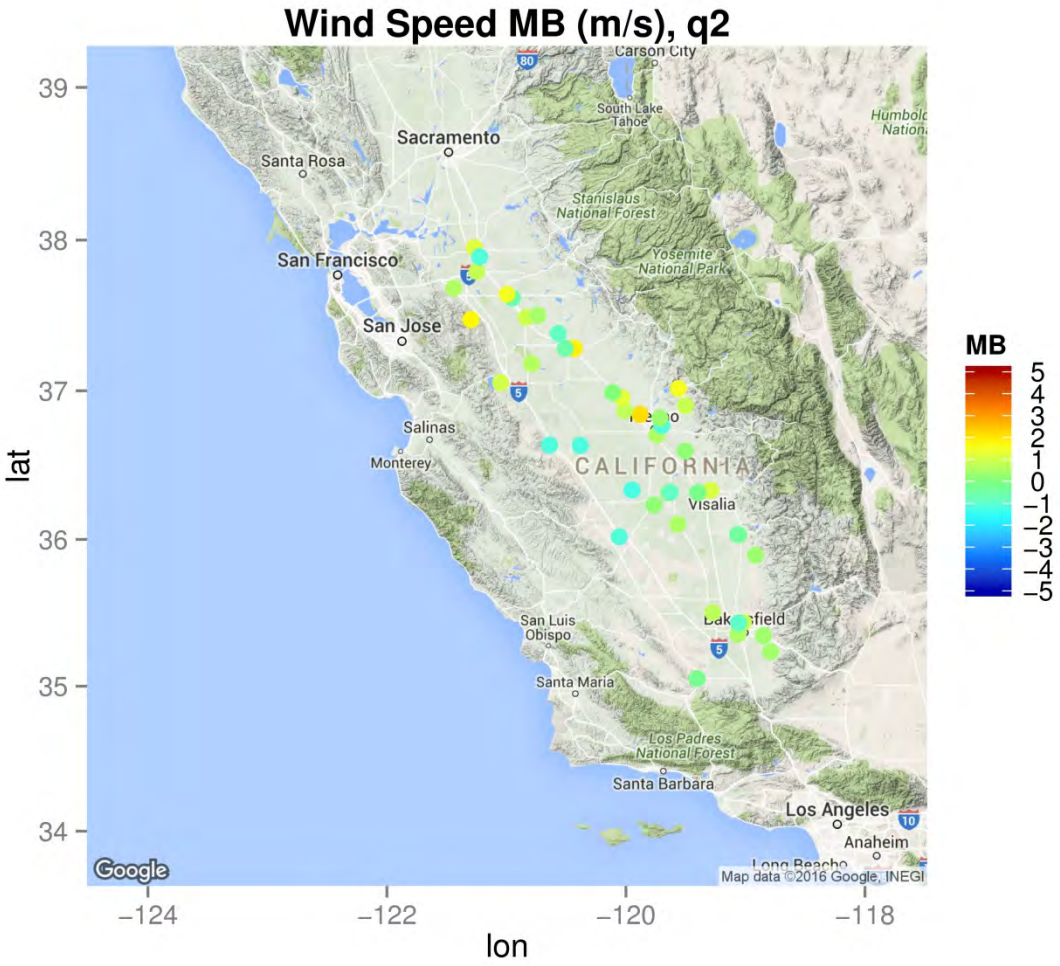

Figure S. 14 Hourly wind speed mean bias in the second quarter of 2013

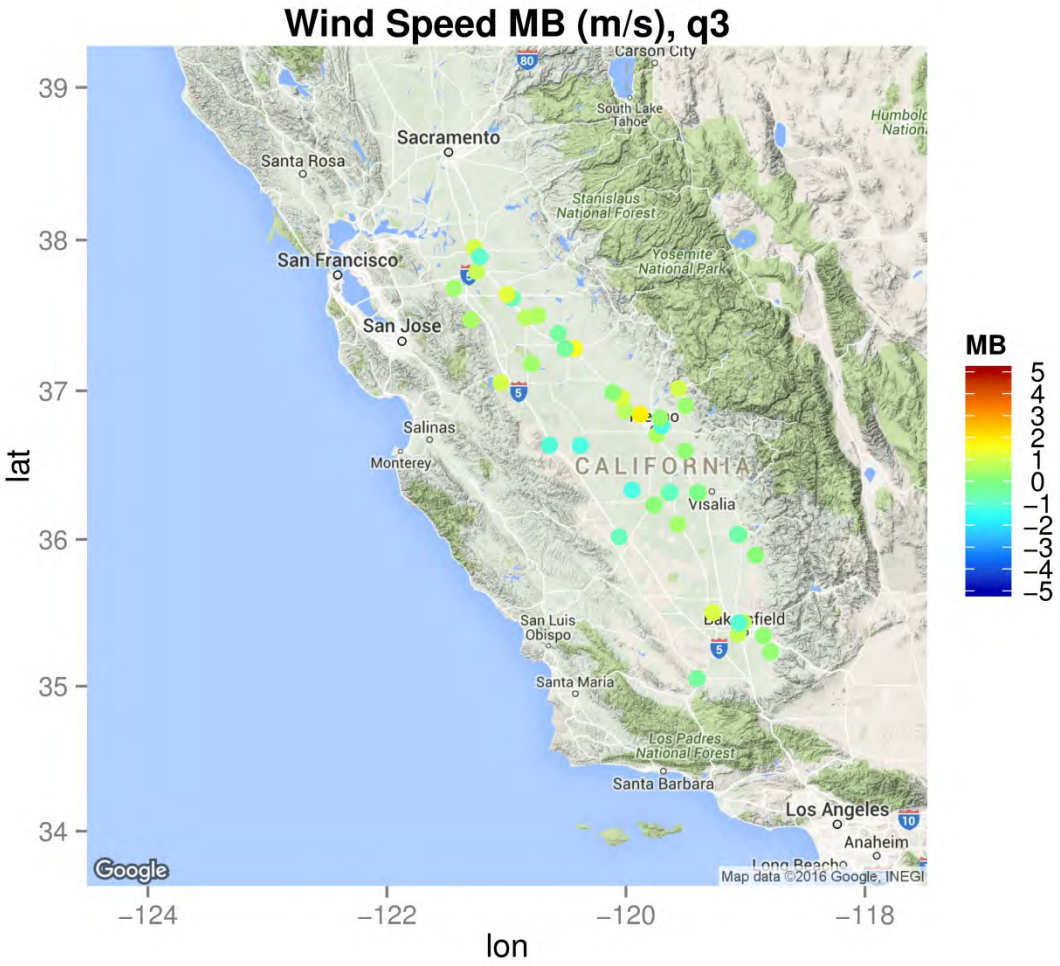

Figure S. 15 Hourly wind speed mean bias in the third quarter of 2013

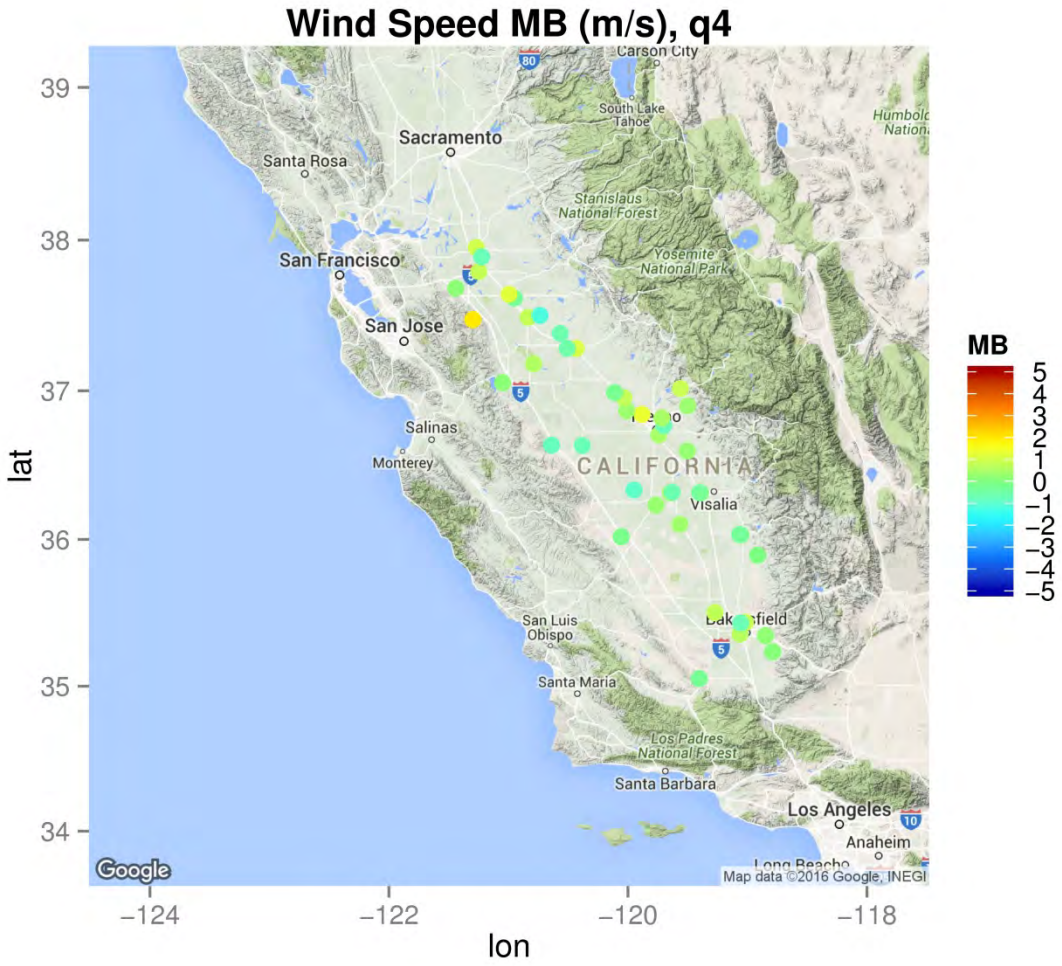

Figure S. 16 Hourly wind speed mean bias in the fourth quarter of 2013

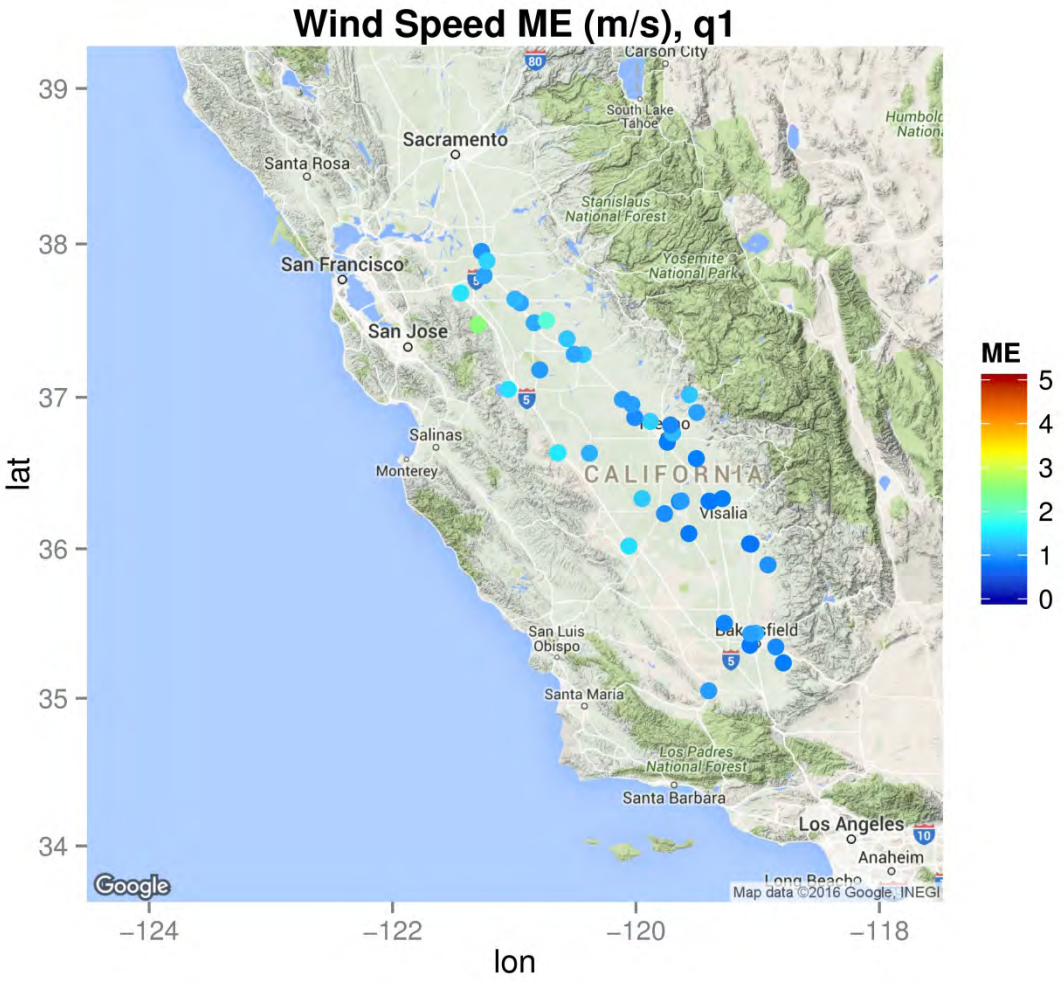

Figure S. 17 Hourly wind speed mean error in the first quarter of 2013

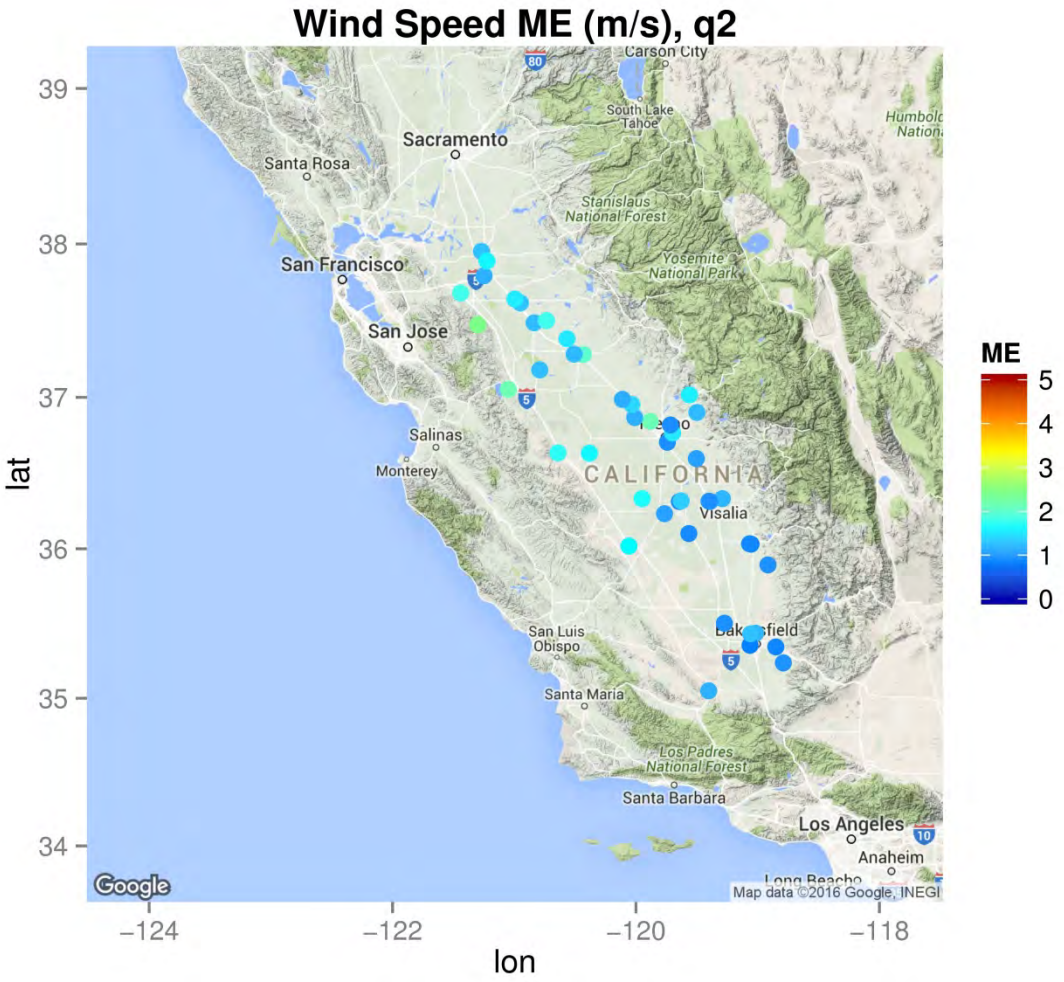

Figure S. 18 Hourly wind speed mean error in the second quarter of 2013

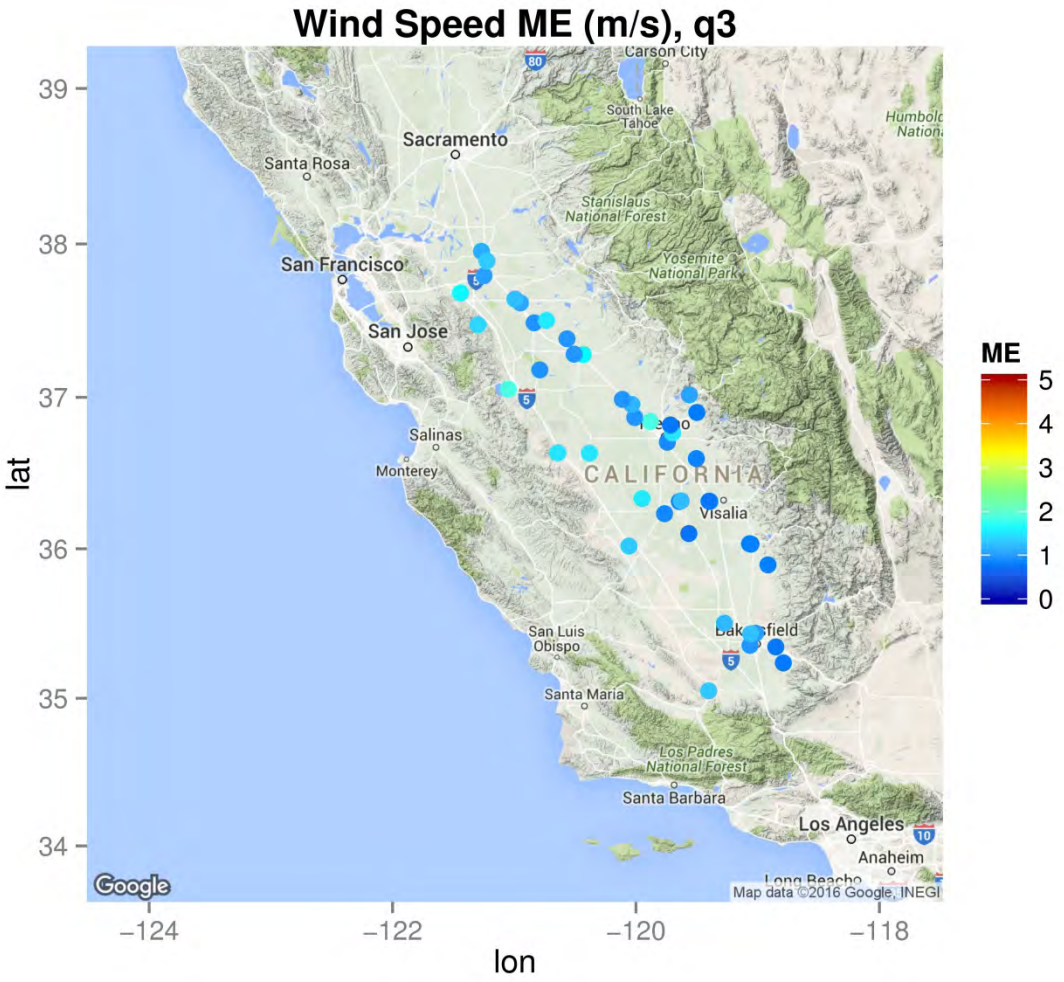

Figure S. 19 Hourly wind speed mean error in the third quarter of 2013

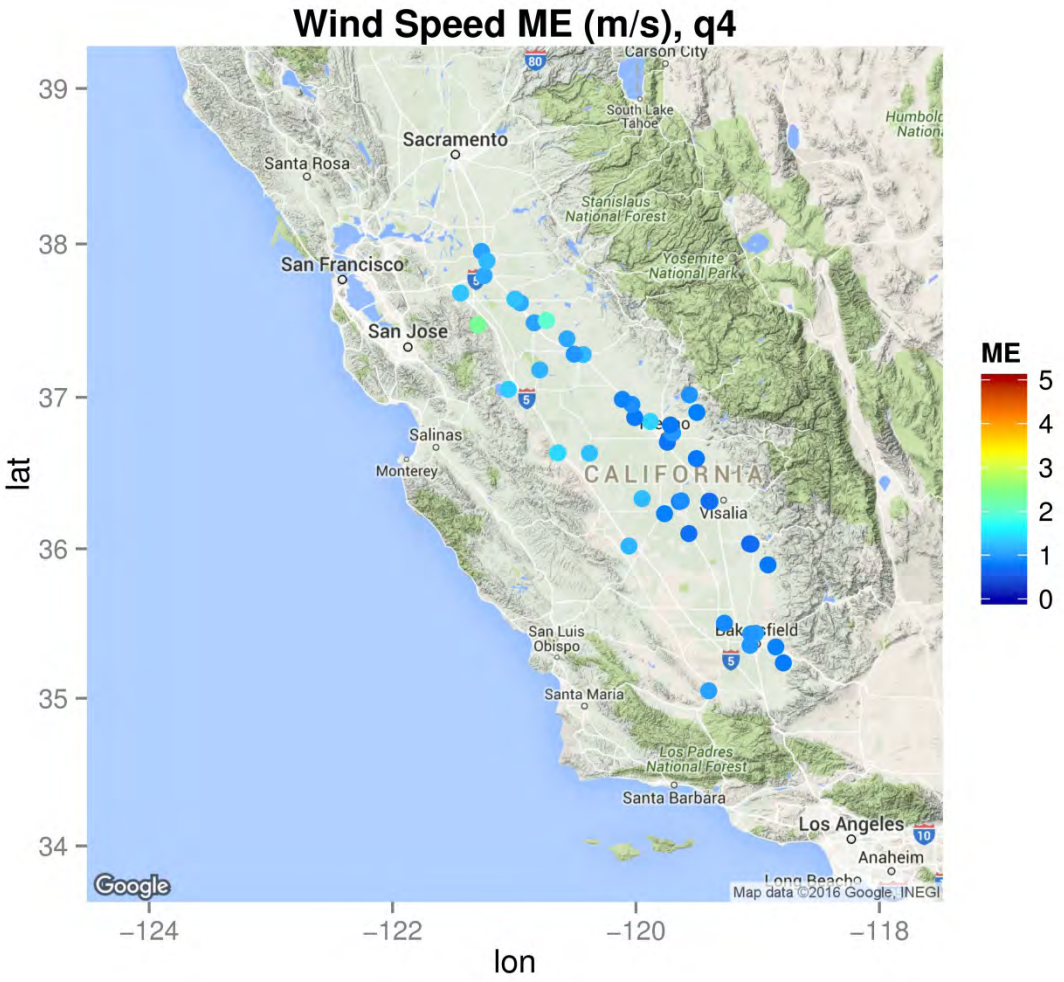

Figure S. 20 Hourly wind speed mean error in the fourth quarter of 2013

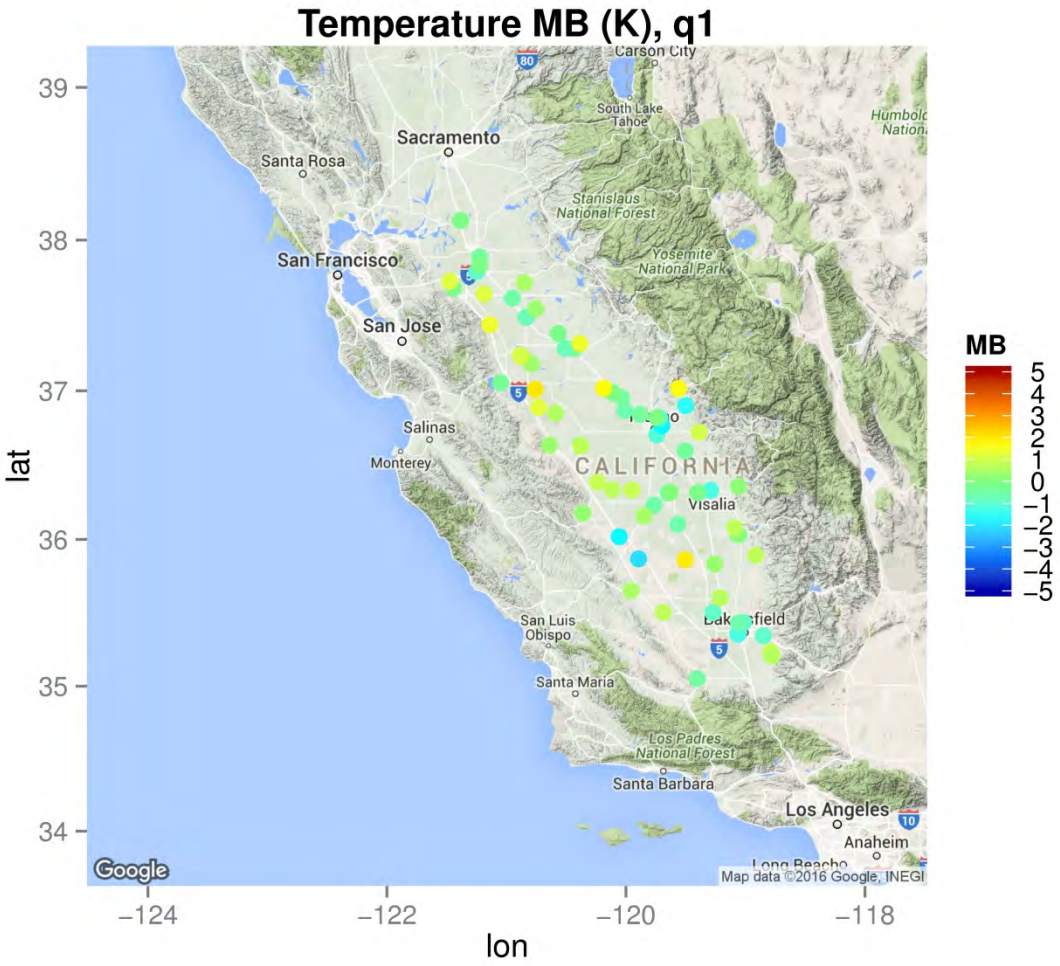

Figure S. 21 Hourly temperature mean bias in the first quarter of 2013

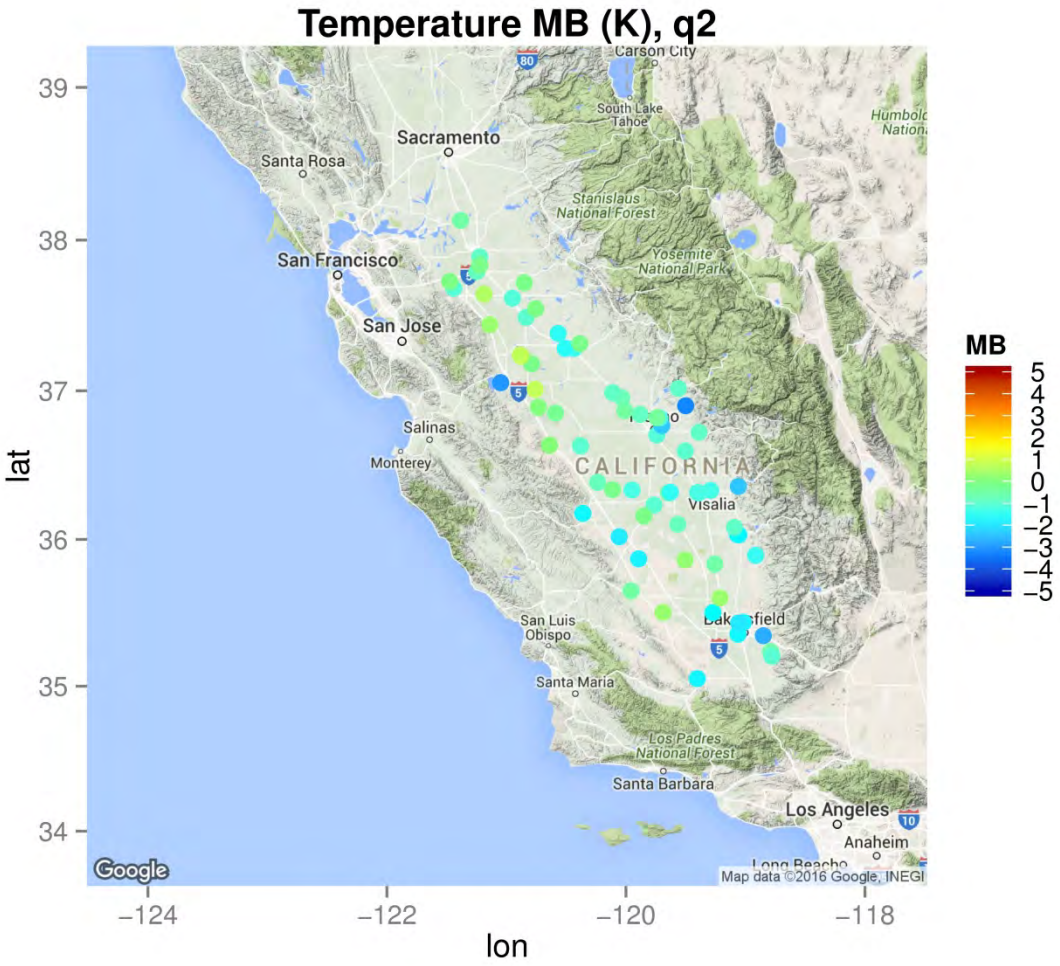

Figure S. 22 Hourly temperature mean bias in the second quarter of 2013

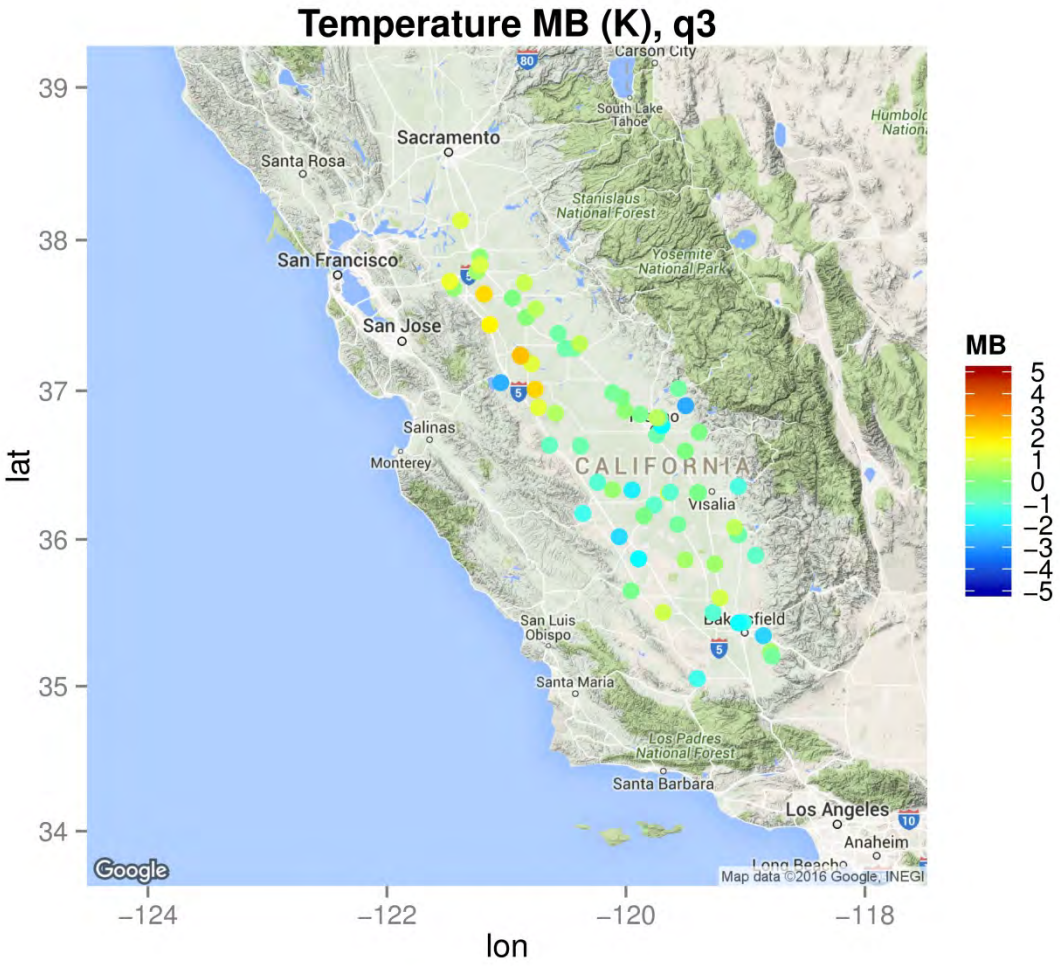

Figure S. 23 Hourly temperature mean bias in the third quarter of 2013

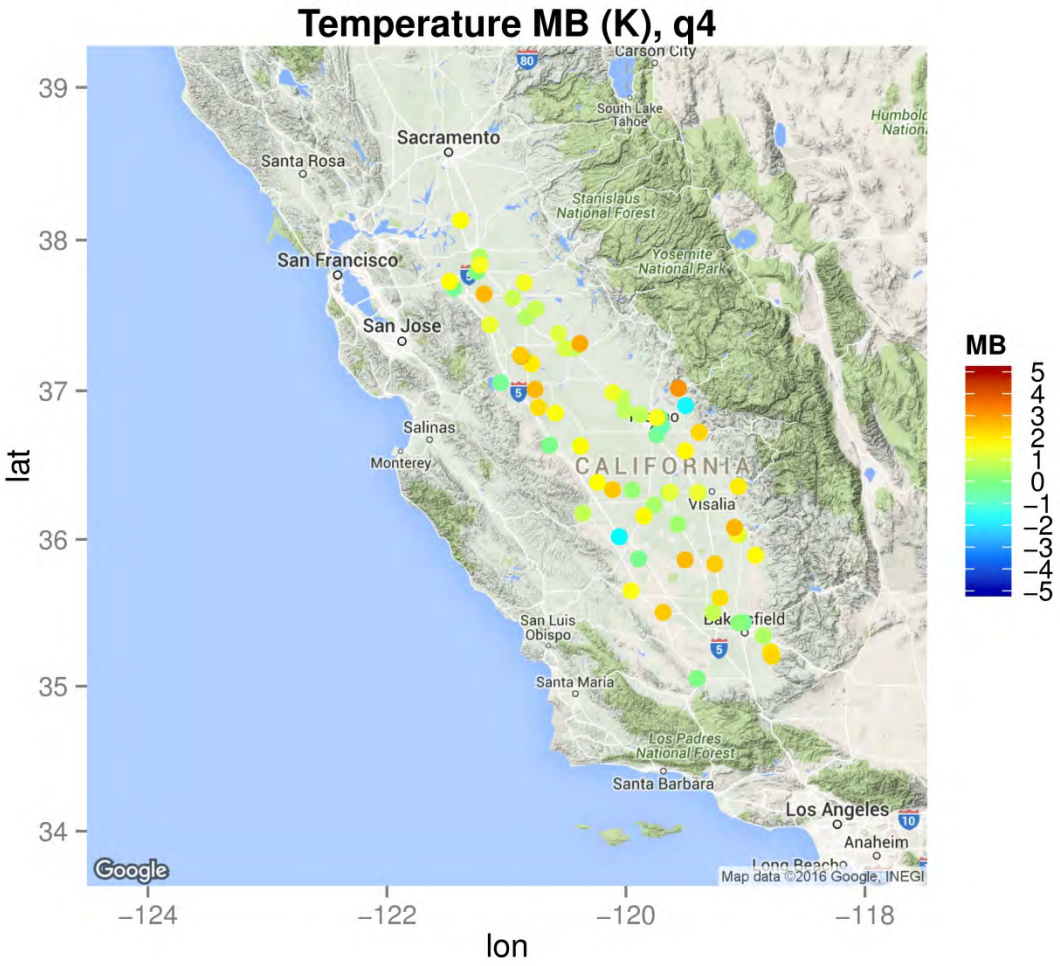

Figure S. 24 Hourly temperature mean bias in the fourth quarter of 2013

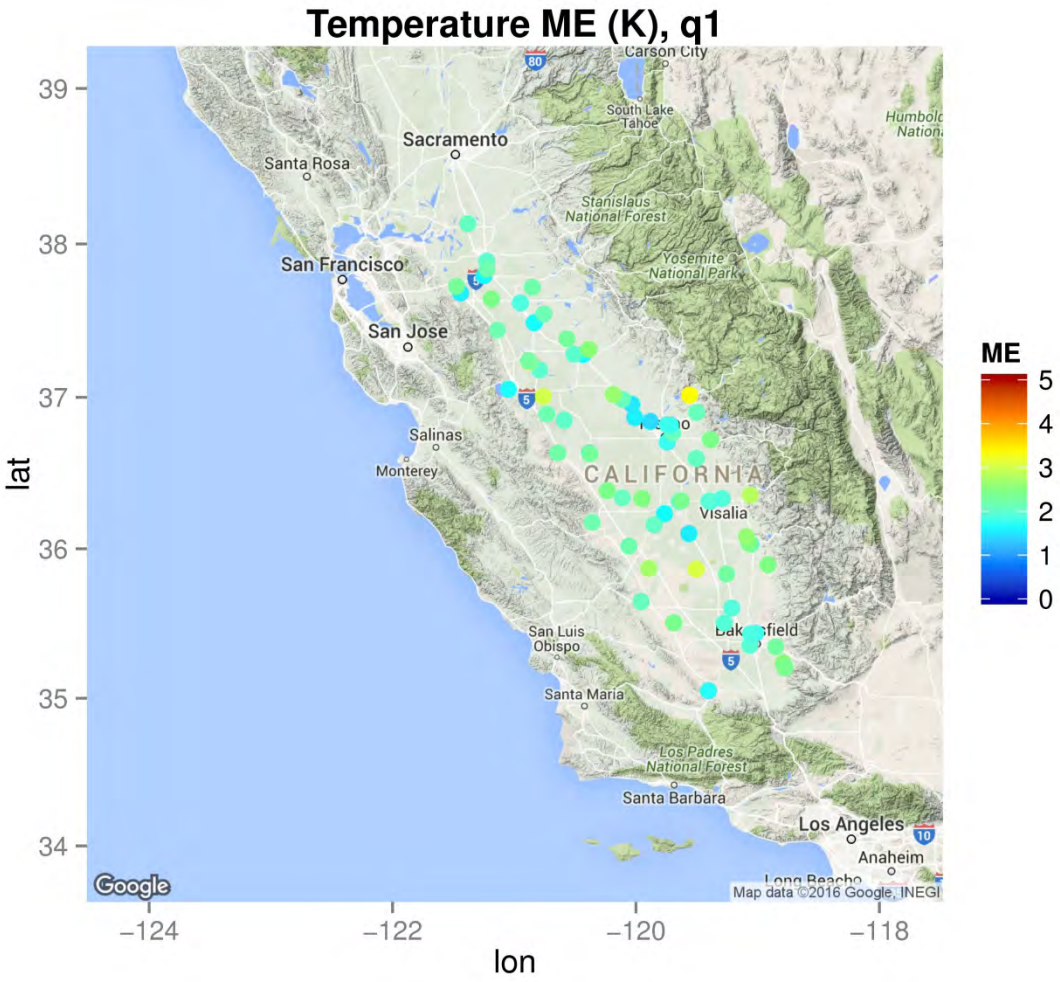

Figure S. 25 Hourly temperature mean error in the first quarter of 2013

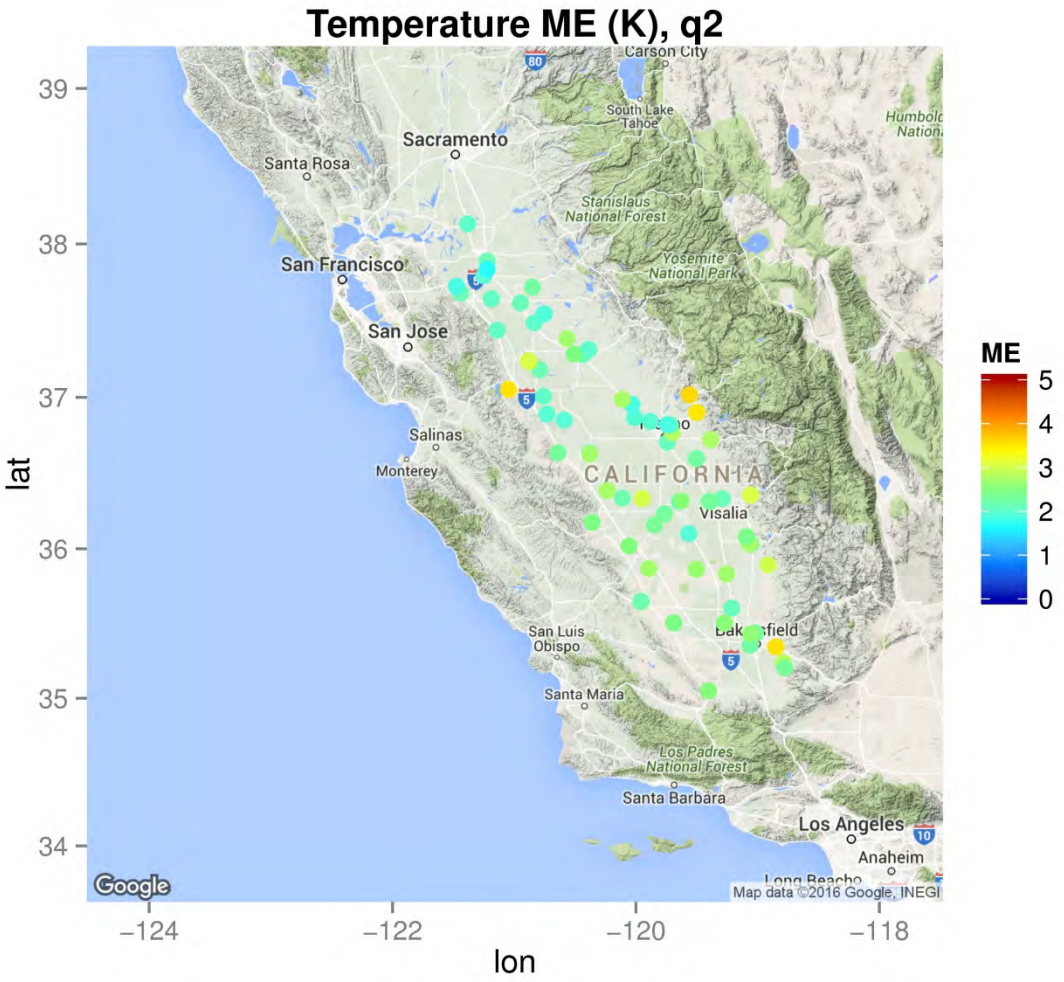

Figure S. 26 Hourly temperature mean error in the second quarter of 2013

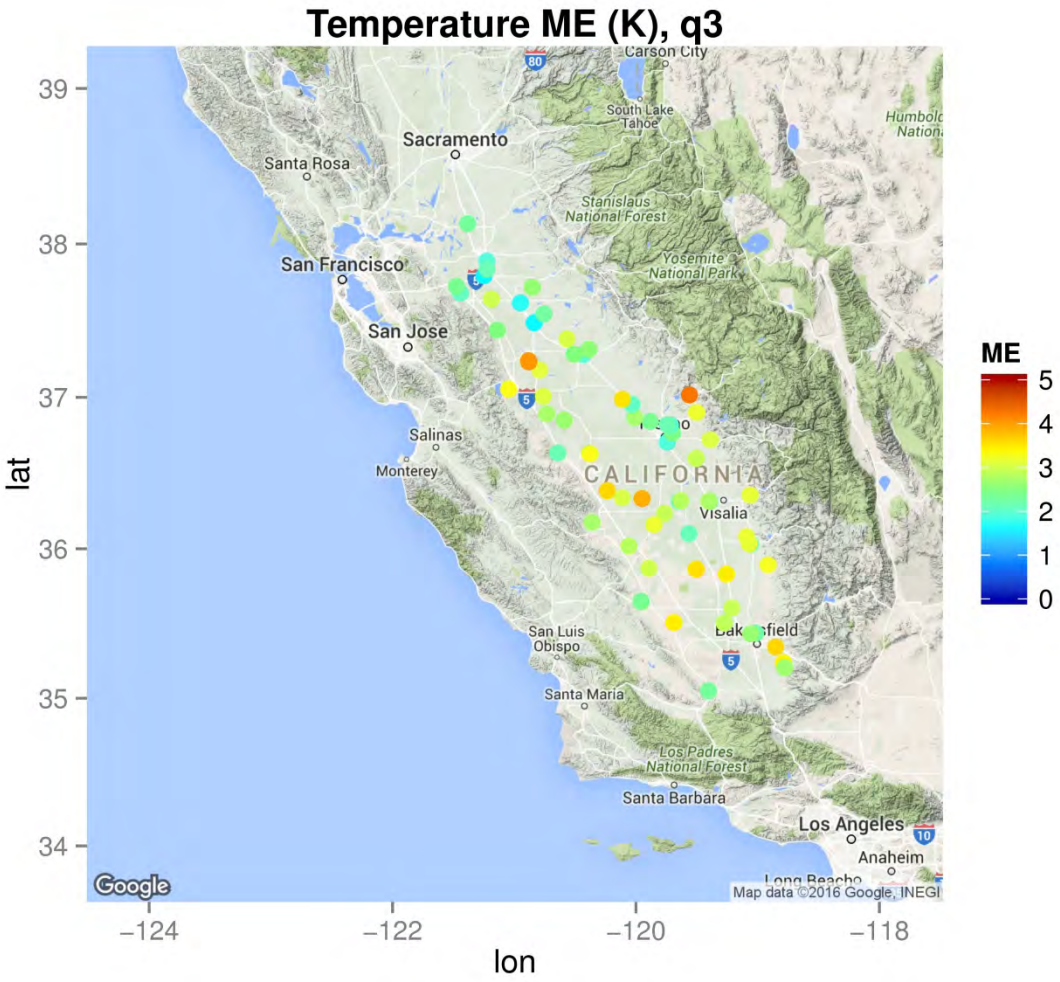

Figure S. 27 Hourly temperature mean error in the third quarter of 2013

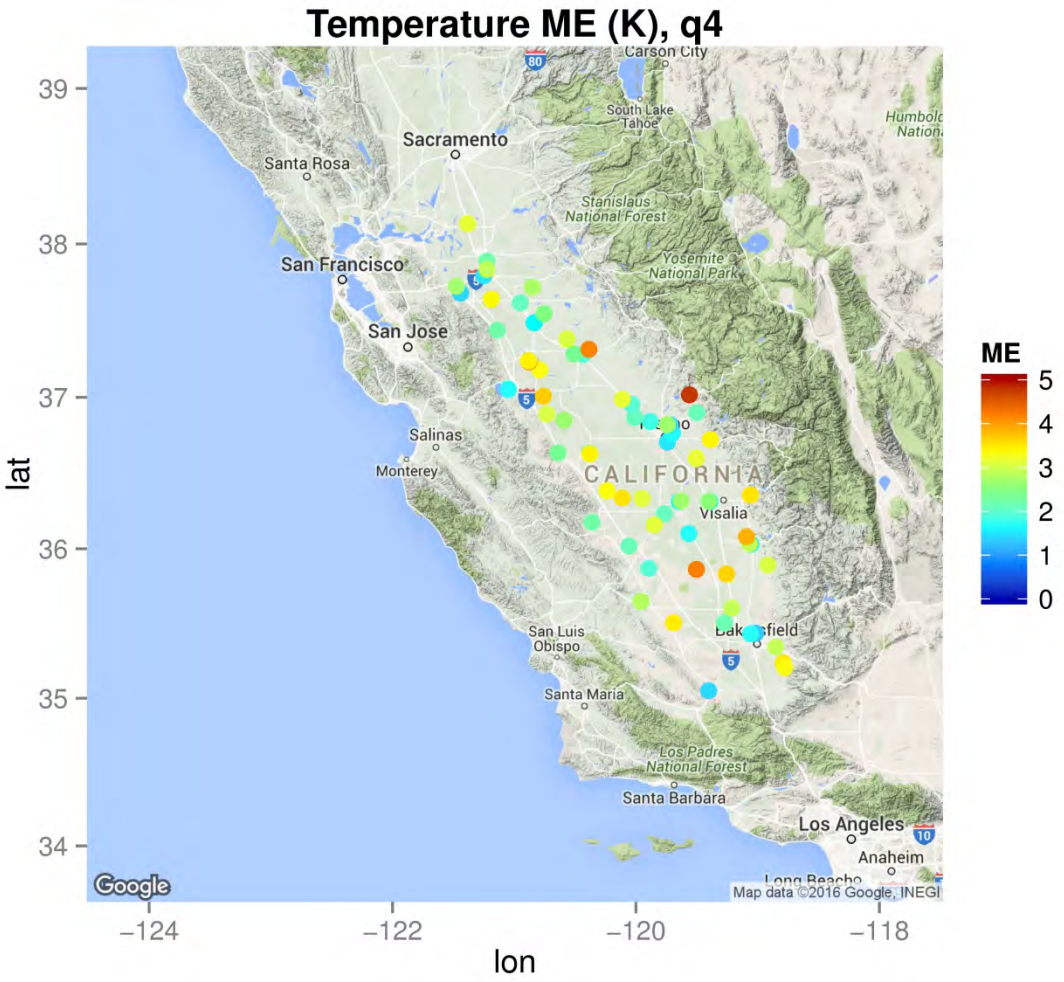

Figure S. 28 Hourly temperature mean error in the fourth quarter of 2013

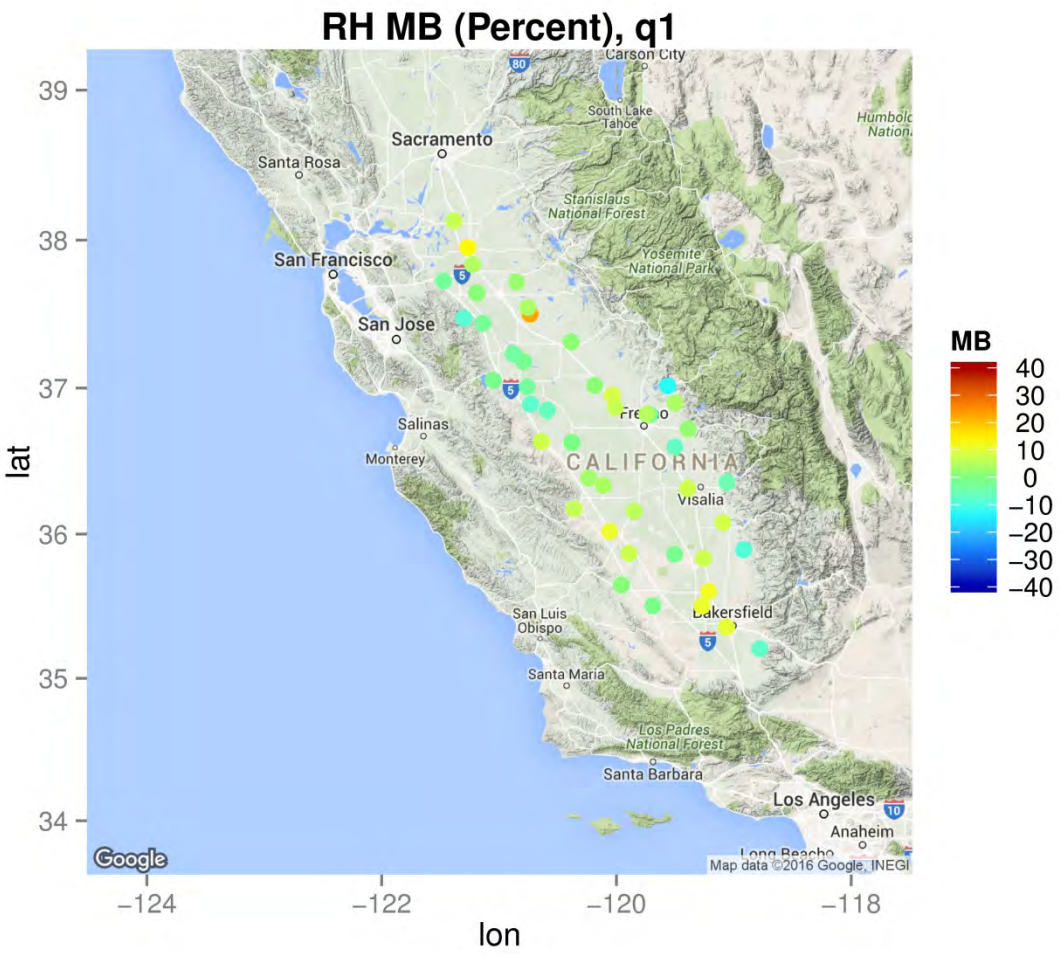

Figure S. 29 Hourly relative humidity mean bias in the first quarter of 2013

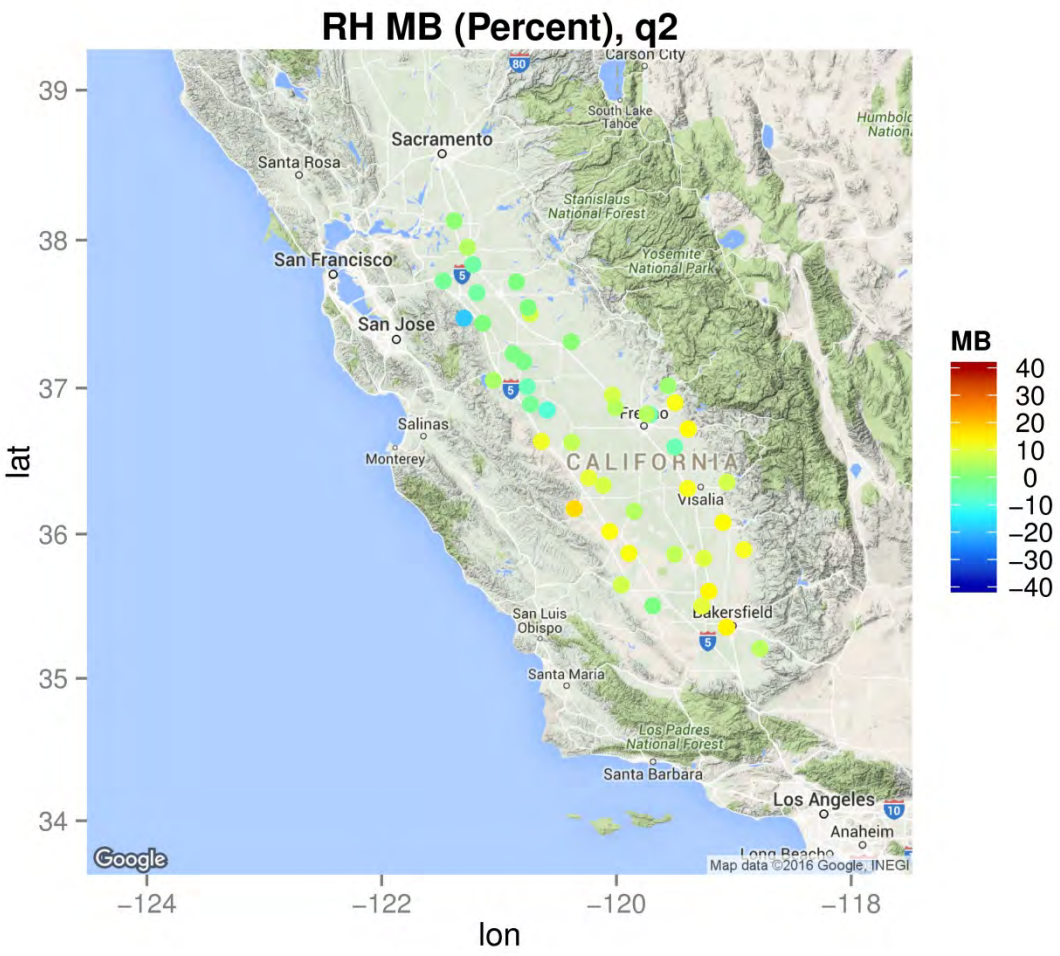

Figure S. 30 Hourly relative humidity mean bias in the second quarter of 2013

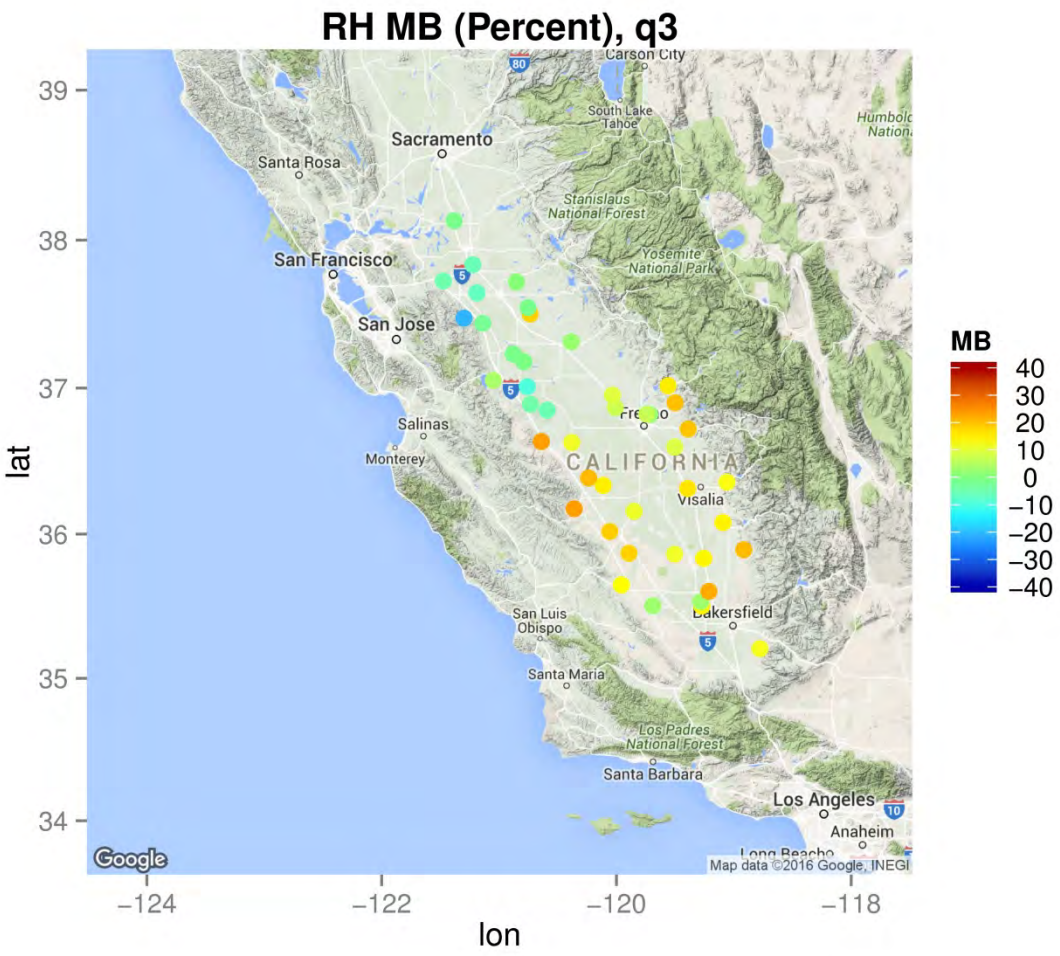

Figure S. 31 Hourly relative humidity mean bias in the third quarter of 2013

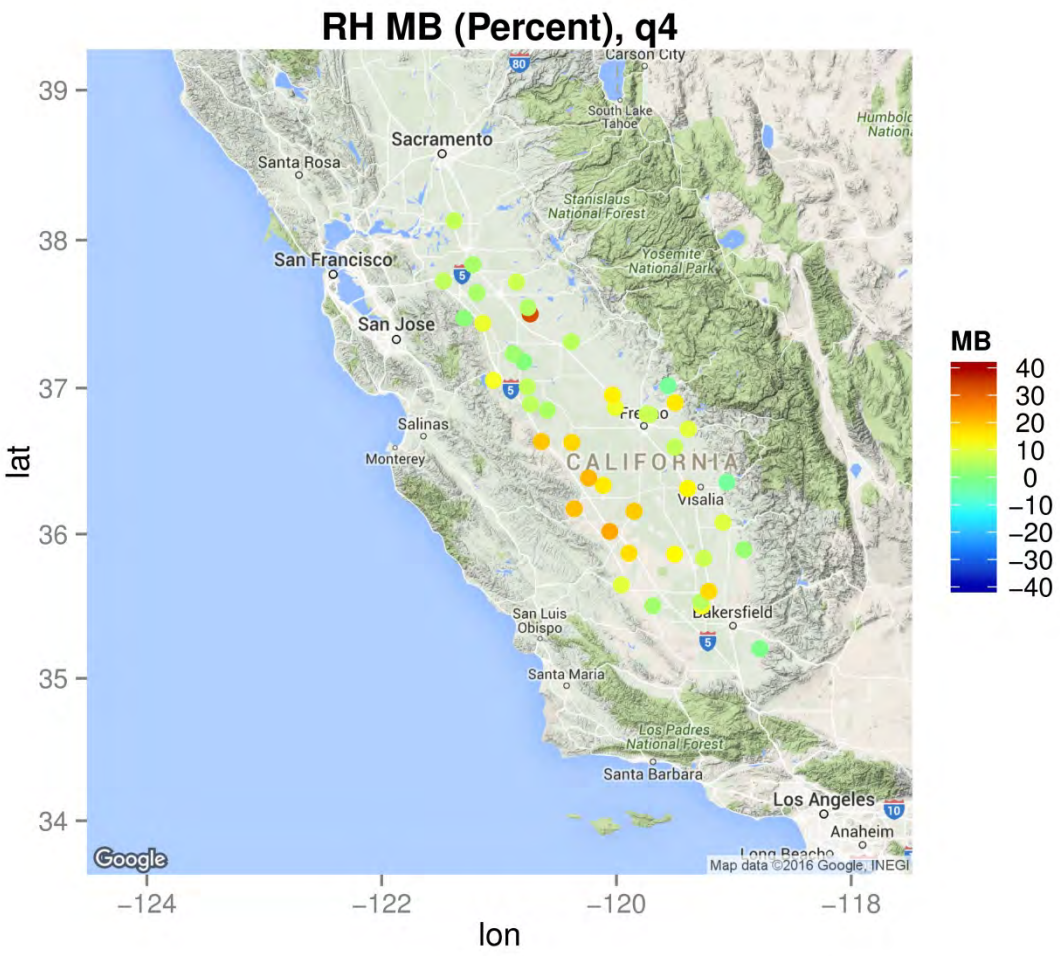

Figure S. 32 Hourly relative humidity mean bias in the fourth quarter of 2013

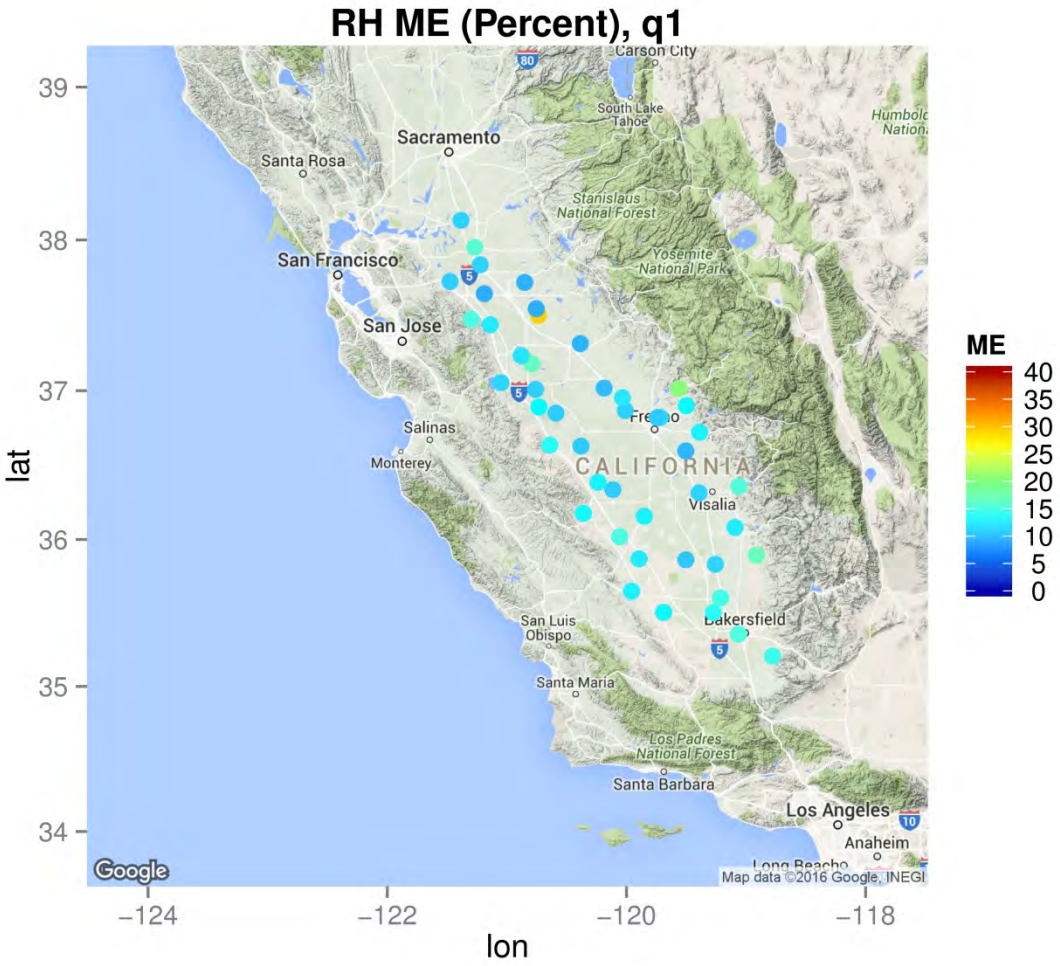

Figure S. 33 Hourly relative humidity mean error in the first quarter of 2013

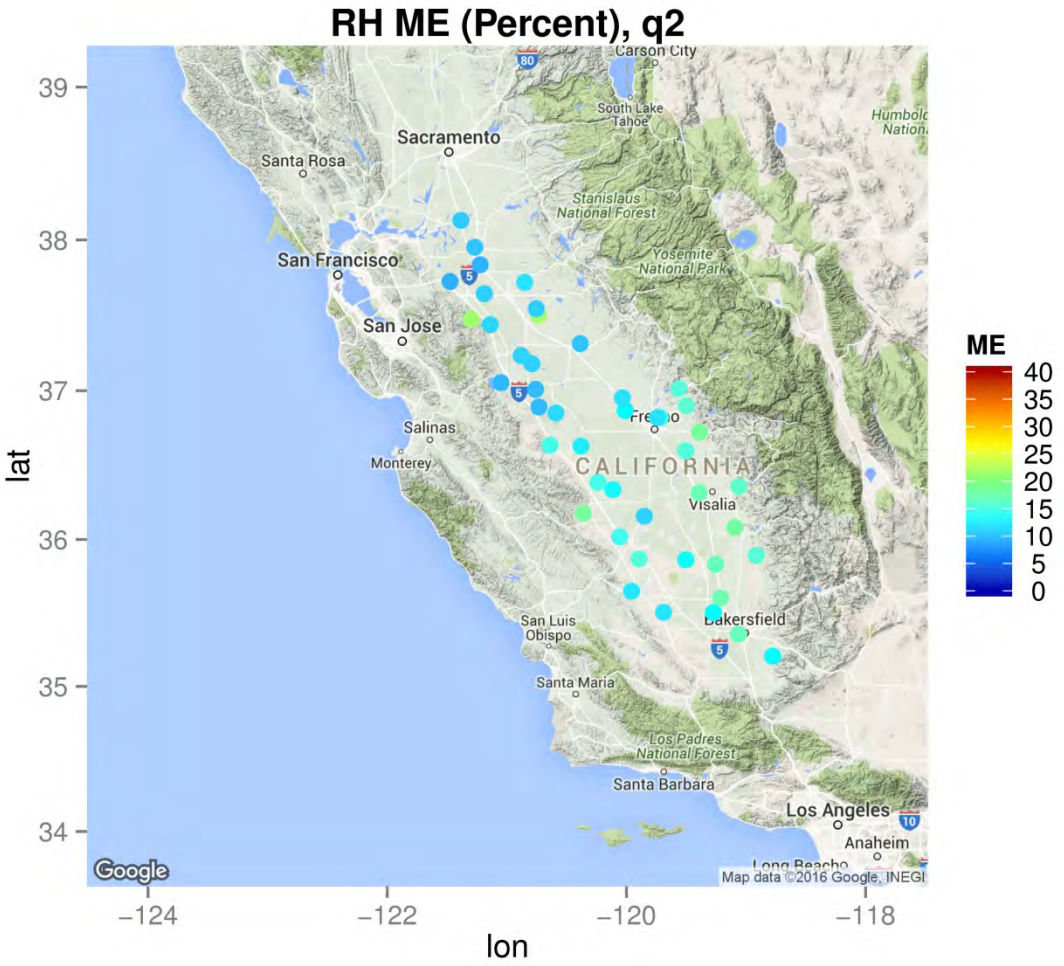

Figure S. 34 Hourly relative humidity mean error in the second quarter of 2013

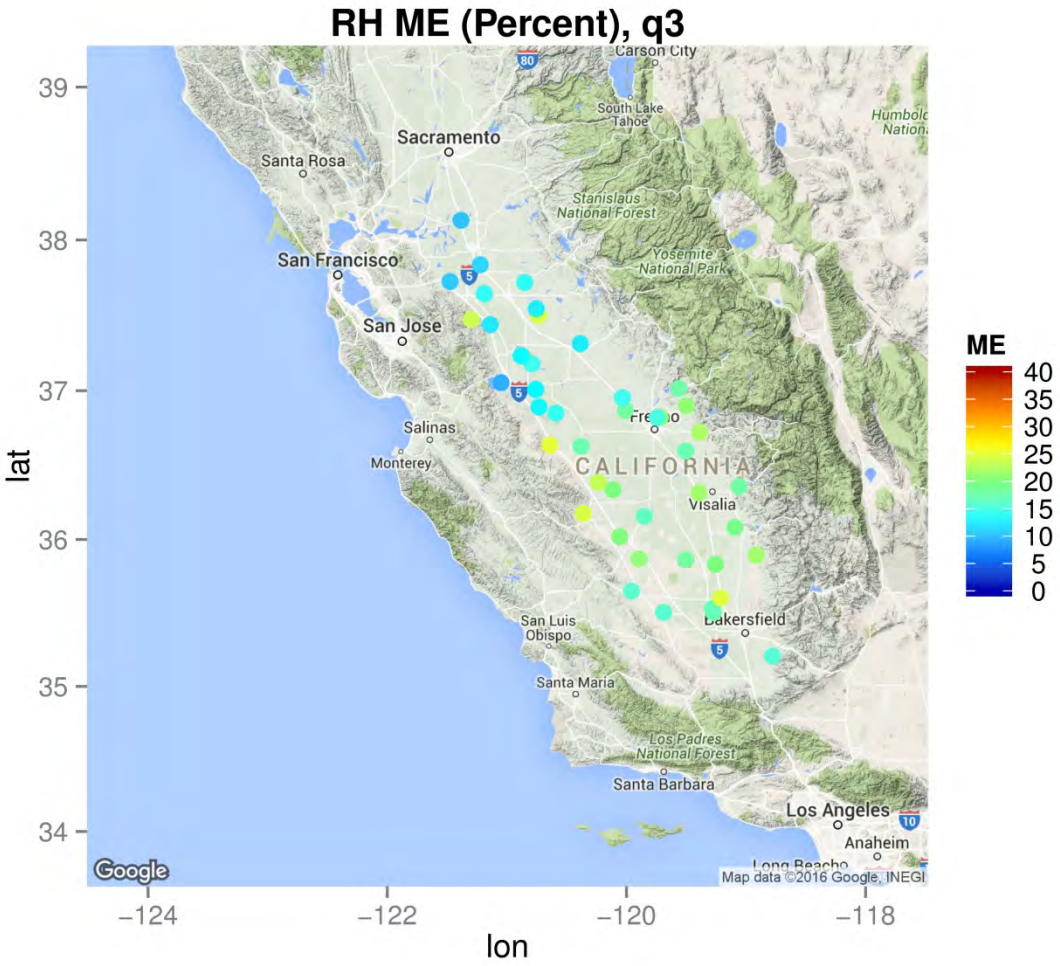

Figure S. 35 Hourly relative humidity mean error in the third quarter of 2013

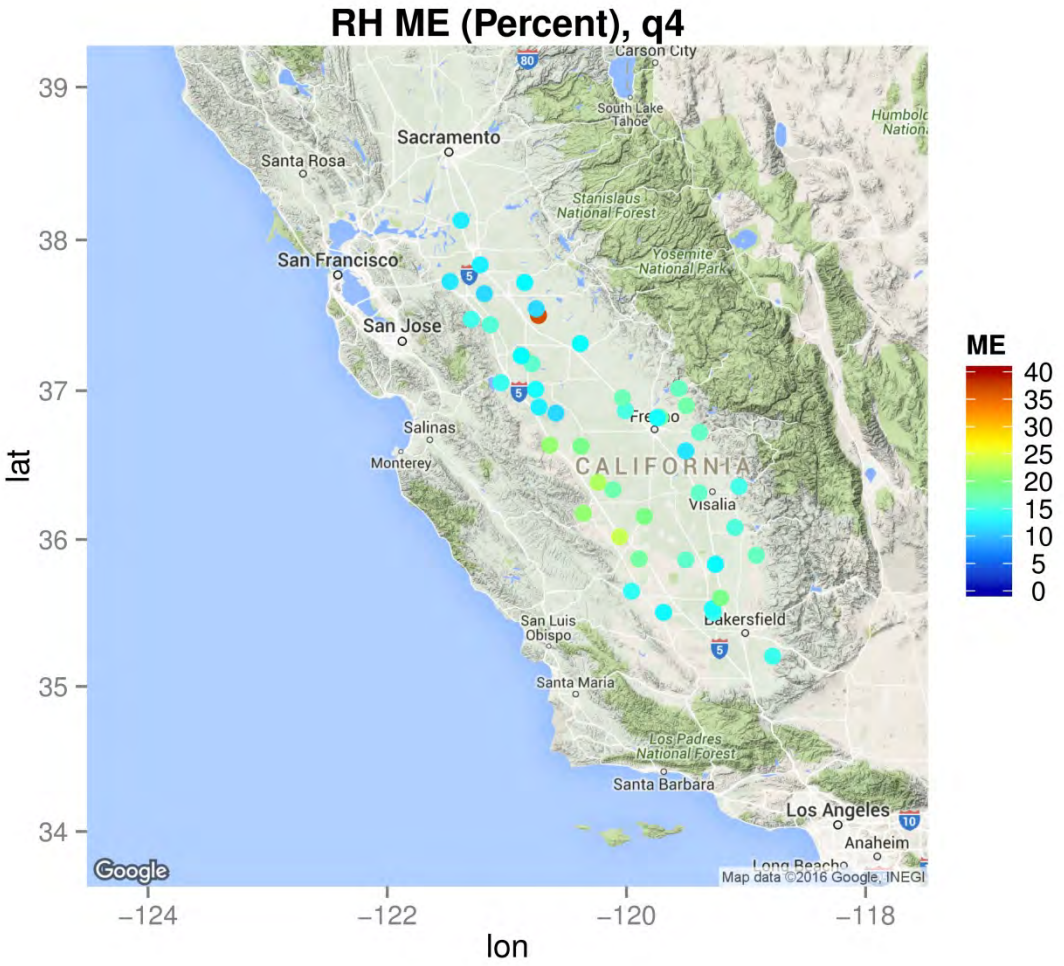

Figure S. 36 Hourly relative humidity mean error in the fourth quarter of 2013

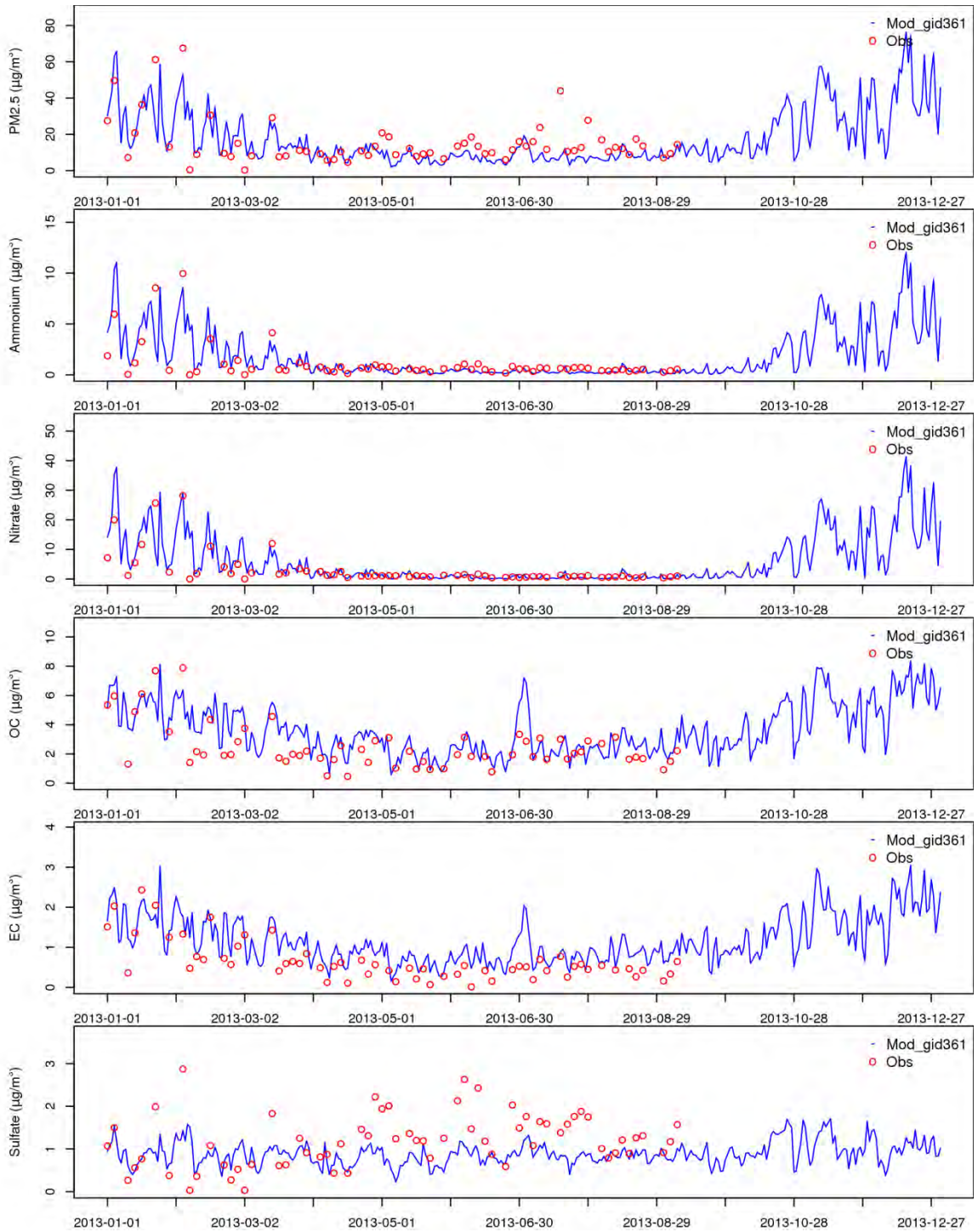

Figure S. 37 Comparison of time series of observed (from CSN measurement) and modeled $PM_{2.5}$ species at Bakersfield

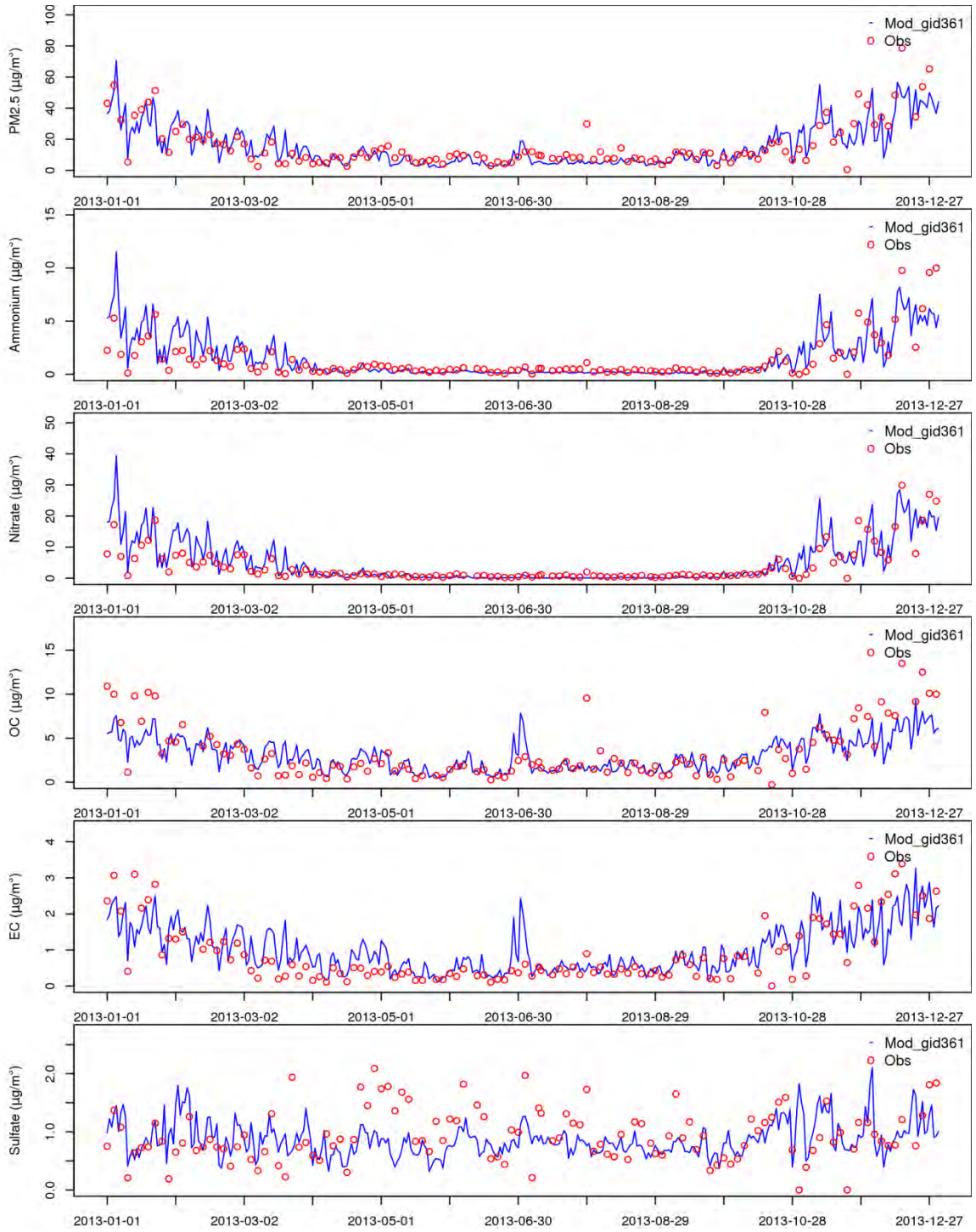

Figure S. 38 Comparison of time series of observed (from CSN measurement) and modeled $PM_{2.5}$ species at Fresno

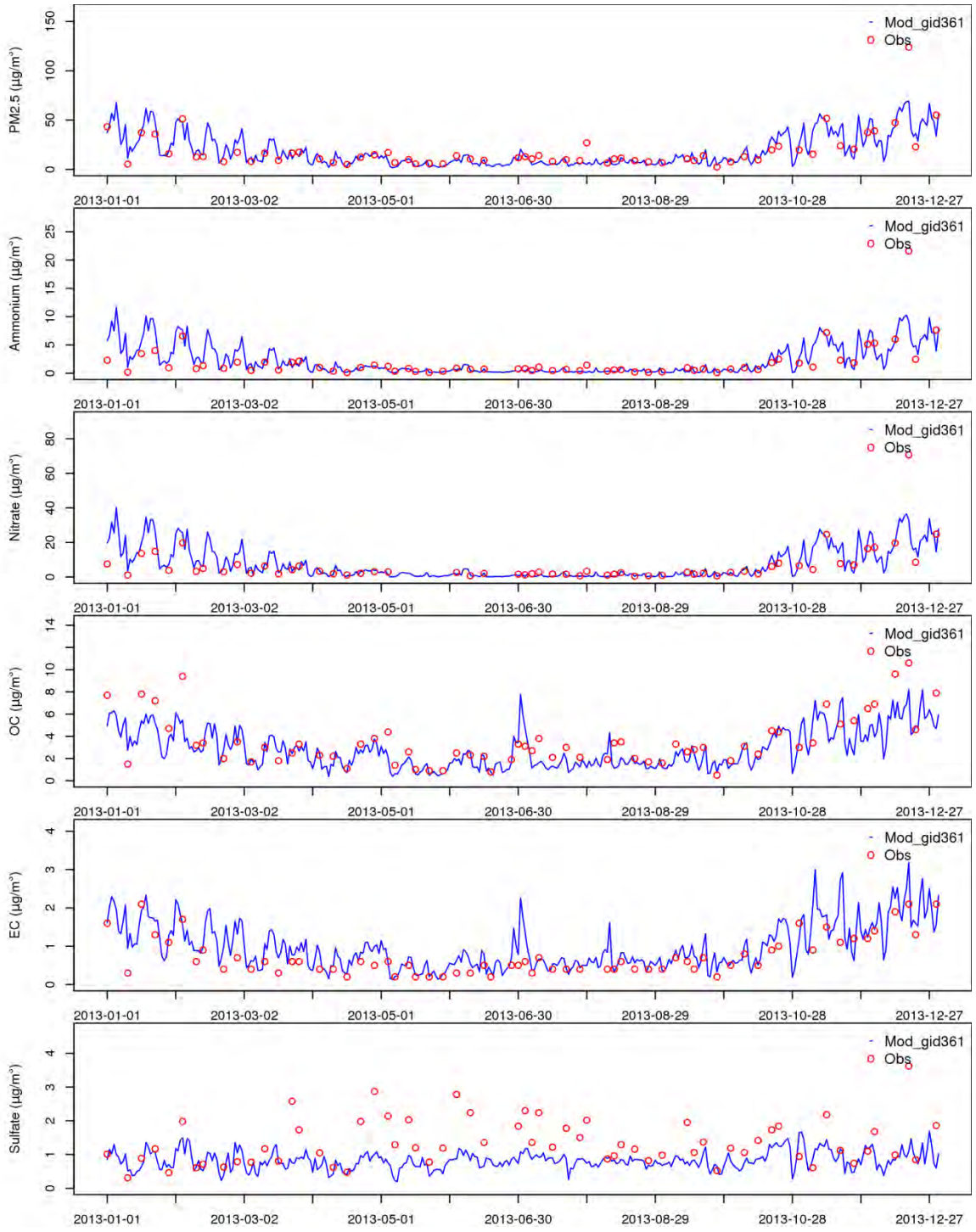

Figure S. 39 Comparison of time series of observed (from CSN measurement) and modeled $PM_{2.5}$ species at Visalia

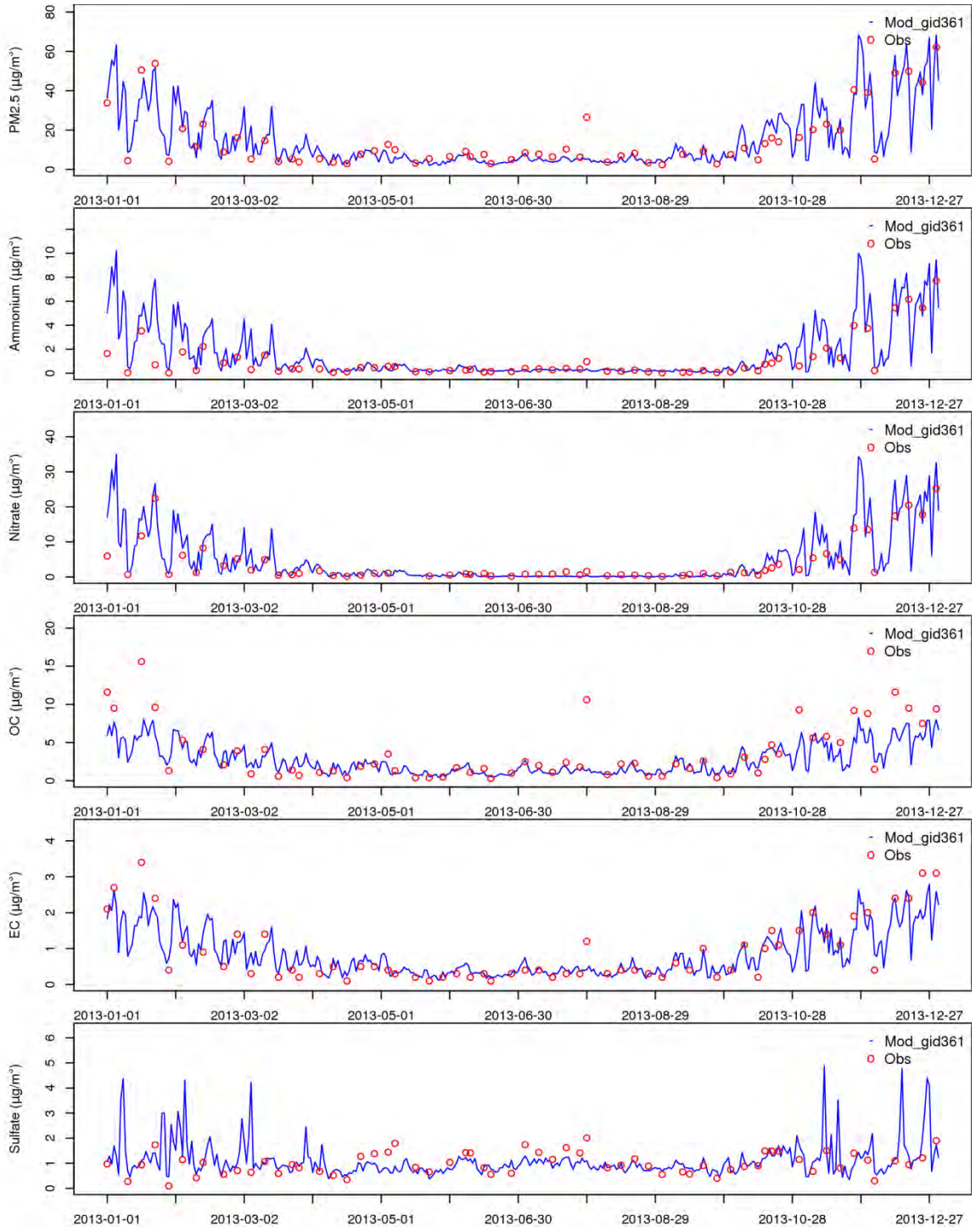

Figure S. 40 Comparison of time series of observed (from CSN measurement) and modeled $PM_{2.5}$ species at Modesto

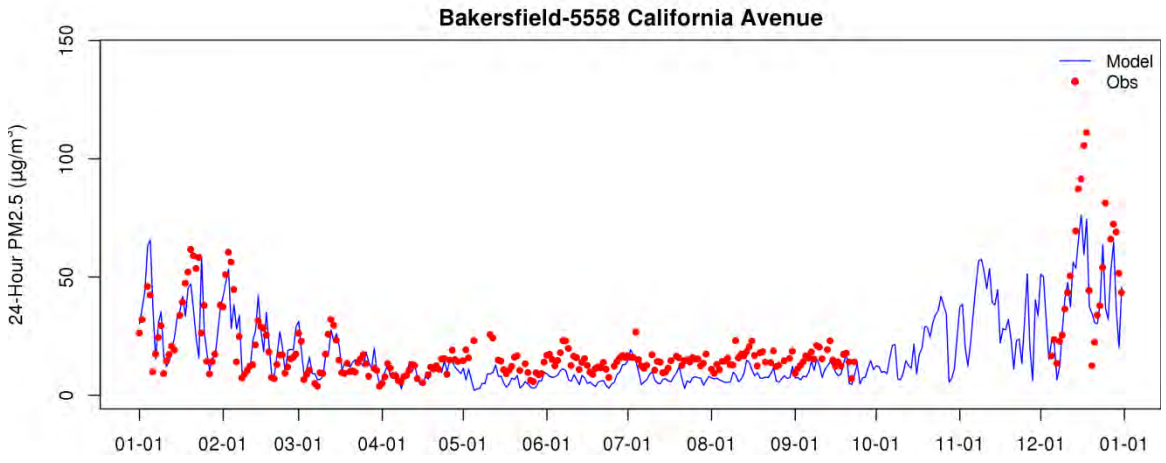

Figure S. 41 Observed and modeled 24-hour average $PM_{2.5}$ at Bakersfield – California Avenue.

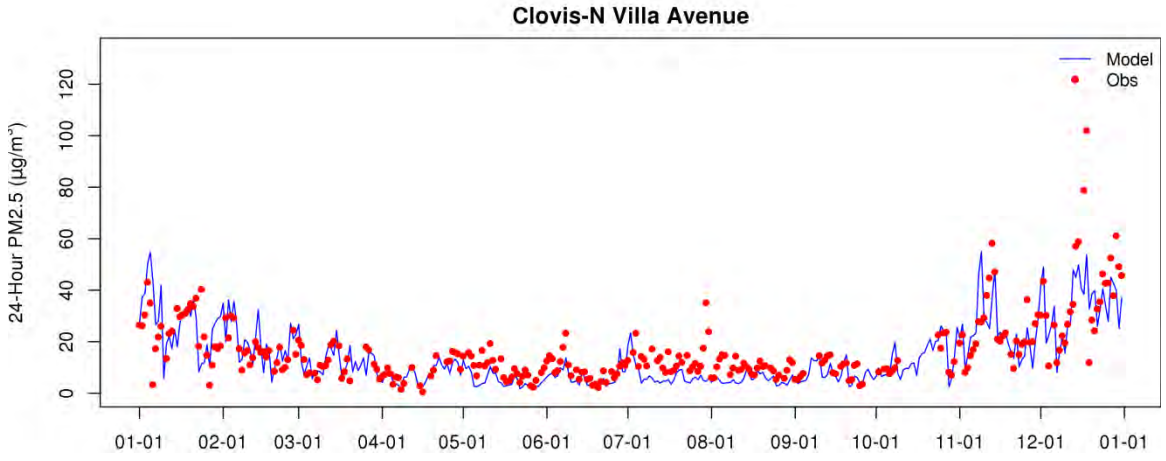

Figure S. 42 Observed and modeled 24-hour average $PM_{2.5}$ at Clovis – Villa Avenue

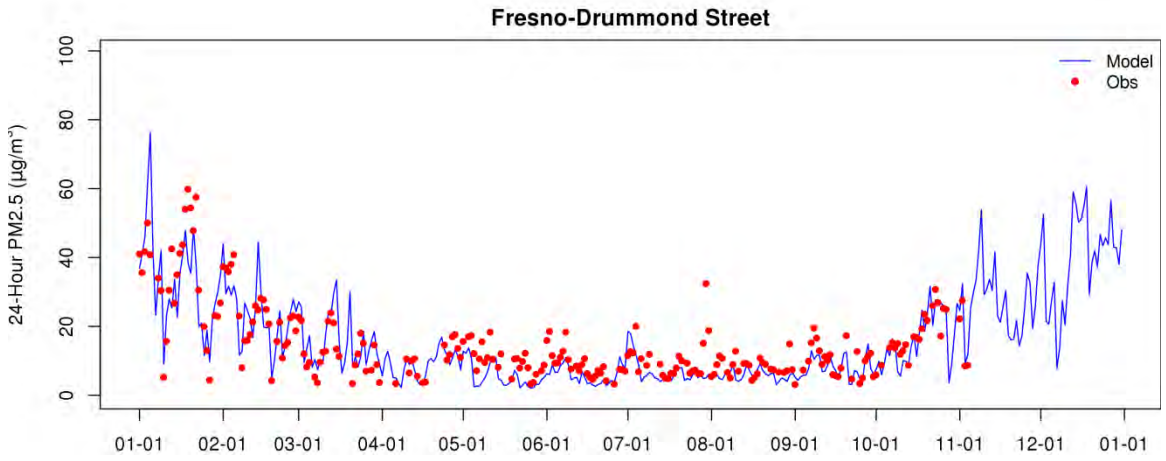

Figure S. 43 Observed and modeled 24-hour average $PM_{2.5}$ at Fresno – Drummond Street

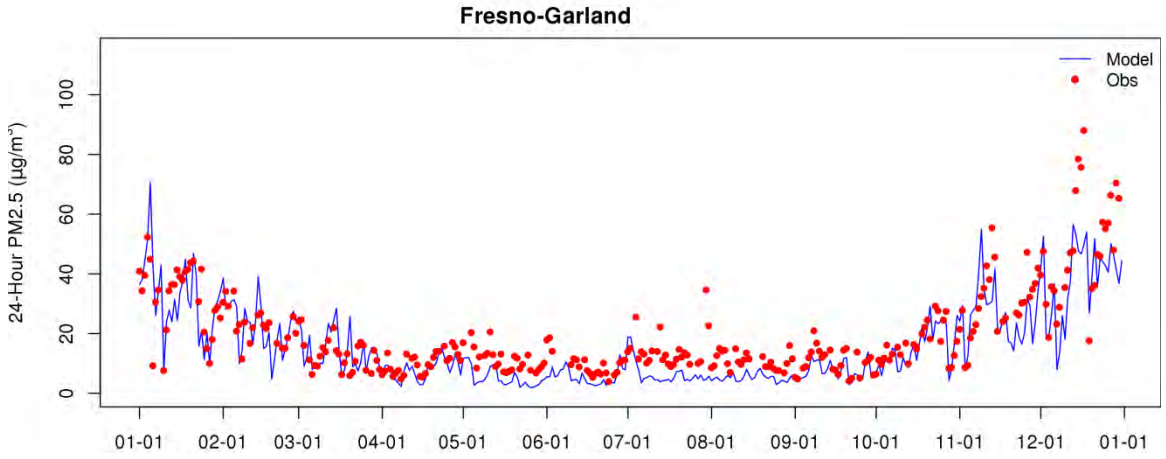

Figure S. 44 Observed and modeled 24-hour average $PM_{2.5}$ at Fresno – Garland

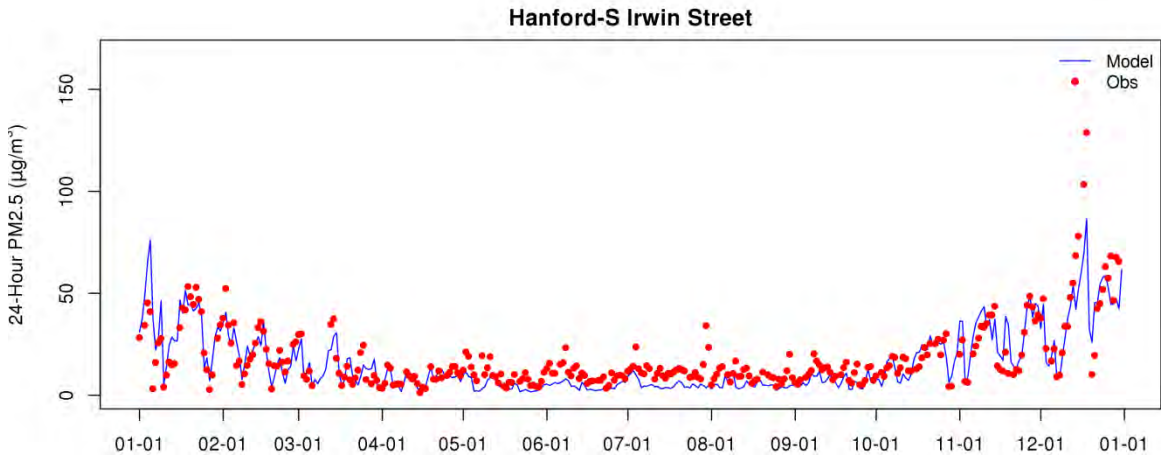

Figure S. 45 Observed and modeled 24-hour average $PM_{2.5}$ at Hanford – Irwin Street

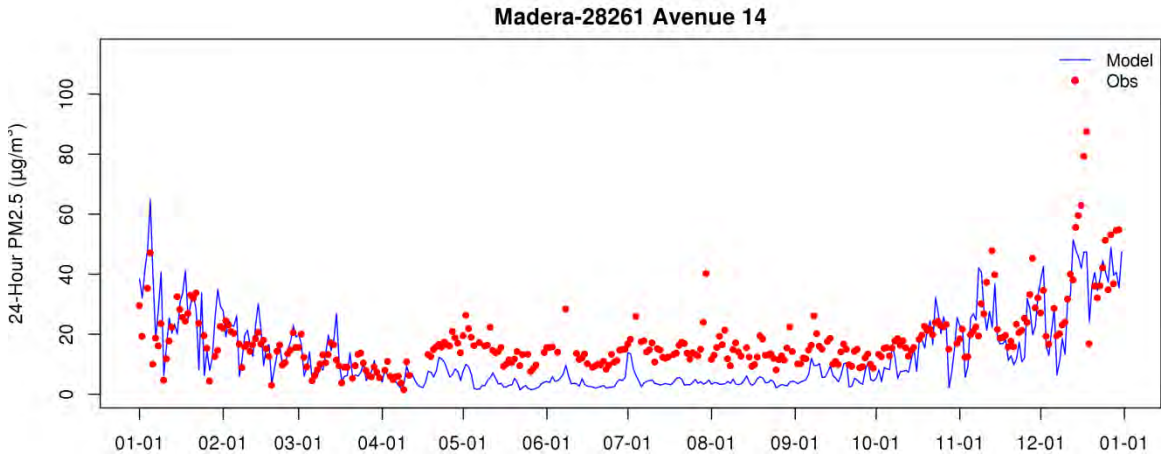

Figure S. 46 Observed and modeled 24-hour average $PM_{2.5}$ at Madera – Avenue 14

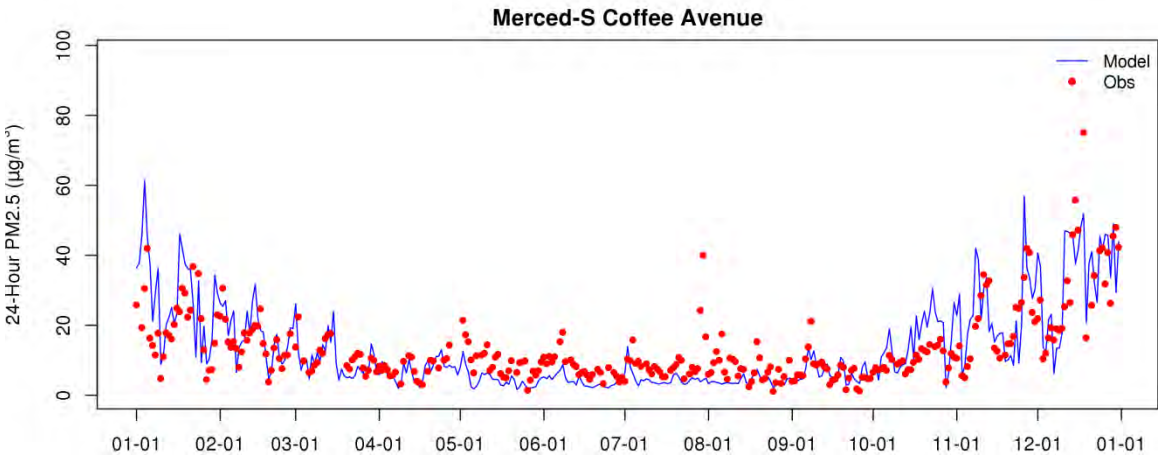

Figure S. 47 Observed and modeled 24-hour average $PM_{2.5}$ at Merced – S Coffee Avenue

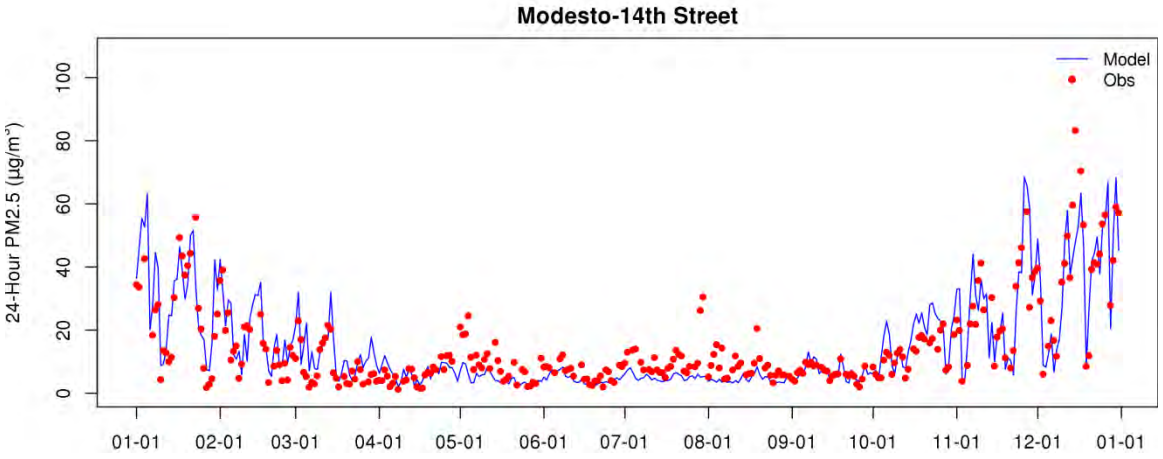

Figure S. 48 Observed and modeled 24-hour average $PM_{2.5}$ at Modesto – 14th Street

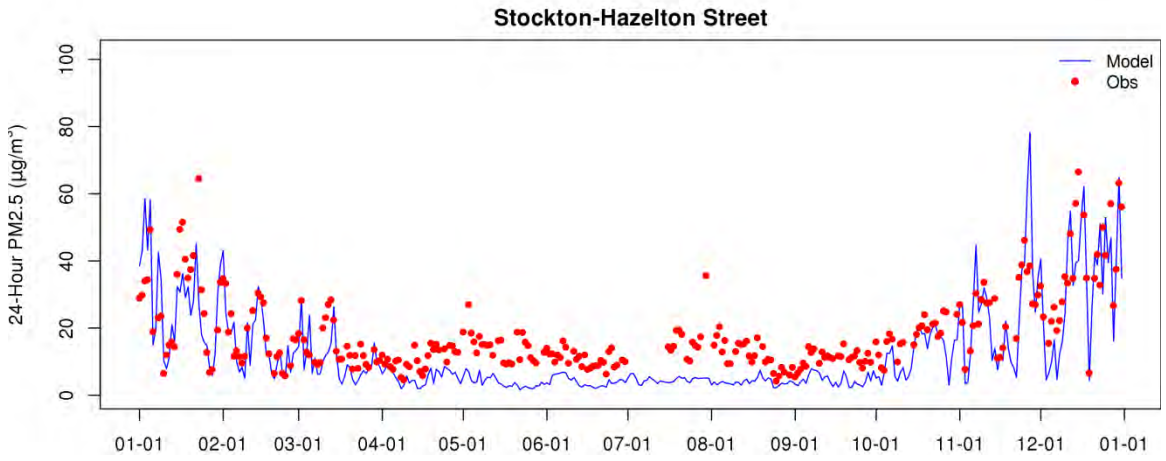

Figure S. 49 Observed and modeled 24-hour average $PM_{2.5}$ at Stockton – Hazelton Street

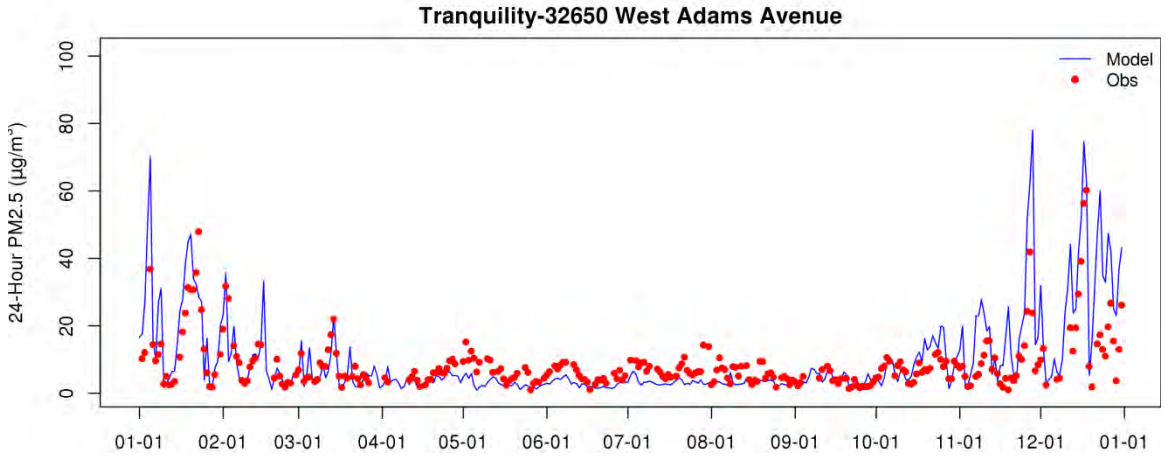

Figure S. 50 Observed and modeled 24-hour average $PM_{2.5}$ at Tranquility – West Adams Avenue

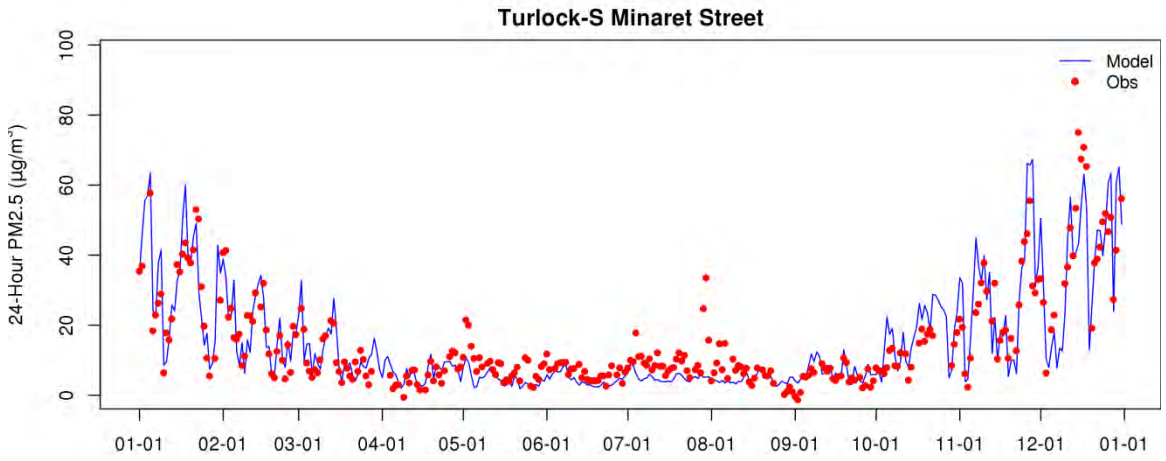

Figure S. 51 Observed and modeled 24-hour average $PM_{2.5}$ at Turlock – Minaret Street

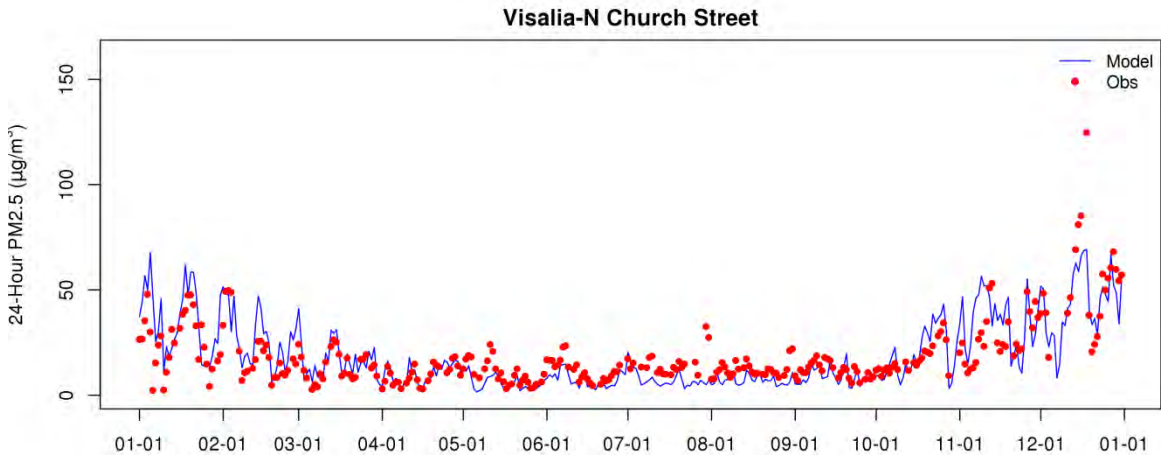

Figure S. 52 Observed and modeled 24-hour average $PM_{2.5}$ at Visalia – Church Street

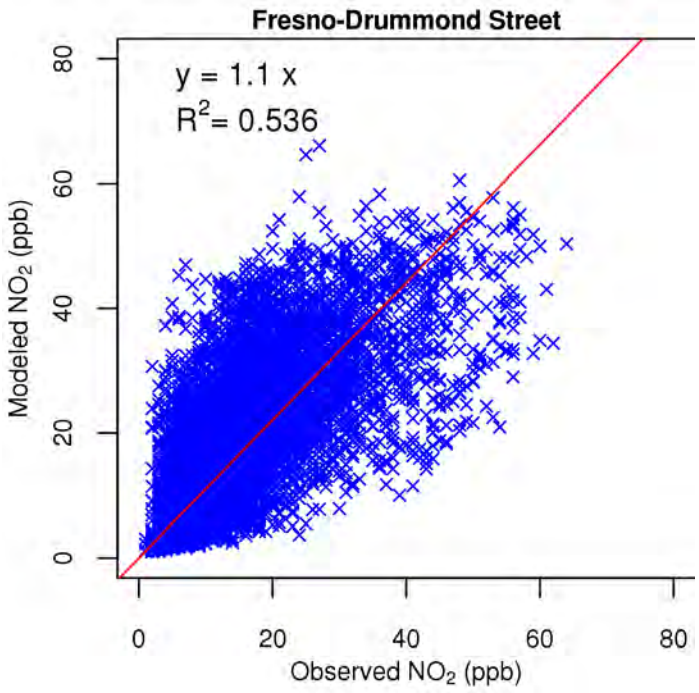

Figure S. 53 Scattering plot of observed and modeled 1-hour NO_2 mixing ratio at Fresno – Drummond Street

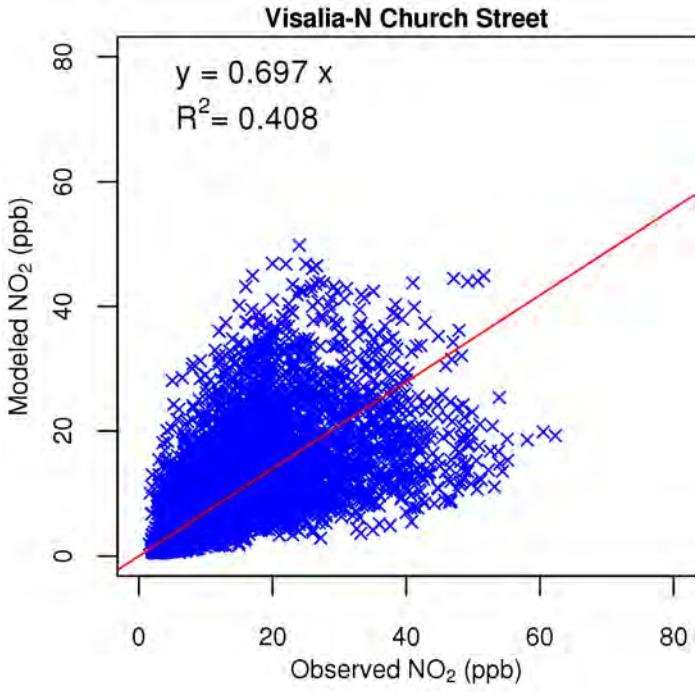

Figure S. 54 Scattering plot of observed and modeled 1-hour NO_2 mixing ratio at Visalia

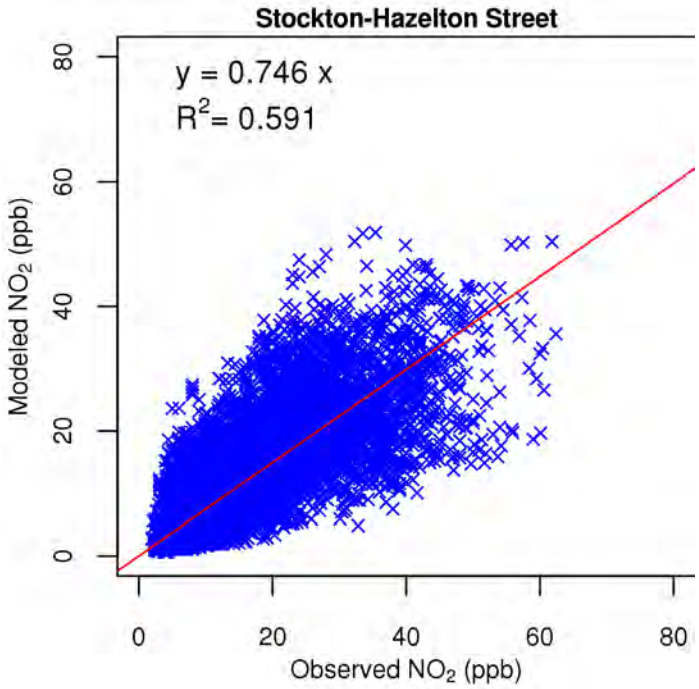

Figure S. 55 Scattering plot of observed and modeled 1-hour NO_2 mixing ratio at Stockton

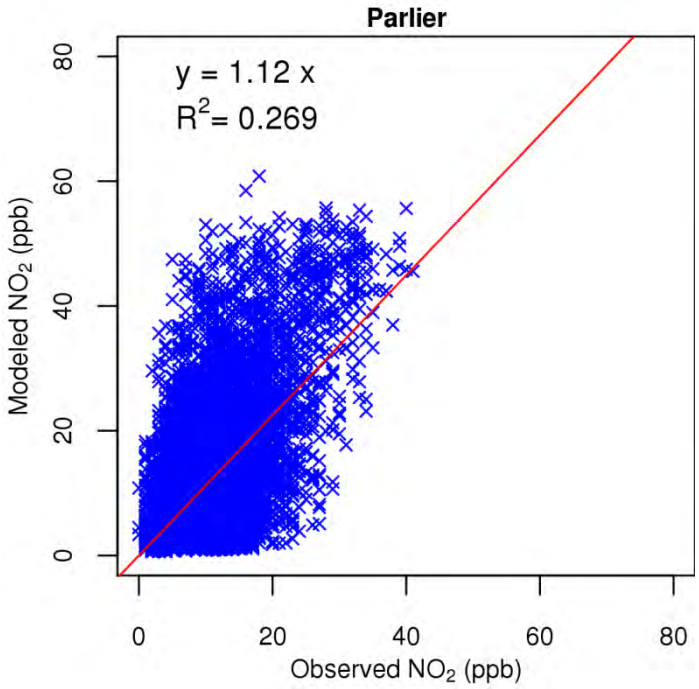

Figure S. 56 Scattering plot of observed and modeled 1-hour NO_2 mixing ratio at Parlier

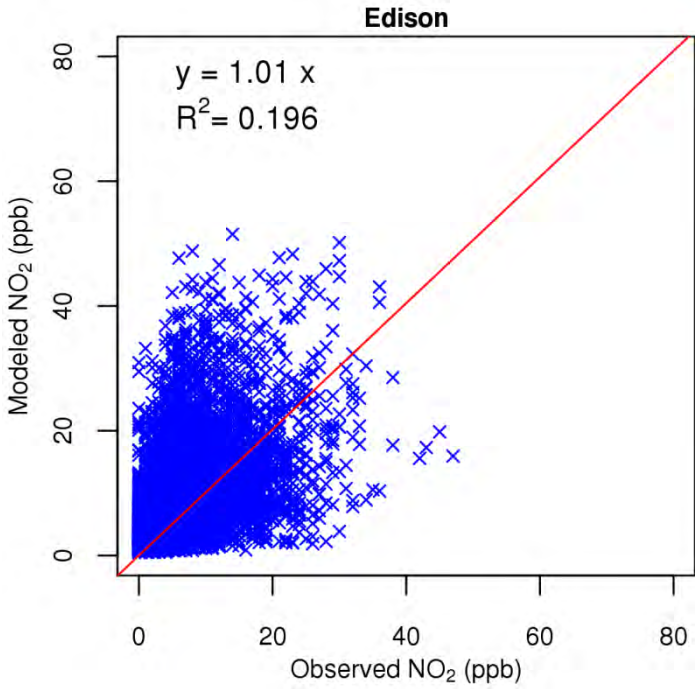

Figure S. 57 Scattering plot of observed and modeled 1-hour NO_2 mixing ratio at Edison

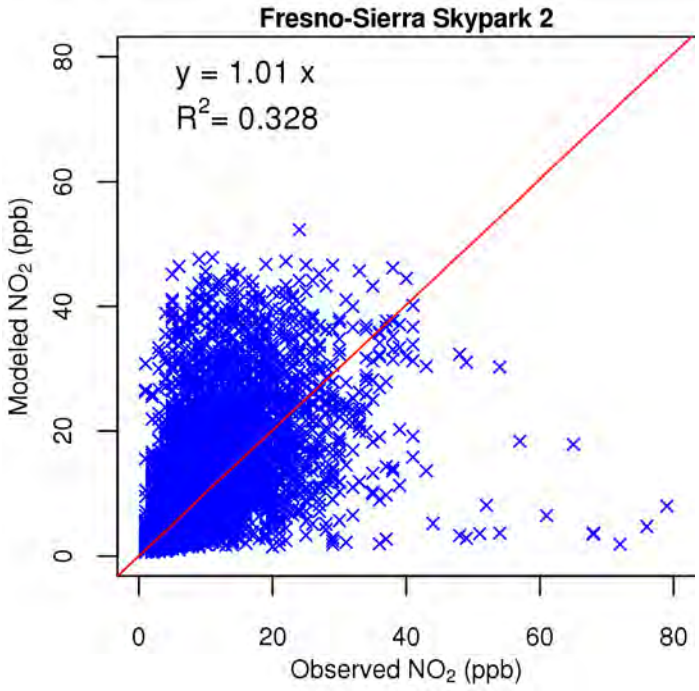

Figure S. 58 Scattering plot of observed and modeled 1-hour NO_2 mixing ratio at Fresno – Sierra Sky Park

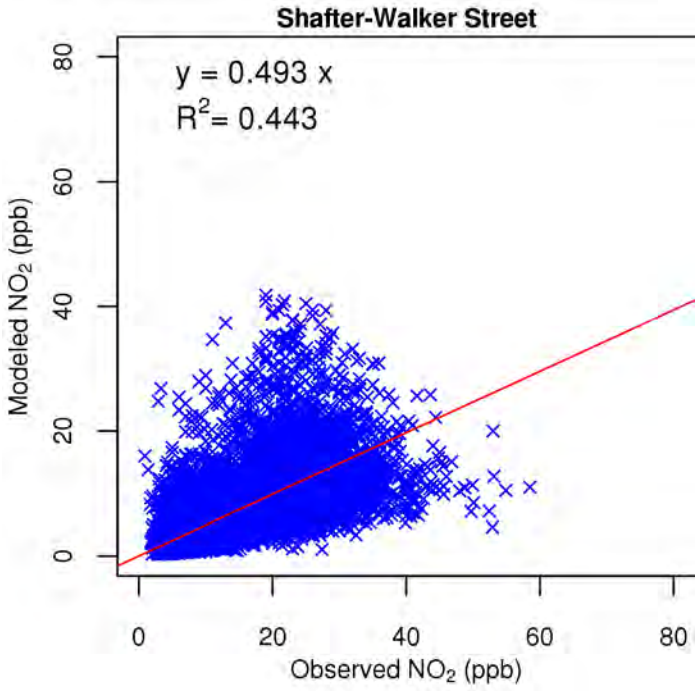

Figure S. 59 Scattering plot of observed and modeled 1-hour NO_2 mixing ratio at Shafter

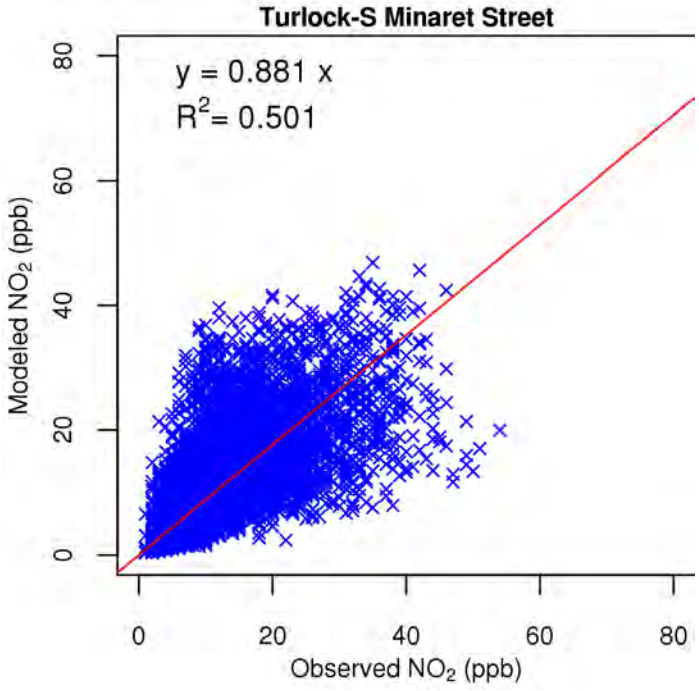

Figure S. 60 Scattering plot of observed and modeled 1-hour NO_2 mixing ratio at Turlock

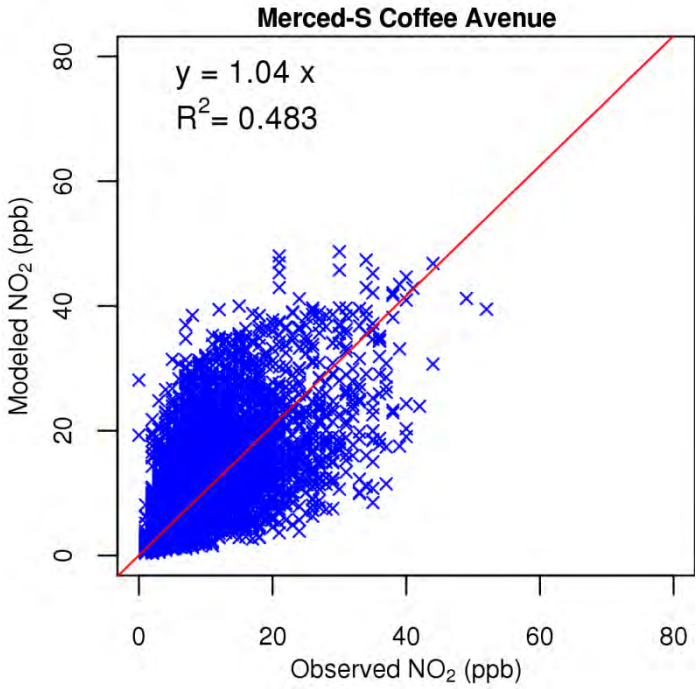

Figure S. 61 Scattering plot of observed and modeled 1-hour NO_2 mixing ratio at Merced

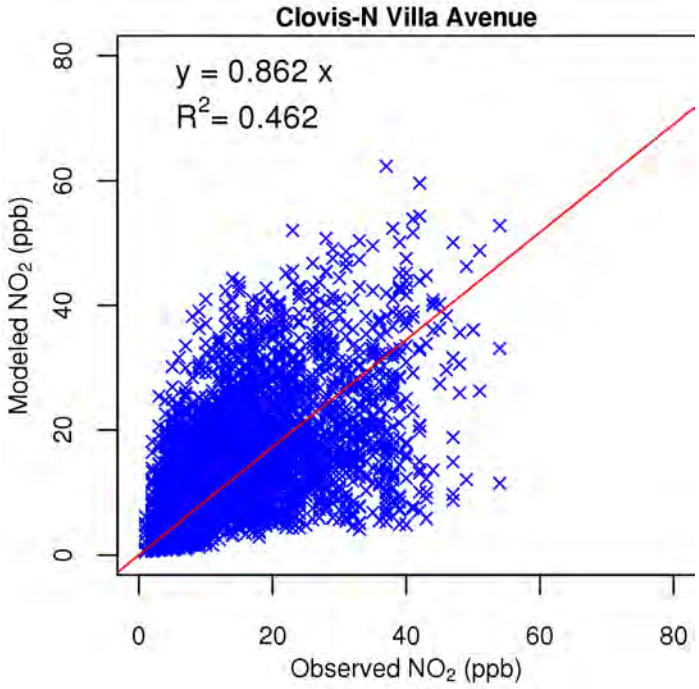

Figure S. 62 Scattering plot of observed and modeled 1-hour NO_2 mixing ratio at Clovis

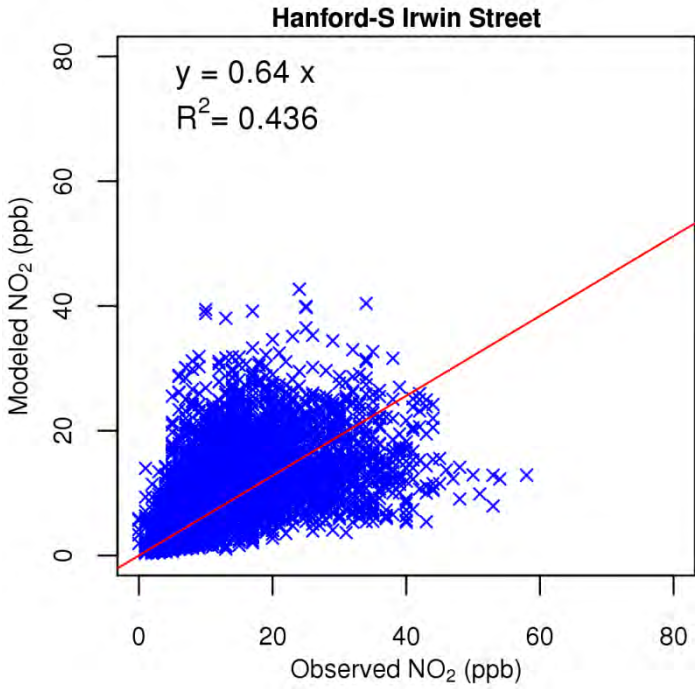

Figure S. 63 Scattering plot of observed and modeled 1-hour NO_2 mixing ratio at Hanford

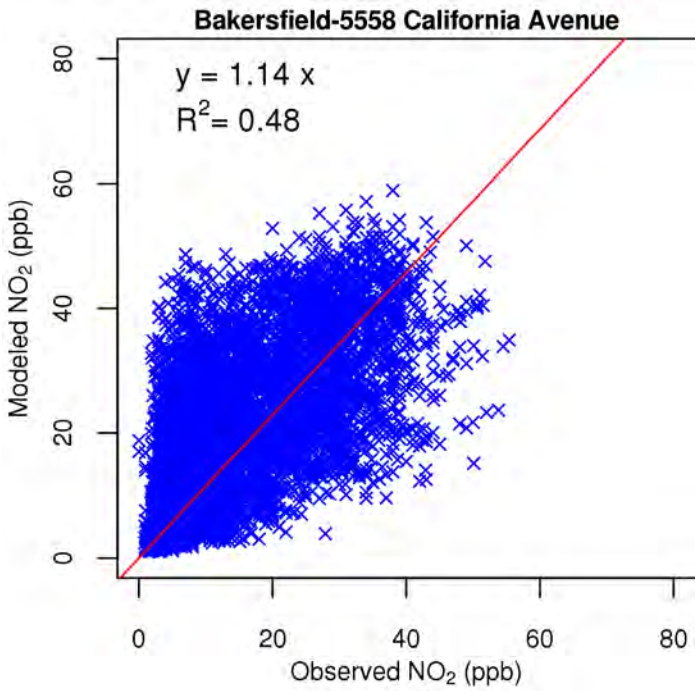

Figure S. 64 Scattering plot of observed and modeled 1-hour NO_2 mixing ratio at Bakersfield – California Avenue

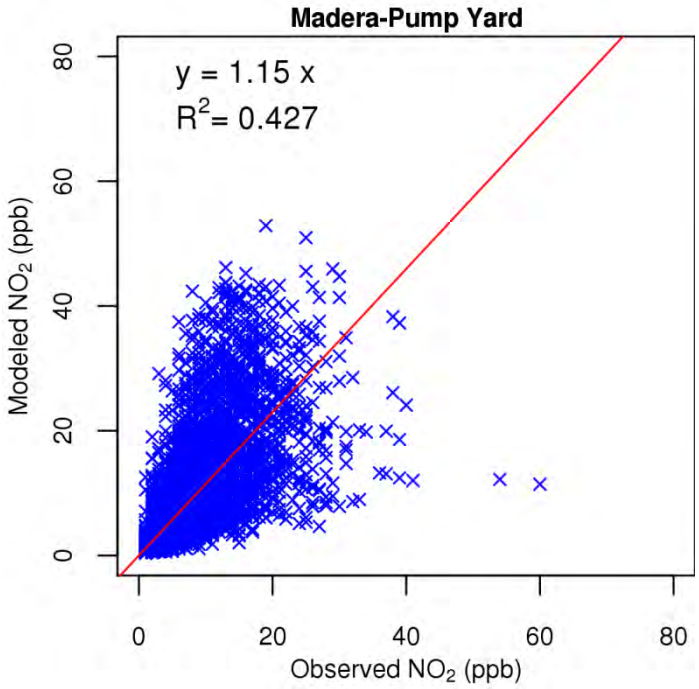

Figure S. 65 Scattering plot of observed and modeled 1-hour NO_2 mixing ratio at Madera

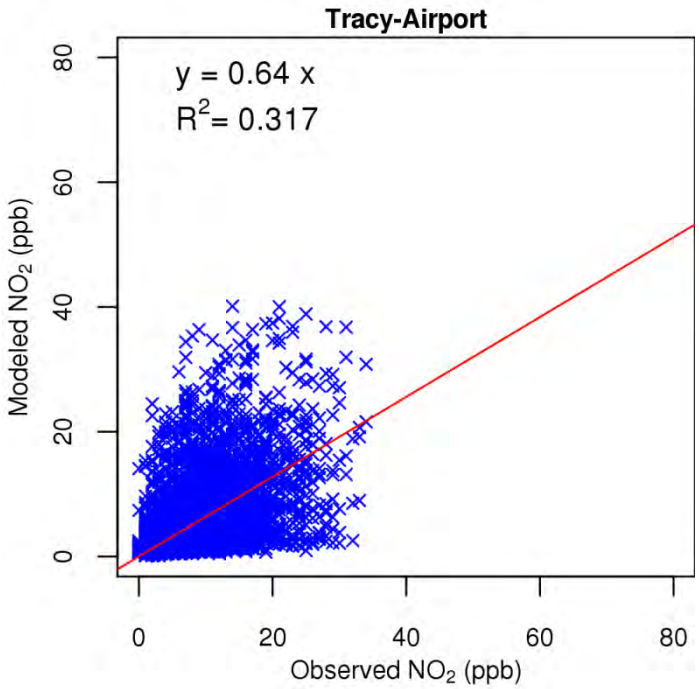

Figure S. 66 Scattering plot of observed and modeled 1-hour NO_2 mixing ratio at Tracy

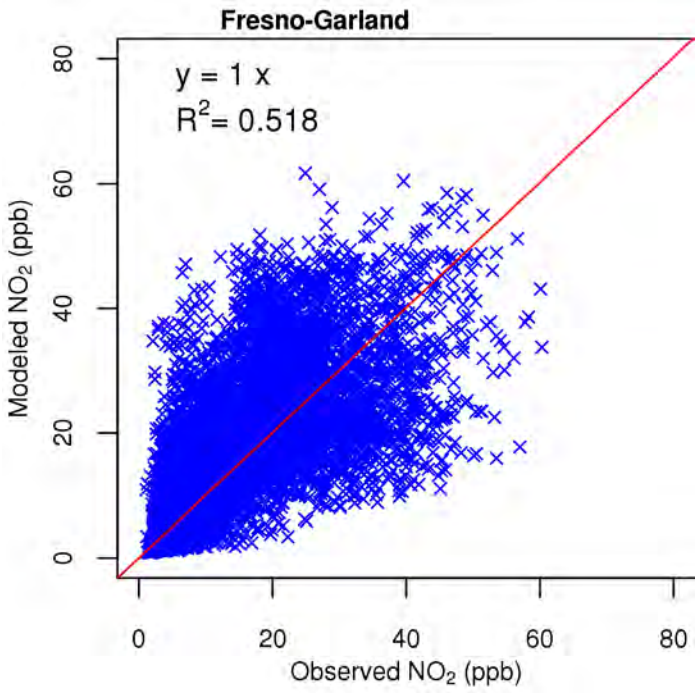

Figure S. 67 Scattering plot of observed and modeled 1-hour NO_2 mixing ratio at Fresno – Garland

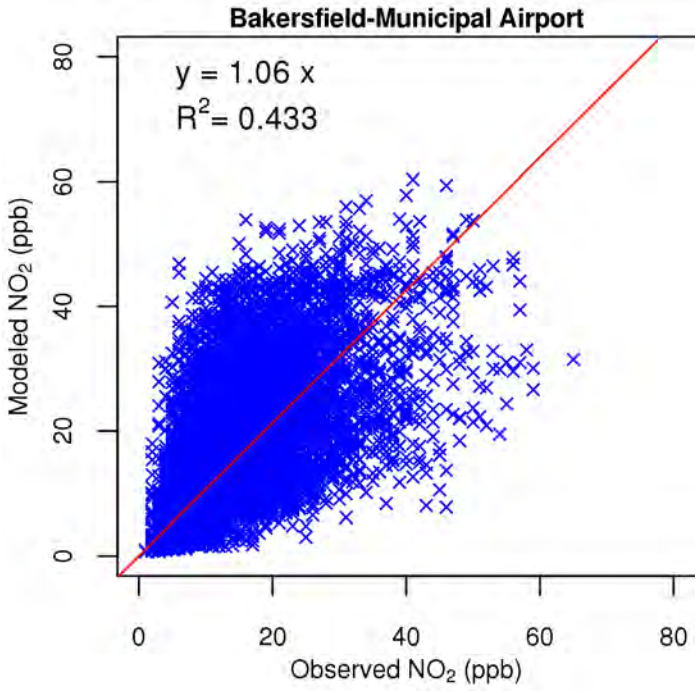

Figure S. 68 Scattering plot of observed and modeled 1-hour NO_2 mixing ratio at Bakersfield – Municipal Airport

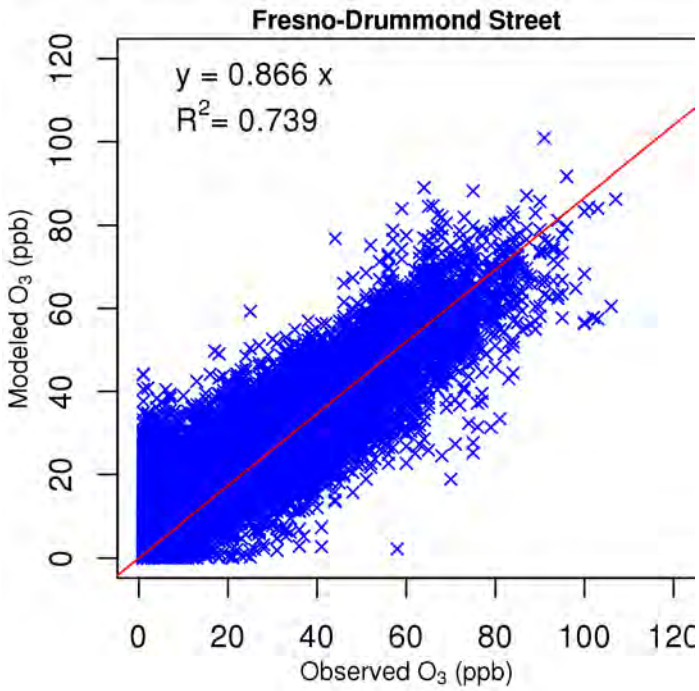

Figure S. 69 Scattering plot of observed and modeled 1-hour O_3 mixing ratio at Fresno – Drummond Street

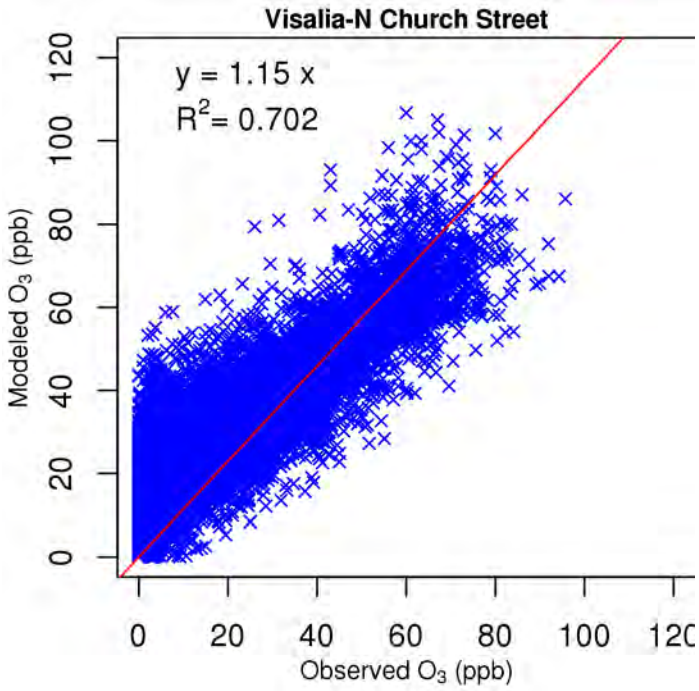

Figure S.70 Scattering plot of observed and modeled 1-hour O_3 mixing ratio at Visalia

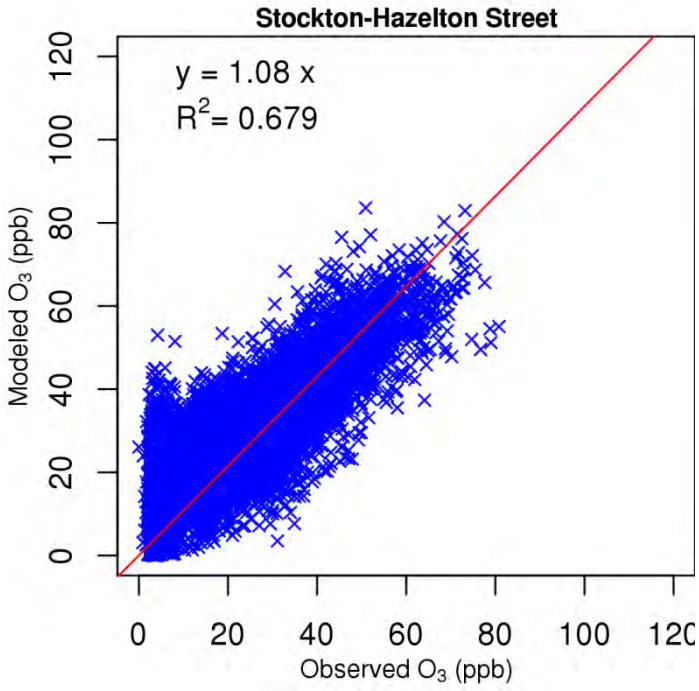

Figure S. 71 Scattering plot of observed and modeled 1-hour O_3 mixing ratio at Stockton

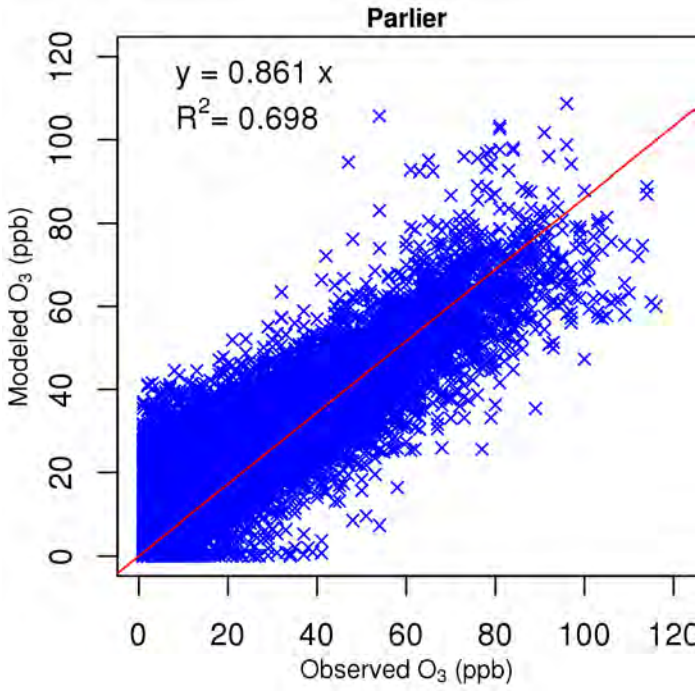

Figure S. 72 Scattering plot of observed and modeled 1-hour O_3 mixing ratio at Parlier

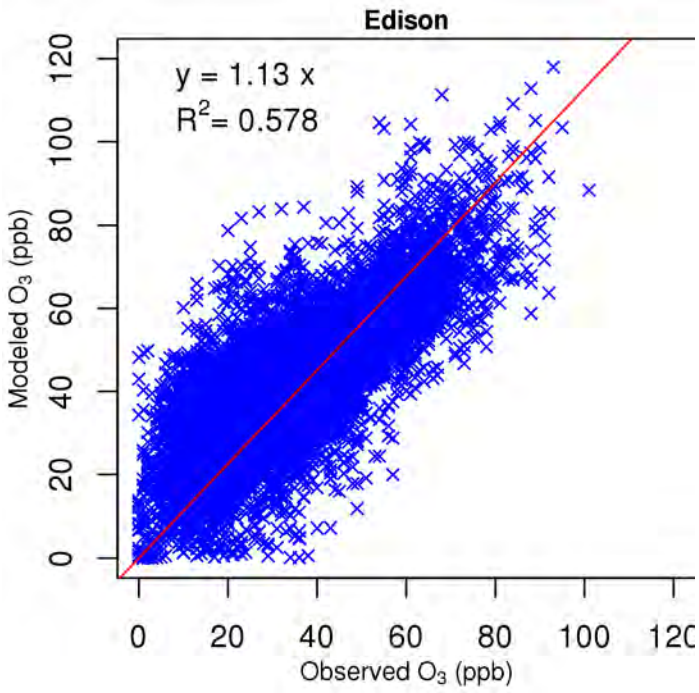

Figure S. 73 Scattering plot of observed and modeled 1-hour O_3 mixing ratio at Edison

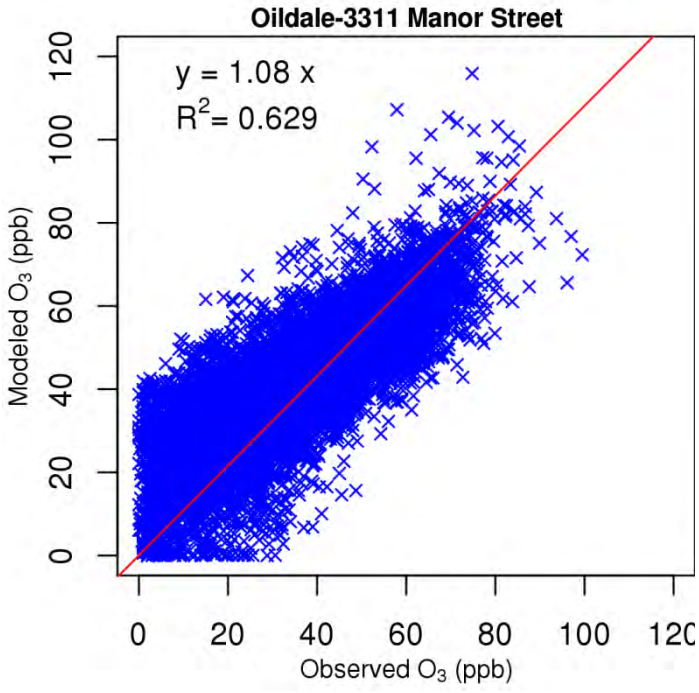

Figure S. 74 Scattering plot of observed and modeled 1-hour O_3 mixing ratio at Oildale

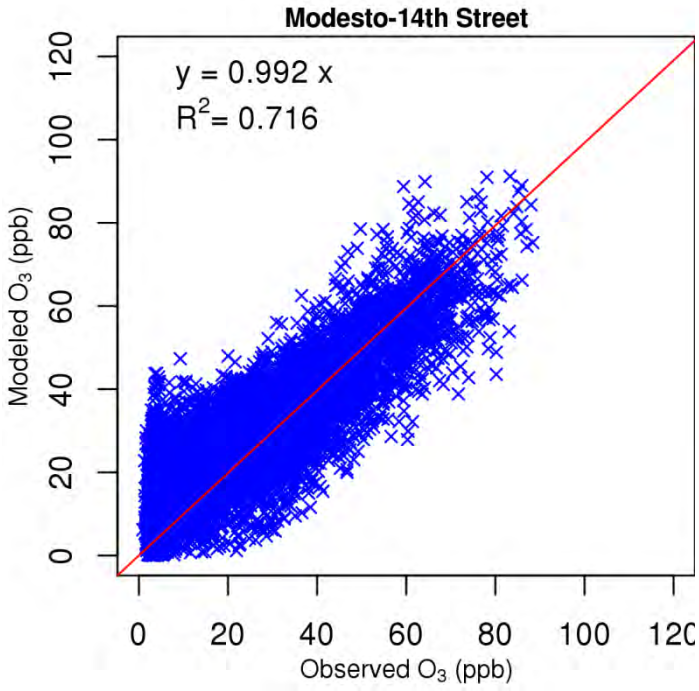

Figure S. 75 Scattering plot of observed and modeled 1-hour O_3 mixing ratio at Modesto -14th Street

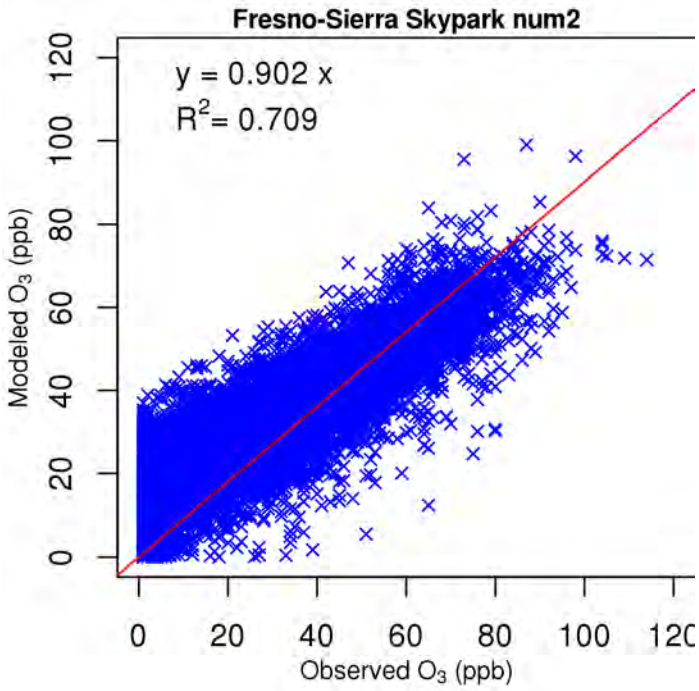

Figure S.76 Scattering plot of observed and modeled 1-hour O_3 mixing ratio at Fresno – Sierra Sky Park #2

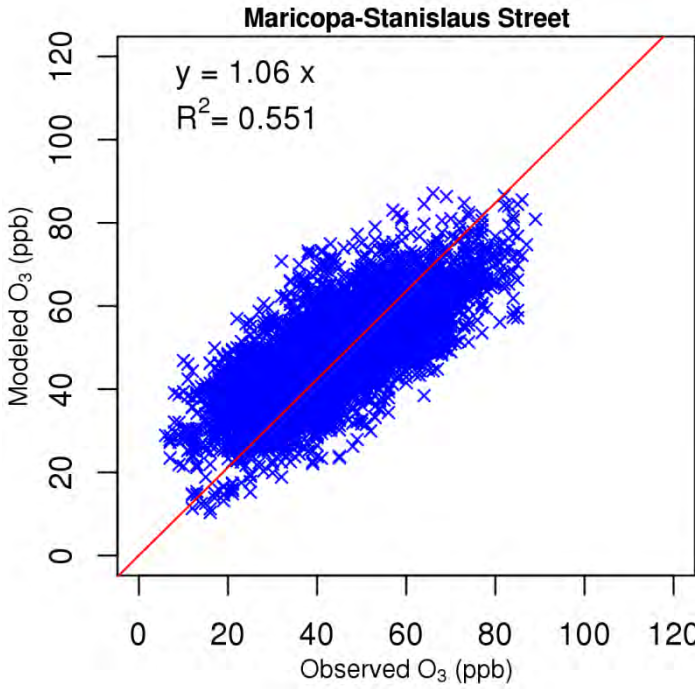

Figure S. 77 Scattering plot of observed and modeled 1-hour O_3 mixing ratio at Maricopa

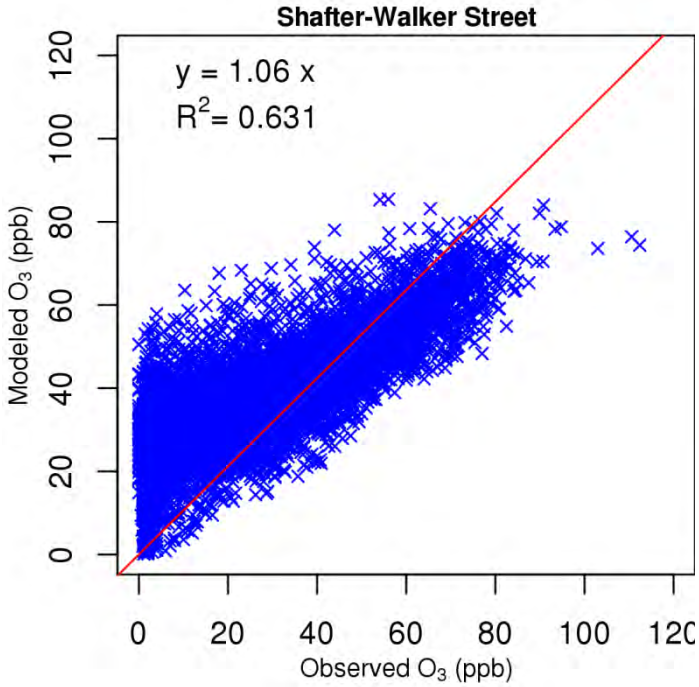

Figure S. 78 Scattering plot of observed and modeled 1-hour O_3 mixing ratio at Shafter

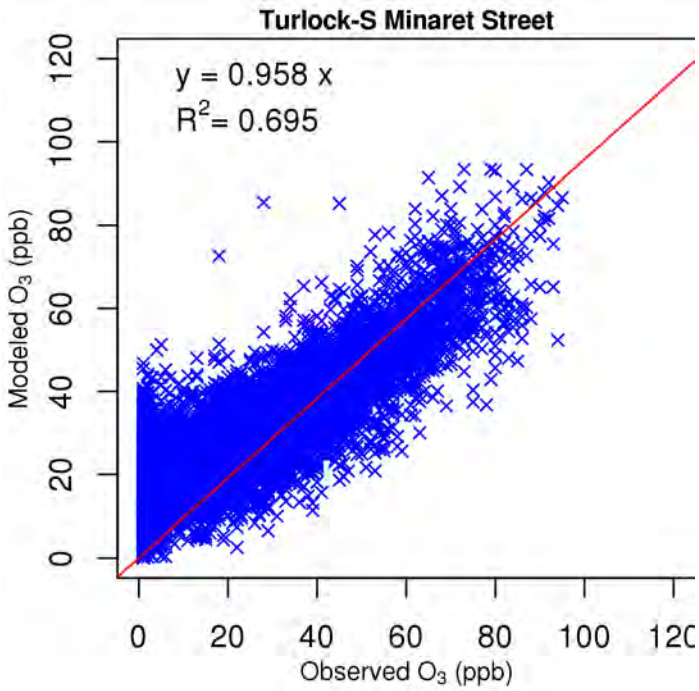

Figure S. 79 Scattering plot of observed and modeled 1-hour O_3 mixing ratio at Turlock

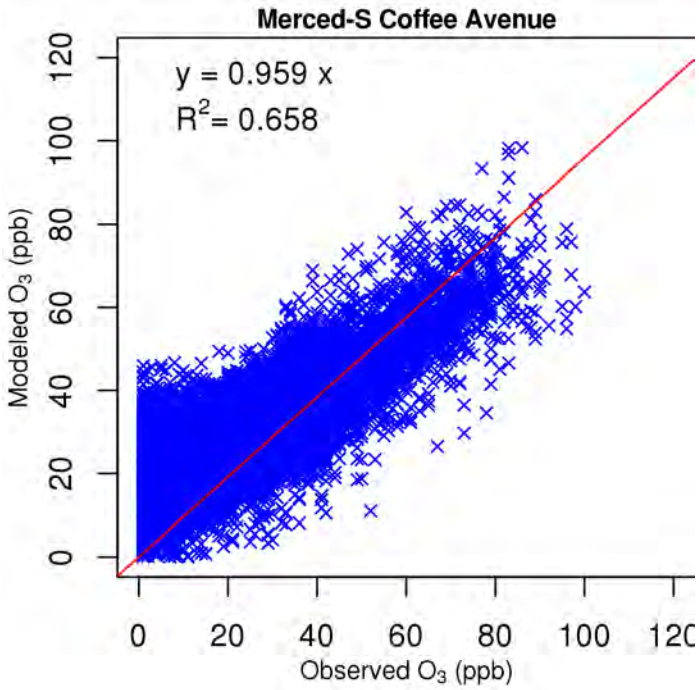

Figure S. 80 Scattering plot of observed and modeled 1-hour O_3 mixing ratio at Merced – S Coffee Avenue

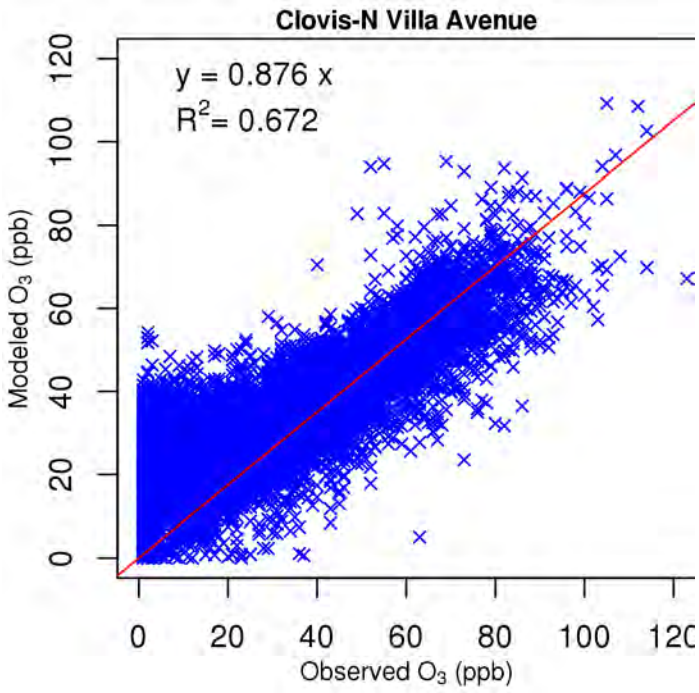

Figure S. 81 Scattering plot of observed and modeled 1-hour O_3 mixing ratio at Clovis

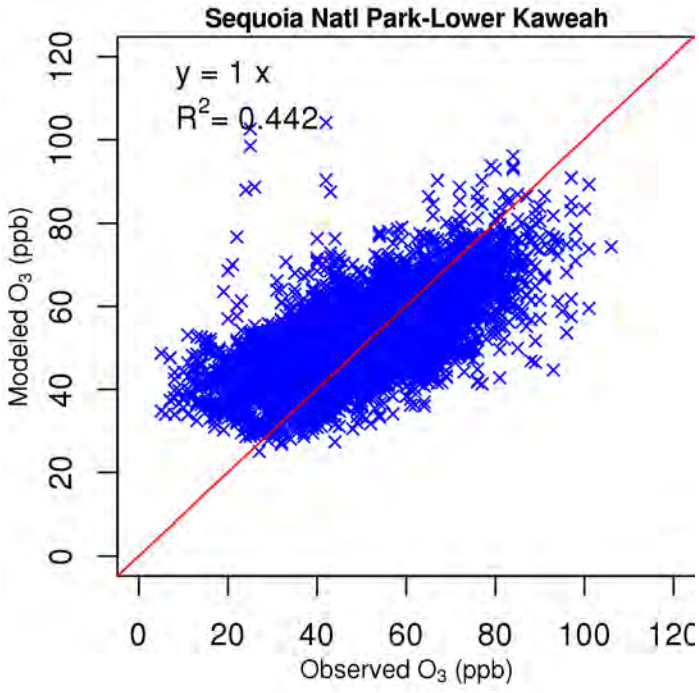

Figure S. 82 Scattering plot of observed and modeled 1-hour O_3 mixing ratio at Sequoia National Park

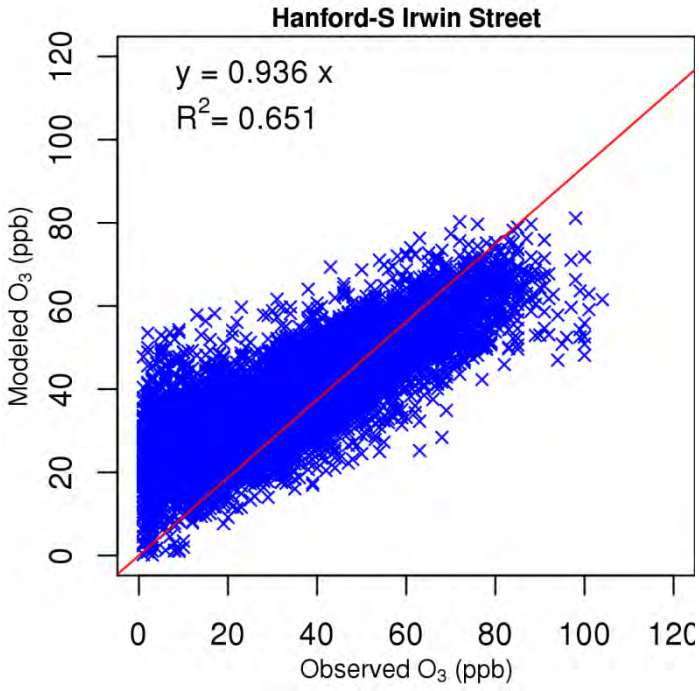

Figure S. 83 Scattering plot of observed and modeled 1-hour O_3 mixing ratio at Hanford

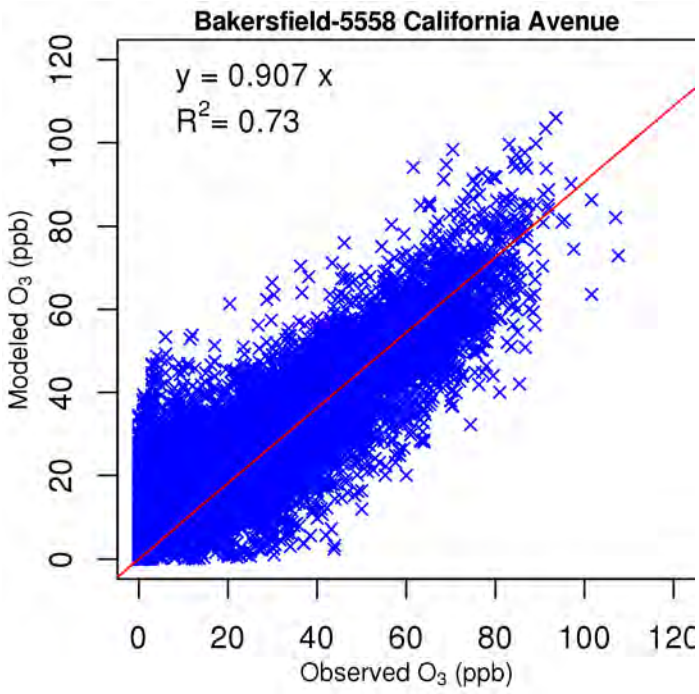

Figure S. 84 Scattering plot of observed and modeled 1-hour O_3 mixing ratio at Bakersfield – California Avenue

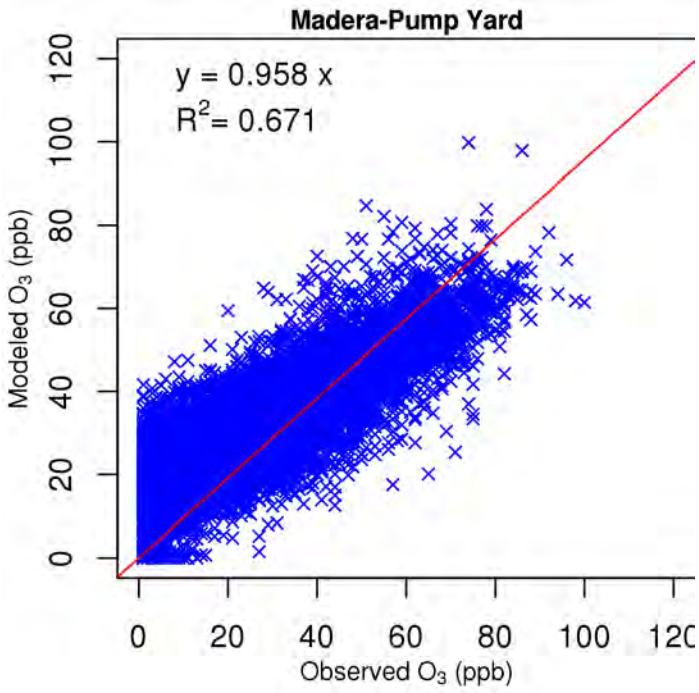

Figure S. 85 Scattering plot of observed and modeled 1-hour O_3 mixing ratio at Madera – Pump Yard

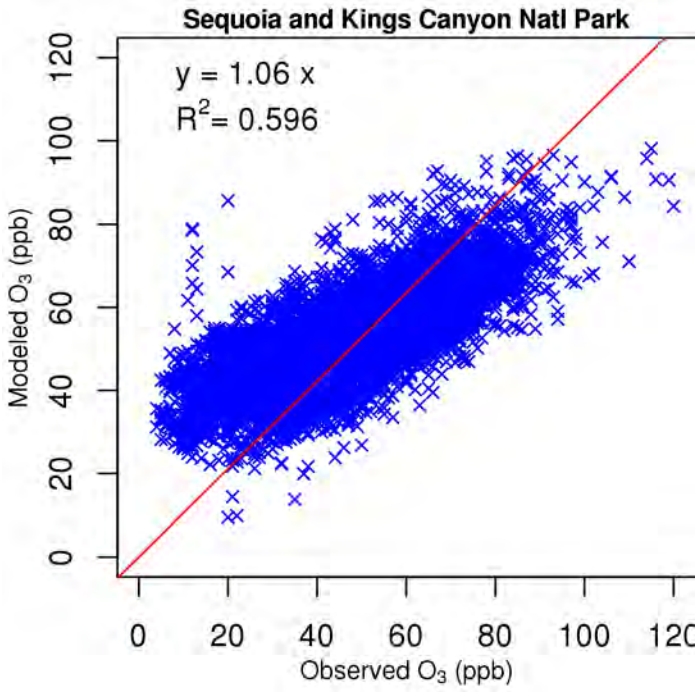

Figure S. 86 Scattering plot of observed and modeled 1-hour O_3 mixing ratio at Sequoia and Kings Canyon National Park

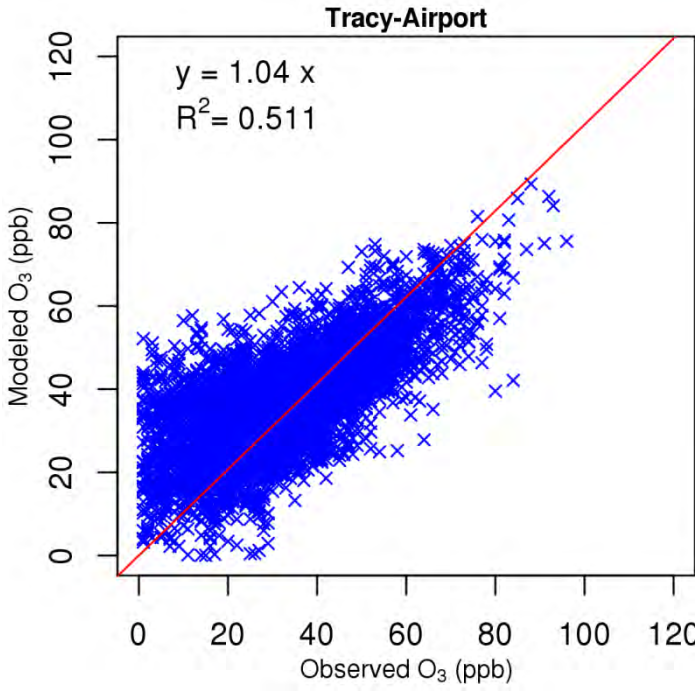

Figure S. 87 Scattering plot of observed and modeled 1-hour O_3 mixing ratio at Tracy

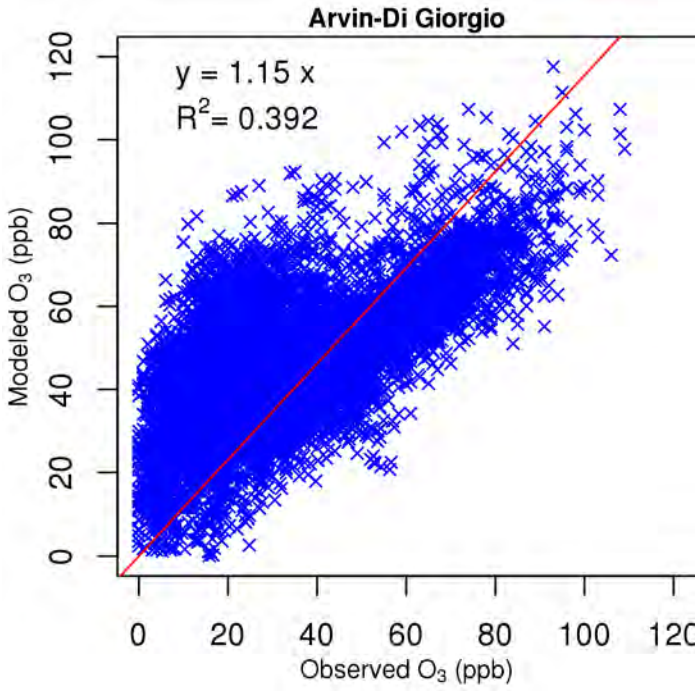

Figure S. 88 Scattering plot of observed and modeled 1-hour O_3 mixing ratio at Arvin

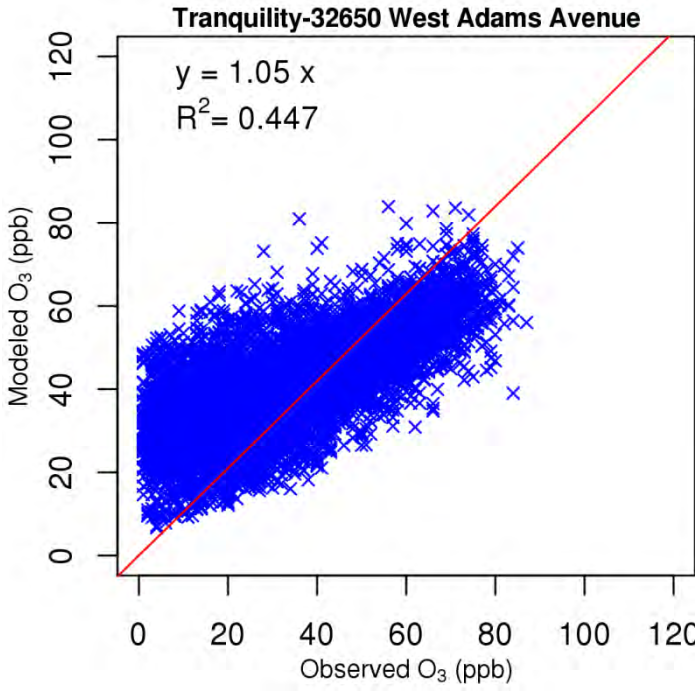

Figure S. 89 Scattering plot of observed and modeled 1-hour O_3 mixing ratio at Tranquility

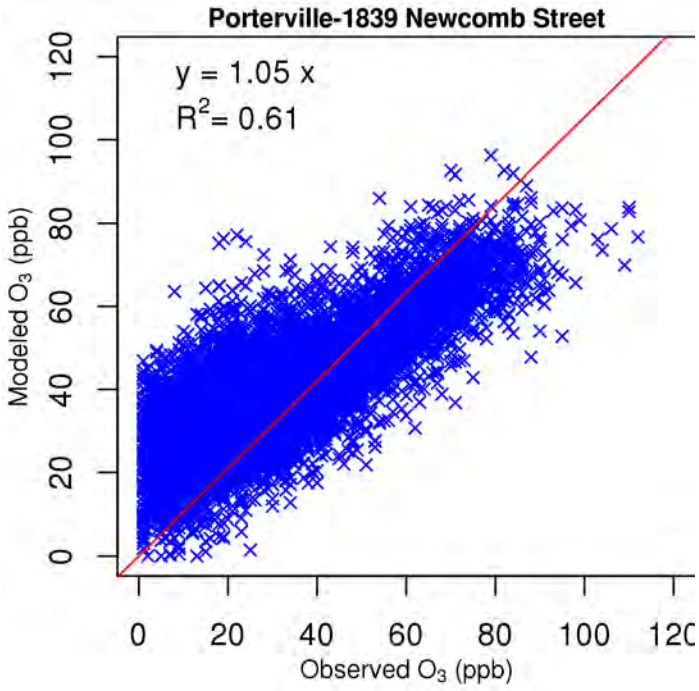

Figure S. 90 Scattering plot of observed and modeled 1-hour O_3 mixing ratio at Porterville

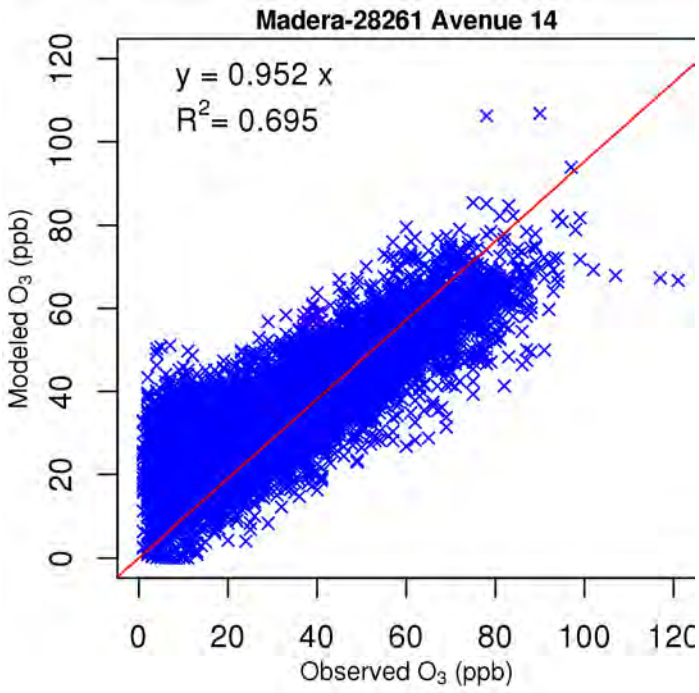

Figure S. 91 Scattering plot of observed and modeled 1-hour O_3 mixing ratio at Madera – 28261 Avenue 14

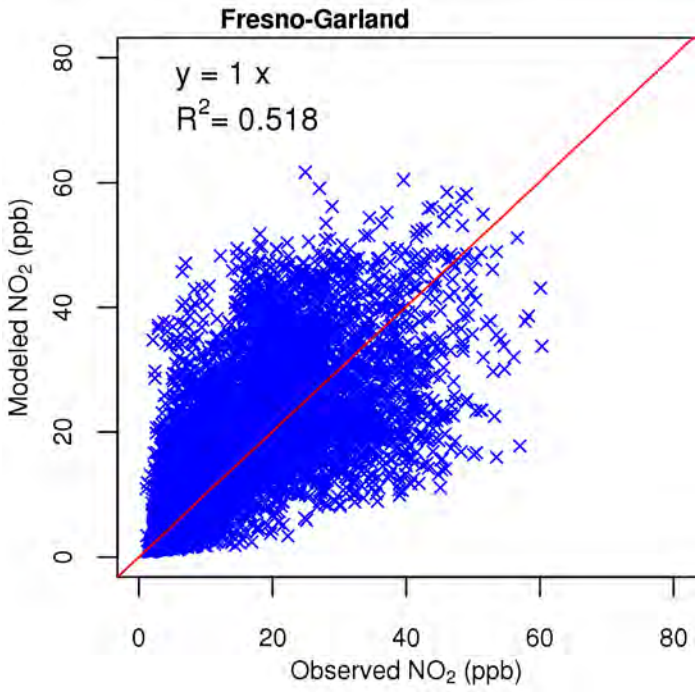

Figure S. 92 Scattering plot of observed and modeled 1-hour O_3 mixing ratio at Fresno-Garland

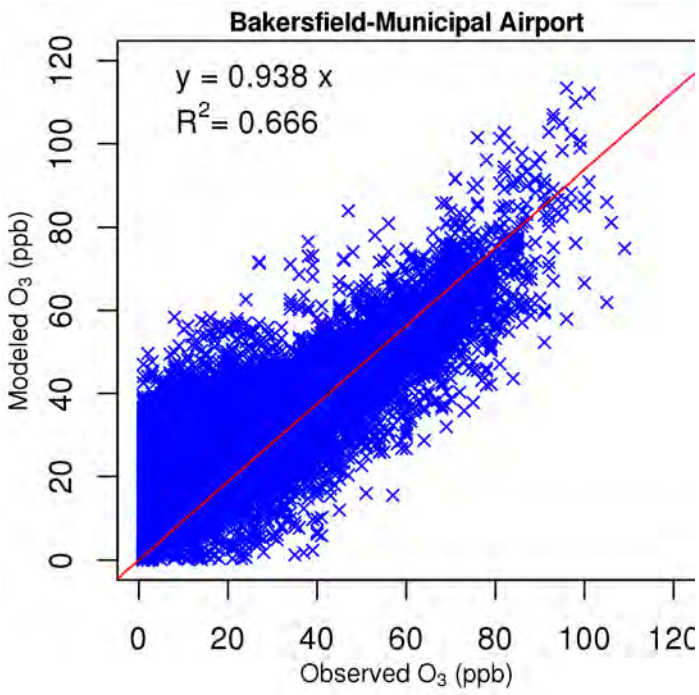

Figure S. 93 Scattering plot of observed and modeled 1-hour O_3 mixing ratio at Bakersfield – Municipal airport